The Effects of Crude Oil and Chemical Dispersant Exposure on *Danio rerio* (zebrafish) Embryonic Development

by

Erfaan Ghiassi

3 November, 2014

Director of Thesis: Edmund J. Stellwag, Ph.D.

Department of Biology

East Carolina University

Abstract

Crude oil has been shown to cause defects in cardiovascular development in a variety of teleost species. We used the zebrafish, *Danio rerio* as a model to test the effects of oil and dispersant on cardiac development and function during early embryogenesis. The aim of this study is to understand the effects of crude oil and chemical dispersant exposure on the gross anatomy and cellular morphology of cardiac development using the zebrafish (Danio rerio) model. This work was carried out through a histological examination of the phenotypic defects in cardiac development induced by exposure of embryonic zebrafish to crude oil and chemical dispersant. Embryonic exposure to Macondo crude oil and chemical

dispersant at 150-250 ppm causes teratogenic effects in cardiac development of zebrafish embryos with phenotypic abberations in form and function evident as early as 48 hpf. Developmental effects on cardiac development include a change in chamber morphology and positioning, coupled with a reduction of cardiac function; leading to cardiac stasis and embryonic death. Specifically, there is progressive yolk sac and cardiac edema, defective and reduced looping of the cardiac chambers, alteration in chamber morphology and positioning, reduction of cardiac function and circulation, and even a reduction in size of the eye and otic vesicle. These results provide a basis for further investigation of the toxicokinetic and toxicodynamic mechanisms through which exposure to crude oil and dispersant cause developmental toxicity. In addition, integrating the results of this study with gene expression profiles obtained from genome-wide transcriptomics at comparable time points promotes the formulation of future hypotheses aiming to more thoroughly understanding the pathways and genetic mechanisms though which PAH toxicity affects the zebrafish heart. Understanding the nature and mechanisms of oil exposure is especially critical for assessing toxicity of PAH contaminated environments.

A Thesis

Presented To the Faculty of the Department of Biology

East Carolina University

In Partial Fulfillment

Of the Requirements for the Degree

Master of Science in Cell Biology

By

Erfaan Ghiassi

3 November, 2014

The Effects of Crude Oil and Chemical Dispersant Exposure on *Danio rerio* (zebrafish) Embryonic Development

by

Erfaan Ghiassi

APPROVED BY:

DIRECTOR OF THESIS:_____
Edmund J. Stellwag, Ph.D.

COMMITTEE MEMBER: _____
Anthony Capehart, Ph.D.

COMMITTEE MEMBER: _____
Anthony Overton, Ph.D.

COMMITTEE MEMBER: _____
Randall H. Renegar, Ph.D.

CHAIR OF THE DEPARTMENT
OF BIOLOGY: _____
Jeff McKinnon, Ph.D.

DEAN OF THE
GRADUATE SCHOOL: _____
Paul J. Gemperline, Ph.D.

DEDICATION

For my beloved cousin Dr. Payman Houshmandpour who was taken from us on April 11, 2012. You left fingerprints of grace on our lives. You shan't be forgotten.

'Lord, make me an instrument of your peace. Where there is hatred, let me sow love; where there is injury, pardon; where there is doubt, faith; where there is despair, hope; where there is darkness, light, where there is sadness, joy.

O' Divine Master, grant that I may not so much seek to be consoled as to console; to be understood as to understand; to be loved as to love.

For it is in giving that we receive; it is in pardoning that we are pardoned; and it is in dying that we are born to eternal life.'

-- Saint Francis of Assisi

ACKNOWLEDGEMENTS

First and foremost, I would like to thank God, for giving me the blessing and opportunity to continue my education; for giving me a loving family that has stood by my side through thick and thin; for giving me the strength and ability to persevere through difficult times; and for the opportunities that lie ahead.

My sincere appreciation and thanks goes out to Dr. Edmund J. Stellwag, for giving me the opportunity to work with him throughout the course of my graduate career. The time and energy he has invested in me is invaluable, and I aspire to be as knowledgeable, hard working, and dedicated as he is. I am proud to have been able to learn, grow and mature into the individual I am today under your support and guidance.

I would also like to extend my gratitude to my thesis committee members, Dr. Anthony Capehart, Dr. Anthony Overton, and Dr. Randall H. Renegar. You all have been excellent mentors and support figures. The wealth of knowledge and expertise each of you posses has been of utmost importance, and critical to my success as a graduate student. I greatly appreciate all the guidance, support, and time you have dedicated to me throughout the years.

It would be very remiss of me not extend a great deal of thanks to Dr. Tom Fink for all that he has done for me. He allowed me to work in his laboratory throughout my endeavors as a

graduate student, and has been there to support and guide me through the entirety of my project; serving as my mentor and friend throughout the years. Without him, there would be no graduation. I am thankful for his positive attitude and all the time he has invested in me.

And lastly, my appreciation is extended to Dr. Yong Zhu. Thank you for your mentorship and for guiding me through the obstacles I faced as a gradate student.

TABLE OF CONTENTS

LIST OF TABLES

LIST OF FIGURES

LIST OF ABBREVIATIONS

A	Atrium
AhR	Aryl hydrocarbon receptor
ANOVA	Analysis of Variance
A-P	Anterior-posterior
AP	Alkyl phenol
AVC	Atrio-ventricular canal
AVc	Atrio-ventricular cushions
AVJ	Atrio-ventricular junction
BA	Bulbus arteriosus
BP	British Petroleum
BPM	Beats per minute
BTEX	Benzene, Toluene, Ethylbenzene, and Xylene
BVc	Bulbo-ventricular cushions
C	Celsius
CCV	Common cardinal vein
CH1	Anti-Tropomyosin antibody
CYP1A	Cytochrome P450 1A
DNA	Deoxyribonucleic acid
E	Eye
EMT	Epithelial to mesenchymal transition

En	Endocardium
Ep	Epicardium
Fgf	Fibroblast growth factor
H	Heart
Hpf	Hours post fertilization
L-R	Left-right
MC252	Macondo 252 crude oil
MHC	Myosin heavy chain
Mm	Millimeter
MO	Morpholino
MODU	Mobile Offshore Drilling Unit
My	Myocardium
Nc	Notochord
O+D	Oil and Dispersant
Ov	Otic Vesicle
PAH	Polycyclic aromatic hydrocarbon
Pc	Pericardium
Ppm	Parts per million
RA	Retinoic acid
SE	Standard error
SHF	Secondary heart field
SV	Sinus venosus
Tr	Trabeculae

Untr	Untreated
V	Ventricle
VBC	Ventriculo-bulbar canal
WSF	Water soluble fraction
WT	Wild type
Ys	Yolk sac
µm	Micrometer

The Effects of Crude Oil and Chemical Dispersant Exposure on *Danio rerio* (zebrafish) Embryonic Development

INTRODUCTION

Crude Oil

On April 20, 2010, the United States came face to face with the worst man made environmental disaster in history; the Macondo Well Gulf of Mexico oil spill was twenty times greater than the Exxon Valdez oil spill in 1989. As a result of a wellhead blowout, an explosion on the Deepwater Horizon semi-submersible Mobile Offshore Drilling Unit (MODU) initiated a massive oil spill in The Gulf of Mexico that flowed unabated for over three months (Freudenburg et al., 2011). As the largest accidental marine oil spill in the history of the petroleum industry, it has been estimated that the well was leaking an estimated 53,000 barrels per day, accumulating up to 4.9 million barrels of oil (210,000,000 US gallons). It is further estimated to have affected a geographic area of up to 68,000 square miles, encompassing eight US national parks as well as the Gulf islands and marshlands. Over eight thousand species of organisms, including but not limited to fish, birds, mollusks, crustaceans, turtles and other reptiles, as well as a host of marine mammals were severely affected by this environmental disaster (Freudenburg et al., 2011). Accordingly, much attention has been directed towards assessing the biological effects of crude oil and dispersant exposure on marine and terrestrial organisms. Of particular interest to the scientific community, is the effect crude oil exposure has on the embryonic stages of development. Does crude oil exposure result in overt toxicity and immediate embryonic death, or does it lead to specific defects that affect the short or long term survival of exposed organisms? In order to address these and similar questions,

scientists have performed field studies assessing the ecological impacts and toxicity of large-scale oil spills on native organisms. In the laboratory, scientists have used the zebrafish model of embryogenesis to conduct experiments aimed to identify the genotypic and phenotypic effects of crude oil and chemical dispersant exposure during early embryonic development of teleosts. Results from these experiments have shown that crude oil and chemical dispersant exposure of wild fish from Purdoe Bay, Alaska following the Exxon-Valdez oil spill and more recently from the Gulf of Mexico oil spill, causes a significant increase in larval mortality by induction of alterations in cardio-respiratory parameters of embryos and larvae. Moreover, recent results from laboratory exposure of zebrafish embryos to crude oil treated water show inherent toxicity causing defects in specific developmental processes including but not limited to yolk sac edema, hemorrhaging, cardiovascular abnormalities, defective craniofacial development, and reduced locomotive behavior, severely affecting embryonic survivability (de Soysa et al., 2012).

Over the past 30 years, the zebrafish *Danio rerio* has become an important vertebrate model for genetics, development, physiology, behavior, and evolution (Parichy et al., 2009). It was one of the first vertebrate species to have its genome fully sequenced. There are a variety of advantages to using this fish as a model organism. They are small, physiologically hardy, easy to cultivate in the laboratory, undergo rapid embryonic development, have a short generation time, and spawn frequently. Moreover, they have transparent embryos and larvae, which allows detailed microscopic observation of embryonic and early life history stages on live specimens (Kemadjou et al., 2012). Oil spills

such as he 1989 Exxon Valdez spill and the 2010 Deepwater Horizon disaster pose major threats to the health and population vitality of numerous aquatic and terrestrial organisms (Hicken et al., 2011). Both spills have prompted research efforts to discern how to detect defects in development and survival. Crude oil is highly unstable in the aquatic environment, and quickly loses volatile fractions through weathering (Pauka et al., 2011). As oil weathers, the proportional composition of dissolved PAHs (polycyclic aromatic hydrocarbons) becomes dominated by tricyclic fluorenes, dibenzothiophenes, and phenanthrenes (Hicken et al., 2011). The water-soluble fraction (WSF) of crude oil is a mixture of polycyclic aromatic hydrocarbons, monoaromatic hydrocarbons referred to as BTEX (benzene, toluene, ethylbenzene and xylene), phenols and heterocyclic compounds containing nitrogen, sulfur, and heavy metals (Pauka et al., 2011). PAHs and APs (Alkylphenols) are two groups of diverse chemicals of natural origin (Holth et al., 2008). PAHs consist of the fusion of two or more homo and hetero – cyclic benzene rings that may be alkylated. They are categorized as carcinogenic and non-carcinogenic compounds based on size, structure, and solubility (Holth et al., 2008). Alkylphenols are phenols with a carbon-chain of varying length and structure attached. The toxicity of dissolved polycylic aromatic hyrdocarbons (PAHs) has been the focus of considerable research in the recent decades. A study performed in 2008 by Carls showed that no negative effects were observed by coating, and that particulate oil is not involved in the toxic effects to fish embryos (2008). He concluded that dissolved PAHs caused the observed toxicity in the absence of particulate oil. The study aimed to distinguish between oil effects on wildlife due to physical processes (coating) and oil effects due to chemical toxicity (Carls et al., 2008). The deleterious effects of PAHs on fish early-life stages have been investigated

extensively after the 1989 Exxon Valdez oil spill in Prince William Sound, Alaska (Incardona et al., 2005). Zebrafish and other species demonstrated a common syndrome of oil-induced embryo-larval toxicity, characterized by pericardial and yolk sac edema, jaw reductions, curvature of the body axis, and other morphological and physiological deformities (Incardona et al., 2005).

In addition, the absorption of the WSF of crude oil by teleost fish has been reported to cause alterations that compromise their survival (Pauka et al., 2011). Moreover, the toxic components of crude oil are capable of causing genetic damage, alterations in reproductive and feeding behaviors, cellular aberrations, and effects on steroidogenesis (Pauka et al., 2011). The complex cardiac dysfunction caused by crude oil exposure suggests additional targets, including pacemaker currents and plasma membrane or sarcoplasmic calcium channels (Hicken et al., 2011). It is widely held that PAH toxicity is linked to aryl hydrocarbon receptor (AhR) binding and cytochrome P450 1A (CYP1A) induction (Incardona et al., 2005). Xenobiotic biotransformation enzymes belonging to the P450 families play central roles in the oxidative metabolism of a wide range of exogenous and endogenous compounds (Arukwe et al., 2008). The CYP 1, 2 and 3 superfamilies are known to metabolize a wide variety of compounds, including oil-based compounds (Arukwe et al., 2008). Although the exact mechanisms leading to PAH-associated malformations during development are not fully understood, it is known that most PAHs bind the aryl hydrocarbon receptor. AhR is a ligand activated transcription factor that controls the expression of a battery of genes encoding enzymes that convert PAHs to water-soluble derivatives that are excreted, including mixed-function oxygenases such as cytochrome

P450 1A family members (Incardona et al., 2005). Data presented in studies conducted by Incardona et al. demonstrated that different PAH classes act through distinct toxic mechanisms during development. Studies conducted by Aruwke et al., (2008) showed that exposure of zebrafish to WSF produced an apparent concentration-specific increase of AhR1 and CYP1A. CYP1A has been detected in several organs and tissue types including the brain and liver. Because of its critical role in detoxification and activation of foreign compounds, alteration of the expression of hepatic CYPs affects the potential benefits as well as risks of xenobiotics (Arukwe et al., 2008). A recent study examining the effects of crude oil and its harmful PAHs on embryonic development of zebrafish showed abnormalities which included reduced larval heart rate, cardiac arrhythmia, cardiac and yolk edema, reduced jaw and craniofacial development, curvature of the spine and dorsal tail, hemorrhaging, and reduced vascularization (de Soysa et al., 2012). They proposed that the malformations in cardiovascular and craniofacial development observed in the study are likely associated with reductions in specific rostral migratory streams of cranial neural crest cells (Figure 1) (de Soysa et al., 2012).

Current studies identify and describe a host of gross morphological defects associated with embryological exposure to crude oil. Exposure to crude oil or the water-soluble, polycyclic aromatic hydrocarbons that make up much of the oil have been shown to cause cardiovascular abnormalities and pericardial edema in topsmelt and Pacific herring embryos, as well as additional defects in jaw and spinal cord development in the crimson-spotted rainbow fish (de Soysa et al., 2012). Such phenotypes could potentially be explained by a reduction in cell proliferation or increase in apoptosis (de Soysa et al.,

2012). Experiments conducted in 2012 by de Soysa et al., showed that Mancondo crude oil exposure did not affect cell proliferation, but did in fact induce programmed cell death. It has been suggested that a component of the crude oil actively induces cell death or plays a role in the repression of a survival factor (de Soysa et al., 2012). Crude oil, fuels, oils, and specific PAH's have been documented to up-regulate known apoptotic proteins in juvenile cod, to increase programmed cell death in cultured dolphin renal cells, and to trigger apoptotic DNA fragmentation in ovarian and liver cells of the juvenile channel catfish (Figure 2) (de Soysa et al., 2012).

Apoptosis

Cell death is a driving force in morphogenesis of developing tissues as a major factor in homeostasis of organs and tissues. Developing organisms commonly produce excess cells that are subsequently removed by cell death as a step in normal development (Jacobson et al., 1997). The process of apoptosis is highly conserved and follows a distinct morphological patterns. The term 'apoptosis' was first used by Kerr and colleagues (1972) to describe the cellular shrinkage, membrane blebbing, nuclear condensation, and nuclear fragmentation that are now commonly recognized as the hallmarks of apoptotic cell death (Cole and Ross, 2001). Cell interactions and environmental influences can also promote apoptosis, with mechanisms including excitotoxicity (Choi, 1992), intracellular ion deregulation (Trump and Berezesky, 1995), loss of cell cycle control (Herrup and Busser, 1995), secretion of cytotoxic proteins by the cell or its neighbors (Williams and Smith, 1993; Wood and Youle, 1995), exposure to environmental pathogens or toxins (Vaux et al.,

1994), changes in hormone levels (Truman and Schwartz, 1984), and inadequate amounts or elimination of a trophic factor (Oppenheim and Nunez, 1982; Lowrie and Vrbova). Any of these proposed mechanisms might interact to initiate apoptosis, influencing various cell types in different ways. Three types of apoptosis have been described in the normal development of vertebrates, including frog, chick, mouse, and rat (Cole and Ross, 2001). Phylogenetic apoptosis is the elimination of embryonic cells or structures characteristic of an evolutionary ancestor that is no longer needed in an adult. Morphogenetic apoptosis acts as a type of 'sculpting' and occurs in areas of folding, bending, separation, fusion, or cavitation. Histogenetic apoptosis is characterized as the removal of cells following tissue maturation or remodeling (Cole and Ross, 2011). The dynamics of apoptosis in the zebrafish embryo generally follows the time course described in other organisms, and previous studies have described a rapid rate of dead cell clearance, with cells being removed within one hour or less (Cole and Ross, 2011). Growth of the zebrafish heart during embryogenesis occurs primarily through proliferation of cardiomyocytes. Soon after, these cardiomyocytes withdraw irreversibly from the cell cycle and subsequent growth of the heart occurs predominantly through hypertrophy rather than myocyte hyperplasia (Olson and Schneider, 2003). There are known to be two types of cardiac hypertrophy, physiological, as occurs as a response of exercise, and pathological, which occurs in response to abnormal levels of cellular stress. Stress signals that induce hypertrophy include hypertension, pressure overload, endocrine disorders, myocardial infarction, and contractile dysfunction from inherited mutations in sarcomeric or cytoskeletal proteins (Olson and Schneider, 2003). Pathological hypertrophy has been noted to frequently progress to dilated cardiaomyopathy, which could be in part due to

cellular activation of apoptotic pathways. There is a general agreement that cardiac hypertrophy is triggered by abnormalities in calcium homeostasis within the cardiomyocyte (Figure 3)(Frey et al., 2000).

Neural Crest Cells

In vertebrates, much of the head skeleton and peripheral nervous system develops from migratory cells of the neural crest (Schilling et al., 1996). Neural crest cells are a transient migratory cell population, multipotent, and unique to vertebrates. They give rise to diverse cell lineages and highly patterned structures including craniofacial cartilage and bone, smooth muscle, components of the nervous system, as well as melanocytes (Kelsh et al., 1996). Underlying the development of the neural crest cells is a gene regulatory network encompassing a plethora of transcription factors, interacting cell signaling pathways, and downstream effector genes responsible for conferring cell potency and migratory properties.

Neural crest cells develop into various types of tissues based on their origins and position along the dorsal regions of the neural tube along the anterior-posterior axis (Schilling et al., 1996). These neural crest tissues comprise four main functional domains; cranial, trunk, vagal and sacral, and cardiac neural crests. Cranial neural crest cells form the mesenchyme that differentiates into various craniofacial cartilage, bone, and cranial ganglia. According to Schilling, the cranial neural crest of the pharyngeal arches in particular is thought to produce signals that organize the patterns of surrounding tissues such as mesodermally

derived myogenic cells (Schilling et al., 1996). Trunk neural crest cells give rise to two cell populations; one is pre-determined to become melanocytes, and the other forms the dorsal root ganglia, sympathetic ganglia, and nerves associated with the aorta. Cardiac neural crest cells develop into melanocytes, connective tissue, cartilage, and neurons of some pharyngeal arches (Raible et al., 1996). This domain also gives rise to development of regions of the heart such as the musculo-connective tissue of the large vessels, the septum that divides pulmonary and systemic circulation, as well as formation of the semilunar valves of the heart. Vagal and sacral neural crest cells are known to develop into parasympathetic ganglia of the enteric nervous system (Schilling et al., 1996). In zebrafish, neural crest cells are known to be the source of patterning for many aspects of craniofacial development, pharyngeal arch formation and musculature of the jaw and gills, as well as development of certain regions of the heart and digestive system. Neural crest cells form the pharyngeal skeleton while mesoderm forms the muscles, and these two populations interact extensively with each other and with surrounding epithelia (Schilling et al., 1996). They eventually form reiterated bones and muscles of the jaw and branchial arches that function in feeding and breathing. Retanoic Acid (RA) affects neural crest development (Wedden et al., 1988) and in chick embryogenesis, neural crest cells form part of the aortic arches and contribute to the septation of the outflow tract and truncus arteriosus (Kirby, 1990). Tracing of fish cephalic neural crest migration suggests that the pattern in fish is similar to that in the chick, i.e., that the major mesenchymal contribution of the crest is to the gill arches rather than to the cardiac chambers (Figure 4) (Sadaghiani and Vielkind, 1990).

Genetic Regulation of Cardiac Development

Cardiac dysfunction and disease remains a leading cause of morbidity and mortality, and many of these diseases are in part due to genetic defects that affect the normal development, maturation, and function of the heart (Lieu and Didier, 2012). The cardiovascular system appears when needs for oxygen and nutrition can not be met by diffusion alone, because of the volume or increased metabolic rate of an organism (Burggren and Pinder, 1991; Pelster and Burggren, 1996). As such, the heart is the first definitive organ to develop and become functional during the course of embryogenesis. A fundamental question in organogenesis addresses the means by which organ progenitor cells are specified. 'The zebrafish heart may provide an ideal system for combining embryological and genetic approaches to the complex process of organogenesis. The formation of bilateral cardiac tubes and their subsequent fusion, the lining of the myocardium by the endocardium, the morphological differentiation of the heart in an arterial to venous direction, paralleled by an acceleration of the heart beat, all contribute to the formation and proper functioning of the heart, and can be readily assayed in the zebrafish embryo" (Didier et al., 1993). Previous studies performed in mouse, chick, and Xenopus have implicated several positive regulators such as Bmp, Activin/Nodal, fibroblast growth factor (Fgf) and Wnt involved in the specification and regulation of progenitor cells (Lieu and Didier, 2012). Keegan et al., 1996, showed that in addition to positive regulation, a repressive mechanism is also involved. Through a combination of genetic, pharmacological, and fate mapping techniques, it was shown that in zebrafish, the potential of naïve cells to adopt a cardiogenic fate is restricted by retinoid acid signaling. Mutants

defective in RA synthesis generated an excess number of cardiomyocytes. RA signaling at early somite stages appear to be mediated by hoxb5b, a hox gene whose expression in the adjacent forelimb field is induced by RA signaling (Lieu and Didier, 2012). The same study showed that in addition to hox5b, Fgf signaling acts downstream of RA signaling to regulate both heart and forelimb formation. It is important to note that cardiac defects caused by RA deficiency could be rescued by morpholino knockdown of fgf8, suggesting that RA signaling acts to temper Fgf signaling to ensure the proper development of the heart (Lieu and Didier, 2012). Didier et al., reported a clear gradient sensitivity of the heart to RA, which causes a dose dependent truncation of the heart tube. Recent advance in cardiac biology has led to the identification of 2 sources of cardiac progenitors. Pater et al., observed 2 different cardiomyocyte populations in the developing heart, 'early differentiated' and 'late differentiated' cells. The first heart field contributes primarily to the linear heart tube, whereas cells from the secondary heart field (SHF) are later recruited to the heart tube, and contribute to the further growth and development into a fully functional organ. The proper formation of the cardiac outflow tract in chick embryos involves the recruitment of cells from a progenitor population located in the pharyngeal mesoderm, or SHF (Figure 5).

Cardiac Fate-map and Development

Having analyzed the origin of cardiac progenitors in the zebrafish embryo by injection of single blastomeres with a lineage tracer dye, Didier et al., (1993), showed that at early blastula (512-cell) stage, most cardiac progenitors lie in a marginal zone that extends from 90º longitude, or midway between the future dorsal and ventral axis, through 180º - 270º

longitude, or the future ventral axis (Didier et al., 1993). Blastomeres located around 90º-longitude give rise to myocardial cells but never to endocardial cells, whereas ventral blastomeres exhibit a more complex lineage pattern and give rise to myocardial, endothelial, endocardial, and blood cells (Didier et al., 1993). It was found that a single cell injected in the early blastula could contribute progeny to both the atrium and ventricle, whereas a single cell injected in the mid-blastula contributes progeny to either the atrium or ventricle, but not both. This finding is suggestive of atrial and ventricular lineages separating as early in development as the mid-blastula (Figure 6).

In vertebrates, cardiogenic precursors appear to migrate medially as part of the lateral plate mesoderm, and generate a pair of tubular primordia, one on either side of the midline (Didier et al., 1993). The tubular primorida fuse to generate a definitive heart tube consisting of an inner endocardial tube and an outer myocardial tube. The heart tube will subsequently differentiate into separate chambers consisting in series of the sinus venosus, the atrium, ventricle, and the bulbus arteriosus. The bulbus arteriosus is continuous with the ventral aorta. Cardiac progenitors are among the first mesodermal cells to involute. After involution, they change their direction of movement, turning towards about 30-60º posterior to the animal pole, and begin to arrive at the embryonic axis around 11 hours post fertilization (hpf), the 8 somite stage (Didier et al., 1993). Post-involution and migration, cardiac cells divide once or twice, coalesce at the embryonic axis, and by the 15 somite stage (16 hpf), form the two tubular primordia in the lateral plate mesoderm. At this stage, the bilateral cardiac primordial extends from the caudal end of the trigeminal ganglia, rostrally, to the otic vesicles (Didier et al., 1993). Cardiac progenitors at the ventral

side of the tubes migrate directly on the syncytial layer of the yolk cell. At the 21-somite stage (19 hpf), the tubular primordia have formed complete tubes and migrate closer to each other. Fusion of these two tubular cardiac primorida seen at the 21-somite stage leads to the formation of a definitive heart tube by 24 hours post fertilization (Figure 7)(Didier et al., 1993). Whole mount immunostaining of intermediate stage embryos with CH1, an anti-tropomyosin antibody specific to striated muscle forms of tropomyosin including cardiac alpha tropomyosin, reveals that the intermediate stage of the developing heart is cone shaped, with the base of the cone arranged on the yolk. The apex of the cone, the future arterial end is continuous with the ventral aorta. The base of the cone, the future venous end, is attached to the visceral pericardium and consists of a single sheet of myocardial cells. Endocardial cells migrate from the apex of the heart cone in both anterior and posterior directions (Figure 8).

Studies performed by Didier et al., helped to delineate the exact timing of various developmental milestones in zebrafish cardiac development (1993). It was shown that around the 22-somite stage (19 hpf), individual myocardial cells begin to contract irregularly, and the heart beats in a coordinated fashion at a rate of about 25 beats/minute by the 26-somite stage or 22 hpf (Didier and Fishman, 1994). It was observed that at 24 hpf, the heart tube beats at approximately 90 contractions/minute and circulation begins shortly after this time.

Morphological differentiation progresses in an arterial to venous direction (Didier and Fishman, 1992), and as in the chick, there is a corresponding shift in the location of the

pacemaker to the venous end, and an acceleration in beat rate accompanied by increased contractility (Didier and Fishman, 1994). At 24 hpf, there is an indication of separation into bulbus arteriosus (BA), ventricle (V), atrium (A), and sinus venosus (SV), but regionalization of cardiac myosin heavy chain (MHC) expression defines chamber boundaries by the 26-somite stage (Figure 9). By 30 hpf, the heart tube was measured to beat at about 140 beats/minute and cardiac looping to the embryo's right hand side had begun. This direction of looping of the heart tube is a feature that has been conserved throughout vertebrate evolution from the cyclostomes to tetrapods (Santer, 1985). Heart looping is complete by 36 hpf and it beats at about 180 beats/minute, providing a strong circulation to the head and trunk. Clear indentations mark chamber boundaries and looping leaves the atrium positioned on the left while bringing the ventricle to the right side of the embryo when observed from the dorsal or ventral perspectives (Figure 10). The sinus venosus (SV) and the bulbus arteriosus (BA) can also be distinguished at the extremities of the heart tube (Stainier and Fishman, 1992). The sinus venosus emerges caudally from the common cardinal vein (CCV) and is considered the inflow tract leading into the atrium. The ventricle leads into the rostrally located bulbus arteriosus (BA), which is considered the outflow tract through which blood exits the heart. When dividing into specific chambers, endocardial cells at the chamber boundaries undergo a complex epithelial to mesenchymal transition to form cardiac cushions (Didier and Fishman, 1994).

At 48 hpf, the zebrafish heart consists of a smooth-walled tube partitioned into all four segments with the definitive structure of sinus venosus, atrium, ventricle, and bulbus arteriosus clearly delineated. Each particular region can be identified by constriction

between the segments (Hu et al., 2000). Morphological analysis conducted by Hu et al., showed the myocardium at this stage was about one cell thick in each segment with the exception of the ventricle, which had two to three layers of cells (2000). The heart is lined with endocardium, which is separated from the myocardium by a layer of cardiac jelly in the atrium and the bulbus arteriosus. It is to be noted that the ventricle and sinus venosus does not seem to contain a cardiac jelly layer. There are no valves separating the segments at 48 hpf, and the heart is enclosed in the pericardial cavity with a pair of pericardial muscles running in the caudo-cranial direction, covered with epicardium (Figure 11)(Hu et al., 2000).

The formation of trabeculae in the ventricle occurs between 72 and 120 hpf. By 120 hpf, the ventricle has developed extensive trabeculation while the inner surfaces of the atrium are still smooth. The atrial wall and trabeculae are one to two-cell layers thick, and the ventricular myocardium is about two to three-cells thick (Kelsh et al., 1996). Positive MF-20 staining showed that the bulbus arteriosus has similar characteristics to the ventricular myocardium at this stage in development (120 hpf). Valves between the atrium and ventricle (AVc) and the ventricle and bulbus arteriosus (VBv) are prominent and distinguishable by 120 hpf. They show two cusps, with the leaflets having a mesenchymal, cushion-like appearance (Figure 12)(Kelsh et al., 1996).

In the zebrafish, the heart is situated anterior of the main body cavity and ventral to the esophagus (Menke et al., 2011). The path of blood flow through the heart begins with deoxygenated venous blood entering the sinus venosus. The walls of the sinus venosus are

thin and mainly composed of collagenous connective tissue (Menke et al., 2011). Subsequently, the deoxygenated blood passes from the sinus venosus, through the sino-atrial valve, and into the atrium. The atrium has a thin muscular wall, and thin trabeculae from a loose meshwork in the lumen (Menke et al., 2011). Blood is forced into the ventricle through the atrio-ventricular valve via a synergistic effect of atrial contraction and ventricular dilation. The ventricular wall is significantly thicker, and is comprised of a compact outer layer of muscle and a spongy inner layer with numerous trabeculae (Menke et al., 2011). High pressure generated by the contraction of the ventricle pumps the blood into the bulbus arteriosus, which exhibits a characteristic 'onion' shape, via the ventricular-bulbar valve. The bulbus arteriosus exhibits high elasticity and has a tick wall consisting of fibro-elastic tissue and some smooth muscle fibers (Menke et al., 2011). From the heart, the ventral aorta distributes the blood to the gills through the afferent branchial arteries (Figure 13)(Menke et al., 2011).

I have conducted a comprehensive histological comparison of embryonic and larval zebrafish exposed to crude oil and chemical dispersant and suitable controls. The scope of this project focuses specifically on phenotypic defects at a gross morphological and cellular level. Image analysis software has been used to quantify differences in cardiac cellularization and tissue structure of embryos and larvae resulting from early and continuous exposure to crude oil and dispersant mixtures. Results from this research aim to provide greater insight into the earliest developmental effects, and the dynamics of tissue-specific developmental changes resulting from crude oil exposure during vertebrate embryogenesis. As such, this research will test a hypothesis concerning the teratogenic

effects of crude oil and chemical dispersant exposure on cardiac organogenesis using *Danio rerio* as the model organism. It also serves to provide a more detailed understanding of the earliest cellular and tissue-specific defects affecting cardiac form and function as a result of crude oil exposure during development.

A 2012 study conducted by de Soysa et al. testing whether the WAF (water accumulated fractions) of the Deepwater Horizon oil could impact specific processes involved in embryonic development, shows that Macondo crude oil causes a variety of significant defects in craniofacial development and circulatory function similar to previous reports. These effects include brain hemorrhaging, dorsal tail curvature, cyst formation, reduction of craniofacial cartilage, reduction of circulation and vasculogenesis, as well as cardiac and yolk sac edema. Furthermore, the results of the study have been linked to earlier defects in neural crest development.

Results from the 2012 study by de Soysa et al. showed that WAF treated embryos exhibited reductions in brain and eye size, indicative of a potential reduction in cell proliferation or increased programmed cell death when compared to controls. Embryos immuno-labeled with Activated Capsase 3, a marker for cells undergoing apoptosis, showed a statistically significant increase in apoptotic cells (De Soysa et al., 2012). A reduction in cell proliferation was ruled out based on a lack of reduction of mitotic cells. Effects of crude oil components on circulation and vasculogenesis included cardiac edema, hemorrhaging in the brain, and a reduction in the amount of blood cells. A reduction in blood volume beyond the bulbus arteriosus was speculated to be due to diminished hematopoiesis, improper

vessel formation or altered cardiac function. Fluorescent quantum dot angiography of embryos showed a loss of posterior arch vasculature and a reduction of circulation to other vessels, suggesting that endothelial vasculature and proper cardiac organogenesis are compromised in WAF-treated embryos (De Soysa et al., 2012). Alcian Blue staining was used to treat control and WAF-treated embryos to assess the effects of crude oil on craniofacial development. Consistent with head vasculature phenotypes, WAF-treated embryos displayed defects in craniofacial cartilage. When compared to controls, WAF-treated embryos showed a dramatic reduction in all the pharyngeal arch cartilages, with a complete loss of the posterior three arches (De Soysa et al., 2012). Neural crest cells are common progenitor cells contributing to smooth muscle of the pharyngeal arch arteries, portions of the heart, septum and cardiac cushion formation, as well as pharyngeal arch cartilage. Crestin is a known marker for of neural crest cells during early specification, and *in situ* hybridization experiments for crestin transcripts in WAF-treated embryos showed a quantitative reduction of crestin-labelled cells in the anterior migratory streams known to populate the pharyngeal arches. Similarly, tg(fli:GFP) transgenic embryos showed a specific loss of posterior pharyngeal arches and correspondingly, vasculature associated with those pharyngeal arches were also reduced (De Soysa et al., 2012). This data demonstrates that water-soluble components of crude oil cause specific teratogenic effects on developing zebrafish embryos.

Objective

The objective of this study is to test the hypothesis that the exposure to crude oil and chemical dispersant leads to specific defects in cardiac development marked by a change in chamber morphology and positioning, coupled with a reduction of cardiac function, leading to cardiac stasis and embryonic death. The test of the hypothesis is conducted by quantifying gross, as well as tissue and cellular level changes in development, resulting from crude oil exposure of zebrafish at specific times throughout early stages (30, 36, 48, 72, & 96 hpf) of zebrafish embryogenesis using stereomicroscopy, histology, and video microscopy. This study provides a comparison of cellular and tissue-specific changes between oil and dispersant treated embryos vs. untreated controls at various stages of development beginning at 30 hpf and ending at 96 hours post fertilization. In testing the hypothesis, this project will focus on addressing how early heart development is affected, and which aspects of cardiac development are most perturbed. It is intended to delineate whether the effects of crude oil exposure begin early in cardiac development, or instead, during a specific stage of development. It will be of interest to note whether particular structures of the developing heart that are more affected than others.

Materials and Methods

Zebrafish Husbandry and Embryo Collection

Danio rerio strain Tuebingen were obtained from the Zebrafish International Resource Center (Eugene, Oregon) and reared as described in Westerfield (1989). Fish were maintained on a 14 hour day, 10 hour night cycle at 28.5°C and fed a formulated diet of Fry Feed Kyowa B (Kyowa Hakko Co., Ltd) two to five times daily *ad libitum* in 10 gallon tanks with recirculating filtered water. Fertilized eggs were collected and washed with system water within one hour of spawning, conventionally staged (Kimmel et al., 1995), and any unviable or defective embryos (typically <5%) were discarded.

Macondo Crude Oil and Nalco Dispersant

Crude oil MC 252, Macondo unweathered crude oil from the Deepwater Horizon spill and a sample of Nalco EC 9500 chemical dispersant was a generous gift of British Petrolium (BP)

Crude Oil and Chemical Dispersant Treatment

Crude oil and chemical dispersant treatment of zebrafish embryos and larvae were carried out in plastic petri dishes (150 mm, Fisher) with up to 300 embryos/dish. Preliminary

experiments conducted to establish conditions for high frequency crude oil and dispersant-dependent tetratogenesis induction were conducted using serial dilutions of crude oil suspended in adult zebrafish tank water, crude oil and dispersant emulsions (1 part chemical dispersant to 9 parts crude oil mixed with an equal volume of tank water and shaken vigorously for 1 minute to generate emulsions with an average micelle size of 100 microns) or chemical dispersant. Results from preliminary experiments revealed that crude oil exposure over a range of 1 part per thousand (ppt) to 1 part per million (ppm) of crude oil resulted in either the absence of any detectable effects or sporadic developmental defects at the highest concentrations. Chemical dispersant treatment below 1 ppt lacked any discernable effects, whereas treatment with higher concentrations of dispersant resulted in immediate destruction of embryos and larvae as evidenced by lysis of embryo and larval cells and tissues. By comparison, treatment with crude oil and dispersant emulsions in the range of 150 to 250 ppm, resulted in high-level reproducible teratogenesis consistent with results reported in this thesis. Given the results from preliminary experiments, the results reported in this thesis were obtained from embryos and larvae exposed to 150-250 ppm for a crude oil and dispersant emulsion prepared as described above. Further preliminary experiments conducted to examine the effects of temporal exposure of embryos and larvae to different crude oil, crude oil and chemical dispersant emulsions or chemical dispersant alone revealed that embryos treated with 150 -250 ppm at 8-10 hour post-fertilization (70-80% epiboly) generated high level reproducible tetratogenesis. Embryos were exposed to crude oil and dispersant starting at 70% epiboly, and maintained in the treatment solution throughout the duration of the experimental treatment. Control embryos were incubated in a volume of 50 ml of tank water. Both

experimental and control embryos and larvae were removed from the Petri dishes after treatment at 30, 36, 48, 72, and 96-hour post fertilization, and fixed for histological examination. Prior to fixation or live embryo imaging, embryo chorions were manually removed using forceps and dissecting scope (LEICA SE4) at 2x magnification. These embryo and larval sampling times were selected because they encompassed the stage of embryogenesis and larval development over which the major organ systems were established and because preliminary experiments revealed evidence that showed a marked effect of crude oil and chemical dispersant relative to untreated control embryos and larvae.

Live Whole Mount Imaging and Videomicroscopy

Live embryos were dechorionated manually using fine-tipped forceps when applicable. Control and O+D treated embryos were embedded in SeaPlaque® (Cambrex Bio Science Rockland, Inc) low melting point agarose (≤65° C), in the desired lateral orientation, and mounted on a 75x25x1 mm glass slide for qualitative and quantitative analysis of physiological effects of exposure to a crude oil and dispersant emulsion. Whole mount imaging and videography was conducted using an Olympus BX41 microscope with an Olympus DP72 camera attachment, and videos were taken using CellSens Standard software (Olympus Corporation, Version 1.11). Images and videos were further processed using iphoto (Apple Inc. Version 9.5.1). Changes in cardiac morphology resulting from crude oil and dispersant emulsion exposure compared to controls and measurements were expressed in micrometers by using Image J software (U.S. National Institute of Health,

Bethesda, MD). The image analysis software was used to measure the area, and perimeter associated with the embryonic eye and otic vesicle. Heart rates were determined from 15-second video segments collected from individual unanesthetized embryos in real time. Mounted specimens were incubated on a temperature controlled warming stage set to 27°C for at least 10 minutes prior to heart rate assessment. Atrial and ventricular beats were counted over 15 s intervals. Specimen ($n \geq 5$) per treatment and time point was used in collecting measurements, and the variation in mean heartbeat rates were compared using a one-way ANOVA. In all cases, embryos were selected for analysis at random.

Histological preparation and analysis of sectioned control and O+D-treated zebrafish embryos and larvae

Fixation, Processing, and Embedding

Control and treated embryos and larvae were removed from Petri plates at 30, 36, 48, 72, and 96 hours post fertilization (hpf), and fixed for histological examination. Zebrafish embryos and larvae treated with crude oil and dispersant as well as untreated controls were fixed in separate 2.0 mL micro-centrifuge tubes (20-30 per time point) in 1.5 mL of Dent's fixative (80% Ethanol + 20% DMSO) for 24 hours, washed immediately with two 30-second washes of 70% ethanol, 1.5 mL each. Following initial washes, embryos were washed five times, at 30-minute intervals for 2.5 hours using 70% ethanol.

Fixed embryos and larvae were dehydrated by subjecting them in bulk to a sequential series of 70%, 80%, 90%, 95%, and 3x100% ethanol washes at 30-minute intervals at room temperature, 1.5 mL each. The zebrafish embryos were stored in 100% ethanol until further processed .

After ethanol storage, the fixed and dehydrated embryos and larvae were processed through a series of 3 xylene, 1:1 xylene:paraffin, 100% paraffin treatments of 1.5 mL each for 30 minutes each in 2.0 mL micro-centrifuge tubes.

Embryos were transferred to a small glass dish containing molten McCormick™ Scientific Paraplast X-TRA (melting point 52° C) tissue embedding medium (5 mL) at 64 °C. The processed embryos and larvae were placed one at a time into a stainless steel histo-base mold (Fisherbrand®) (15 x 15 x 5 mm), incubated on an pre-warmed hotplate set at 72.5 °C. Embryo-housing molds were transferred one at a time under a LEICA S4E light microscope, and embryos were positioned in the desired lateral orientation using insect pins at 2x magnification. After positioning, molds were fitted with plastic tissue embedding cassettes (Fisherbrand® Tissue Path II) and covered with molten paraffin. In all cases, the embryos and larvae were selected randomly for histological preparation.

Sectioning and Staining

Stainless steel molds were placed in an ice water bath for approximately 1 minute to separate the cassette from the mold. Once separated, paraffin blocks were trimmed on each

side of the embryo at approximately 45° angles to the horizontal plane using a standard razor blade. Trimmed blocks were transferred to a Reichert-Jung 2030 rotary microtome for sectioning at 10µm per section using a high-profile disposable blade (VWR®). Serial sections of each embryo were cut, and transferred to a warm water bath set to 37° C and thermally adhered to a glass slide. Serial sections were mounted on 75x25x1 mm glass slides (VWR VistaVision™ Histobond®), placed in staining racks, and allowed to dry for 24 hours. Tissue sections were stained with Accustain® Harris Hematoxylin Solution (Sigma-Aldrich) and Eosin Ploxine (VWR®) as detailed in AFPI Laboratory Methods in Histotechnology, 1992. pp. 56-57, and allowed to dry for 30 minutes, and covered with 1.0 mm coverslips (VWR) using Cytoseal™ 60 mounting media (Richard-Allan Scientific).

Microscopy and Photomicrographs

Histological sections were examined for comparison at 10x and 20x magnifications using an Olympus BX41 microscope. Photographs were taken using an Olympus DP72 camera attachment set to automatic exposure, and images were captured using CellSens Standard software (Olympus Corporation, version 1.11). Images were further processed using iPhoto version 9.5.1 (Apple Inc.). Morphometric data were collected and measured by outlining the myocardium of the cardiac chambers using Image J software (U.S. National Institute of Health, Bethesda, MD). The image analysis software was used to measure the area, perimeter, and length of straight-line distances associated with the atrium, atrio-ventricular junction, ventricle, and bulbus arteriosus. Sections chosen for comparison were based on the ability to view a full section of the atrium, ventricle, and bulbus arteriosus

(when applicable) in one section. Sections used for measurements corresponding with a single chamber were selected from images that represented sections at 10μm increments bracketing the section described in the preceding sentence. The zebrafish eye, notochord, cardiac cushions, ventricle, and bulbus arteriosus were used as points of reference in normalizing sections between treatments. This approach standardized the orientation and sectioning plane in the heart chambers as much as possible for normalization of images and measurements in comparisons between experimental and control specimens. Zebrafish embryos ($n \geq 5$ per treatment and time point) were used in collecting measurements, and the mean area, perimeter, length and width of chamber measurements were used in statistical analysis.

Statistical Analysis

Selected measurements of the area, perimeter, length and width taken from five independent sets of embryos at each time point, representative of an estimate of overall morphological dimension of heart structure, were analyzed by one-way ANOVA, supplemented with Fisher LSD and Bonferroni comparisons, to test the null hypothesis that there is not a difference between the chamber morphology and orientation of the untreated control embryos and the experimental embryos. Data is presented as mean ±standard error (SE) of the mean, and asterisks (*) are indicative of a significant difference between experimental and representative controls. The level of significance was $p \leq 0.05$ for all comparisons. All analyses were performed using the IBM SPSS Statistics, version 20

software package for Macintosh, and presented in tables using Microsoft Excel for Mac 2011, version 14.4.2.

Results

Preliminary comparisons of crude oil and dispersant treated embryos to untreated control embryos using stereomicroscopic observation of gross morphology revealed striking changes in the development of the heart and surrounding tissues as early as 72 hours post-fertilization (hpf). These crude oil and dispersant-induced changes in heart morphology and other correlated developmental changes, culminated in early larval death in greater than 98% of crude oil and dispersant treated embryos. They also resulted in progressive deterioration of the heart over the period from 96 to 144 hpf.

Effects of Crude Oil Exposure on Heart Development at 30 hours post-fertilization

At 30 hpf, the heart tube of control embryos consists of two primary chambers, the atrium and ventricle. Cardiac looping to the embryos right hand side has begun, and is evidenced by the overlap of the atrial and ventricular chambers when viewed from the lateral perspective (Figure 27). The looping from the A-P directionality of the heart tube to L-R position is a process conserved within vertebrates (Didier et al., 1993) Measurement of area, perimeter, length and width of selected sections representative of the atrium and ventricle were compared between experimental and untreated control embryos Sections

for comparison between control and treated embryos were selected based on procedures detailed in the Materials and Methods section. Untreated control and experimentally-treated embryos at 30 hpf showed similar cellular patterning, but statistically significant differences in the physical dimensions of atrial and ventricular chambers.

Quantitative analysis and comparison of the developing zebrafish embryos at 30 hpf exposed to a crude oil and dispersant emulsion shortly after fertilization showed a significant reduction in atrial perimeter, significant increase in atrial width, and no significant changes in atrial length and area relative to untreated control embryos (Figure 27). Histological sections of the developing heart from untreated control embryos showed an average atrial area of 3,873 ±75 μm^2, atrial perimeter of 325 ±18 μm, an atrial length of 135 ±5 μm, and atrial width of 37 ±1 μm. Comparatively, O+D embryos at 30 hpf showed an average atrial area of approximately 4180 ±143 μm^2, an atrial perimeter of 281 ±13 μm, an atrial length of 120 ±7 μm, and an atrial width of 50 ±1 μm (Table 4 & 4.1). A significant reduction in atrial perimeter and 37.63% increase in width can be observed in the embryos exposed to oil and dispersant (Table 4 & 4.1). Despite the altered atrial perimeter and width, the myocardium of both untreated control and O+D embryos is one cell layer thick, and the general organization and shape of cardiomyocytes remain unaffected (Figure 14). When histological images are reviewed in series, no identifiable differences in chamber structure, orientation, or cellularization can be discerned.

Quantitative comparison and analysis of the ventricle at 30 hpf showed a statistically significant difference in area, length and width, but not perimeter when comparing the untreated control to the O+D treated embryos (Figure 27). Control embryos showed an average ventricular area of 3,212 ±77 μm^2, ventricular perimeter of 317 ±11 μm, a ventricular length of 144 ±4 μm, and ventricular width of 29 ±2 μm. Comparatively, O+D embryos at 30 hpf showed a average ventricular area of approximately 3831 ±77 μm^2, perimeter of 315 ±17 μm, length of 128 ±3 μm, and width of 45 ±2 μm (Table 5 & 5.1).

A statistically significant increase of approximately 618 μm^2 (19.25%) in ventricular area, accompanied by a 16 μm (11.34%) decrease in ventricular length, and 16 μm increase in ventricular width is observed when comparing morphometric values of treated embryos to the controls (Table 5 & 5.1). Qualitative analysis of histology does not show any cellular or tissue specific changes in the arrangement or distribution of cells, and the general tube-like nature of the heart characteristic of untreated control embryos are evident across treatments (Figure 19 & 19.1).

To determine whether experimental treatment with crude oil and dispersant were affecting heart development specifically or whether there were correlated changes throughout the developing embryo, comparative analysis of changes in the developing eye and otic vesicle were also conducted. These two developmental structures were chosen for comparison because they were relatively simple structures morphologically and

because they arise from tissue of the ectoderm, which differs from those of the heart that arise from the tissue of the mesoderm.

When comparing the area and perimeter of the embryonic zebrafish eye at 30 hpf, the data shows no statistically significant differences between untreated and O+D treated embryos (Figure 32). Control embryos had an area of 29,693 ±997 μm^2 and perimeter of 616 ±10 μm, while O+D embryos had an average of area and perimeter of 28,797 ±655 μm^2 and 606 ±7 μm respectively (Table 1 & 1.1). Comparison of area and perimeter of the otic vesicle in 30 hpf zebrafish shows there is also no statistically significant differences between treatments (Figure 32). Control embryos had an average area of 5034 ±91 μm^2 and perimeter of 256 ±2 μm, while O+D treated embryos showed an area and perimeter of 4845 ±77 μm^2 and 250 ±2 μm respectively (Table 2 & 2.1). Analysis of cardiac function at 30 hpf shows no statistically significant differences between the heart rate of untreated controls and O+D treated embryos (Table 3 & 3.1). Control embryonic hearts contract at a rate of 60 ±1 bpm (beats per minute) while O+D treated embryos had a slightly reduced cardiac function at 57 ±1 beats per minute (Supplemental videos 1 & 1.1)

Effects of Crude Oil Exposure on Heart Development at 36 hours post-fertilization

Stereoscopic gross analysis of low melting temperature embedded live 36 hpf whole mount zebrafish at 10x magnification shows definitive chamber boundaries between the sinus

venosus, atrium, ventricle, and bulbus arteriosus that can be identified by constrictions of the lumen between adjacent compartments (Figure 28).

The venous return from the systemic circuit returns to the heart through the common cardinal vein, which fans out across both sides of the yolk sac, and comes together cranio-ventrally at the inflow tract or sinus venosus. The bulbus arteriosus or outflow tract leads to systemic circulation via the ventral aorta in a dorso-rostral direction. The boundary of these additional chambers can be distinguished at the extremities of the heart tube by constrictions in the lumen through histological preparation and whole mount imaging (Figure 28).

Comparisons of cellular and tissue structure and organization in histological sections prepared from crude oil and dispersant-treated embryos at 36 hpf, revealed the embryonic heart tube is comprised of two primary cell layers, the inner endocardium, and the surrounding muscular myocardial layer (Figure 15.1, 20.1, & 28). Both the endocardial and myocardial cell layers appear similar in treated and untreated embryos. The endocardium and myocardium are similar in their cellular makeup between treatments being one cell thick and separated by a layer of cardiac jelly (Figure 15.1, 20.1)

Quantitative comparison and analysis of the atrium at 36 hpf showed a statistically significant difference in area and width, but not perimeter and length when comparing the untreated control to the O+D treated embryos. Control embryos showed an average atrial area of 2063 ±115 μm^2, atrial perimeter of approximately 231 ±9 μm, an atrial length of

105 ±2 μm, and atrial width of 29 ±1 μm (Table 4 & 4.1). Comparatively, O+D embryos at 36 hpf showed an average atrial area of approximately 2896 ±90 μm^2, perimeter of 264 ±17 μm, length of 115 ±7 μm, and a width of 36 μm. That data shows a dramatic and statistically significant increase of approximately 833 μm (40%) in atrial area of treated embryos compared to controls. A statistically significant 7.82 μm (27.41%) increase in atrial width in treated embryos is also observed. Atrial perimeter, and length of O+D treated embryos increased slightly (33 μm and 10 μm respectively), but were not statistically compared to controls. (Table 4 & 4.1)

An increase in atrial width and area in O+D exposed embryos supports the notion that crude oil-induced morphologic differences in cardiac development arise early in embryonic development. Analysis of photomicrographic images taken from histological preparations show that the myocardium of both untreated and O+D embryos remain one cell layer thick. The organization and shape of individual cardiomyocytes remain unaffected by crude oil treatment as well (Figure 15 & 15.1).

Morphometric analysis of a section representative of the ventricular chamber revealed no significant difference in area, perimeter, length, or width between experimental and control embryos (Figure 20). The ventricles of both treated and untreated embryos are observed to be one cell layer thick, and qualitative comparative analysis of histology in serial sections shows no observable differences in cellular structure or arrangement of ventricles in comparisons between control and treated embryos (Figure 20.1).

Quantitative analysis of area and perimeter of the embryonic eye and otic vesicle was measured at 36 hpf. Comparison between the area and perimeter of the embryonic eye of untreated controls and O+D treated embryos shows a statistically significant reduction in both the area and perimeter in O+D treated embryos (Figure 33). The average area and perimeter of the eye in untreated embryos is 35,664 ±1131 $\mu m^2$and 678 ±644 μm respectively. In contrast, O+D embryos had an average of area of 30,130 ±649 μm^2, and perimeter of 615 ±7x μm (Figure 1 & 1.1). Comparison of area and perimeter of the otic vesicle in O+D treated embryos to that of untreated controls at 36 hpf shows no statistically significant differences in mean values. Control embryos showed an average area of 6779 μm^2 ±135 and perimeter of 297 ±4 μm, while O+D treated embryos showed an otic vesicle area and perimeter of 5747 ±146 μm^2 and 273 ±3 μm respectively (Table 2 & 2.2)**.**

At 36 hpf, measurement of heart beat rates revealed nearly identical values, with untreated and O+D embryos having a mean heart rate of 78 ±1 bpm and 76 ±1 bpm respectively. This data indicates that crude oil exposure did not affect the physiological activity of the developing heart at this stage of development. (Table 3 & 3.1)(Supplemental videos 2 & 2.2).

Effects of Crude Oil Exposure on Heart Development at 48 hours post-fertilization

At 48 hours post fertilization, the zebrafish heart consists of a smooth walled tube partitioned into all four distinct segments, which are the sinus venosus, atrium, ventricle, and bulbus arteriosus in series. At this stage of development, the zebrafish heart is

essentially identical to the heart of mammals, amphibians, and birds at the same embryonic stage (Vogel). Looping is complete and structures of the sinus venosus, atrium, ventricle, and bulbus arteriosus can be easily identified by whole-mount microscopy as evidenced by constriction between consecutive segments (Figure 29).

Histological analysis of larvae shows that the myocardium remains one cell layer thick throughout the segments with the exception of the ventricle, which was observed to be two or three cells thick in certain regions (Figure 16.1 & 24.1). The heart is lined with the endocardium and is separated from the myocardium by a layer of cardiac jelly, which is absent in the sinus venosus and ventricular chambers. There are no valves present at this stage, however at the end of the second day, endocardial cells at the boundaries of chambers undergo epithelial-mesenchymal transition (EMT) to form intermediate structures known as cardiac cushions. Cardiac cushions are easily identified at the boundary of the atrium and ventricle in both the untreated and treated embryos via histological analysis of tissue. Upon sectioning of the zebrafish heart, the atrioventricular cushions can be observed in the lumen of the atrial canal as two thickenings, one on its dorsal and another on its ventral wall. These thickenings, or cardiac cushions will go on to fuse and remodel to eventually form the valves and septa of the mature adult heart. The junction of these chambers as defined by the presence of cardiac cushions will be referred to as the atrio-ventricular canal (AVC) (Figure 24).

The development of the cardiac cushions by 48 hpf provided a landmark to delineate the location of the AVC in this study. The atrio-ventricular canal was used to as a point of

reference in the normalization process to promote comparison of comparable sections between treatments. The presence of the cardiac cushions allows for additional measurements of area and perimeter of the AVC, as well as the area, perimeter, length, and width of the ventricle and bulbus arteriosus as visible together in the same sagittal section (Figure 24 & 24.1).

Quantitative comparison and analysis of the atrium at 48 hpf showed a statistically significant difference in width, but not area, perimeter, or length when comparing the untreated control to the O+D treated larvae. Control larvae showed an average atrial area of 4328 ±97 um2, atrial perimeter of approximately 290 ±5 μm, an atrial length of 124 μm ±2, and atrial width of 46 ±1 μm. Experimentally treated larvae at 48 hpf showed an average atrial area of approximately 4235 ±184 μm, perimeter of 306 ±15 μm, length of 137 ±5 μm, and a width of 37 ±1 μm (Table 4 & 4.1).

Although the differences in atrial area, perimeter, and length are not statistically significant, they represent a strong trend that reflects a change in chamber dimensions. The significant (20.11%) reduction in atrial width reflects a continuing trend toward narrowing of the lumen of the heart chambers (Table 4 & 4.1).

Qualitative examination of histological images confirms a narrower overall atrial structure in treated larvae as compared to that of the untreated control larvae. There appears to be no visible distinction between the endocardial and myocardial cells of the experimentally

treated and untreated control larve. No identifiable differences can be discerned in cardiomyoctye structure and organization between treatments (Figure 16 & 16.1).

Morphometric analysis of area and perimeter of AVC showed no significant differences in measurements between untreated controls and experimentally treated larvae. The area of the AVC in untreated larvae averaged 567 ±11 μm^2, and the perimeter 85 ±1 μm. In contrast, the area and perimeter of O+D treated larvae is 550 ±14 μm^2 and 85 ±1 μm respectively. Both area and perimeter were almost identical (Table 6 & 6.1). Qualitative histological analysis of sections in series shows a reduction in looping of the atrium and ventricular chambers in O+D treated larvae compared to untreated controls. When comparing histology of O+D treated larvae with that of untreated controls, endocardial cells contributing to cardiac cushion formation in O+D treated larvae are indistinguishable from endocardial cells lining the lumen of the chambers in most larvae. In contrast, endocardial cells contributing to cardiac cushion formation in control larvae can be seen as thickenings and aggregation of cells at the atrio- ventricular junction (AVJ) (Figure 24).

Comparison of O+D and untreated larval ventricular dimensions revealed a statistically significant difference in average ventricular area and perimeter. A ventricular area of 1970 ±66 μm^2, and ventricular perimeter of 16 ±5 μm in untreated controls is observed. O+D larvae had a ventricular area of 3144 ±103 μm^2 and perimeter of approximately 268 ±14 μm. The ventricular area of O+D treated larvae was approximately 1200 μm (59.21%) greater than that of untreated controls, and dramatic 59.62% increase in ventricular area is observed in the treated larvae. Similarly, a 59.16% increase can be seen when comparing

the 168 μm perimeter of untreated control fish to the 268 μm perimeter of O+D larvae (Table 7 & 7.1). This suggests an increase in ventricular size coupled with a change in chamber morphology. No identifiable differences can be discerned in cardiomyoctye structure and organization by visual examination of histology (Figure 24 & 24.1).

Morphometric analysis of the area of the bulbus arteriosus, or outflow tract, showed a statistically significant increase in chamber area and perimeter when comparing O+D treated larvae with untreated controls (Figure 24 &24.1). Control larvae show an average chamber area of 176 ±2 μm^2 and an average perimeter of 48 μm. In contrast, the bulbus arteriosus in treated embryos had an average chamber area of 271 ±15 μm^2, and perimeter of 63 ±2 μm. An increase of 95.38 μm^2 (53.50%) in the area of the bulbus arteriosus in treated larvae can be observed when compared to controls. An increase of 14.92 μm (31.21%) in the perimeter of the bulbus arteriosus can be observed when comparing measurements of treated to untreated larvae. Statistically significant changes in both area and perimeter are indicative of oil and dispersant induced alterations in the size of the outflow tract (Table 8 & 8.1).

Quantitative histological analysis of an additional ventricular section further into the series in control and treated larvae at 48 hpf showed a statistically significant difference in chamber area, perimeter, length and width. An increase of approximately 500 μm^2 in ventricular area (15.83%), 60 μm increase (26.17%) in perimeter, and 42 μm (44.01%) increase in length can be noted in the treated larvae when compared to the controls. In contrast, a significant decrease in ventricular width of treated larvae by approximately 10

μm (20.02%) can be noted when comparing treatments (5 & 5.1). Qualitative analysis of histology at the 48-hour time point confirms the narrowing and elongation of the ventricle in treated larvae (Figure 21).

Quantitative analysis of area and perimeter of the embryonic eye and otic vesicle was measured at 48 hpf (Figure 34). Comparison between the area and perimeter of the embryonic eye of untreated controls and O+D treated larvae shows a statistically significant reduction in both the area and perimeter in O+D treated larvae. The average area and perimeter of the eye in untreated larvae is 43,335 ±1437 μm^2 and 740 ±13 μm respectively. In contrast, O+D larvae had an average of area of 39,247 ±526 μm^2, and perimeter of 708 ±5 μm (Table 1 & 1.1). Comparison of area and perimeter of the otic vesicle in zebrafish larvae 48 hpf shows a statistically significant reduction of both parameters in O+D larvae compared to untreated control larvae. Control larvae showed an average area of 13, 665 ±835 μm^2 and perimeter of 422 ±17 μm in untreated controls. O+D treated larvae showed an area and perimeter of 10,676 ±371 μm^2 and 374 ±8 μm respectively (Table 2 & 2.2). Analysis of heart beat rate embedded in low melting temperature agarose at this stage of development shows an average heart rate of 82 ±1 bpm in untreated larvae and a statistically significant decreased 65 ±2 bpm in experimental larvae. A 21.17% reduction in treated larvae when compared to controls and indicative of a change in physiological function of the developing heart in oil-treated larvae (Table 3 and 3.1) (Supplemental Video 3 & 3.3).

Effects of Crude Oil Exposure on Heart Development at 72 hours post-fertilization

Quantitative histological examination and comparison of images that are representative of different chambers of the heart beginning with the atrium, and ending with the bulbus arteriosus was conducted.

Quantitative comparison and analysis of the atrium at 72 hpf in treated larvae compared to controls showed a statistically significant decrease in atrial area, perimeter and width, but not length (Figure 17). Control larvae showed an average atrial area of 5,765 ±326 μm^2, atrial perimeter of approximately 309 ±8 μm, an atrial length of 115 ±5 μm, and atrial width of 81 ±2 μm. Comparatively, O+D larvae at 72 hpf showed an average atrial area of approximately 3355 ±118 μm^2, perimeter of approximately 271 ±13 μm, length of 113 ±7 μm, and an atrial width of 42 ±5 μm. A decrease in atrial area of 2409 μm^2 (41.79%) can be observed in treated larvae. A 38 μm reduction in perimeter, accompanied by an atrial width reduced by roughly one half of that in controls larvae (39 μm) correlates with the dramatic narrowing in atrial shape and size previously described for fish following crude oil-and dispersant exposure. The length of the atrium between larvae is roughly equivalent (Table 4 & 4.1).

Qualitative analysis of the structure and organization of cardiomyocytes comprising the atrial wall indicates that the cells of treated larvae appear less abundant, and less compact than those of untreated controls. This contributes to the extended tube-like appearance of atria in treated larvae. The shape and cellular organization of the atrial chamber was

dramatically affected in O+D larvae, and is evident at the gross and cellular level. Histological comparison between untreated controls and O+D treated larvae show a thinning of the myocardium characterized by a reduction in musculature observed, as well as a scattered distribution in conjunction with a lack of organization of endocardial cells along the lumen of the chamber in oil and dispersant treated larvae (Figure 17&17.1)

Quantitative analysis of the AVC showed a significant increase in the perimeter but not area in treated larvae, but not area. O+D larvae showed a mean area of 840 ±15 μm^2, a 32.85% decrease when compared to the 1252 ±8 μm^2 area in untreated control larvae. A reduction of 24 μm (18.21%) was observed when comparing the 104 ±1 μm perimeter of O+D larvae to the 128 ±1 μm perimeter of control larvae (Table 6 & 6.1). This data suggest an overall difference in shape but not size of the AVC of larvae exposed to O+D, characterized by the narrowing and elongation of cardiac chambers and their junction. Qualitative analysis of serial sections confirms the narrow and elongated cardiac chamber morphology in crude oil-exposed fish. Histological comparisons of the AVC and its associated cardiac cushions between control and experimental larvae revealed extensive thinning, reduction in density, and alteration in arrangement of endocardial cells contributing to cardiac cushion modeling and formation in O+D treated larvae. (Figure 25 & 25.1). The cardiac cushions in control larvae were organized around the lumen of the AVC, consisting of 2-3 cell layers in most regions, and arranged into two leaflets anchored to the myocardial wall. These modified cardiac cushions are distinct from endocardial cells of the chambers as evident by their organization and positioning between the atrial and ventricular chambers at the atrio-ventricular junction (AVJ). In contrast, cardiac cushions in O+D treated larvae are 1

cell layer thick and show no leaflet type organization (Figure 25 & 25.1). Despite their defective organization, distribution, and appearance; endocardial cells comprising the cardiac cushions in O+D treated larvae can be distinguished from the endocardial cells lining the chamber lumen by their positioning and aggregation at the atrio-ventricular canal and junction (Figure 25 & 25.1).

Comparative measurements of the heart ventricular tissue compartment from the same sectional plane used to collect data for comparisons of the AVC, showed a significant reduction in the ventricular area but no significant change in ventricular perimeter (Figure 25). Untreated larvae had an average ventricular area of 2611 ±120 μm^2, and perimeter of approximately 208 ±5μm. In contrast, O+D treated larvae displayed a ventricular area of 2224 ±105μm^2 with a perimeter of approximately 204 ±10μm. The area of the treated larvae was reduced by approximately 400 μm (14.83%) when compared to that of the control larvae. There was only a 2.07% decrease in perimeter between O+D and untreated larvae. A reduction in area but not perimeter in the ventricle is indicative of overall narrowing and elongation of the ventricular chamber that can be readily observed in photomicrographs of these sections (Table 7 & 7.1). Qualitative assessment of histology at 72 hpf shows the ventricular myocardium of both untreated and experimental larvae consisted of cardiomyocytes densely organized surrounding the endocardium. The myocardium of untreated control larvae is organized into two cell layers, while the myocardium of O+D larvae is only one cell layer in thickness (Figure 25 & 25.1). As a result of a reduction of one cell layer from the myocardium in experimental larvae compared to untreated controls, a reduction of trabeculation associated with the ventricular

myocardium is also observed. Qualitative analysis of histology shows thinning of the endocardium evident by the reduction of cells in combination with the lack of compact arrangement of cells lining the lumen of the ventricular chamber (Figure 25 & 25.1).

Comparisons between histological sections from experimental and control larvae revealed statistically significant differences in both the area and perimeter of the bulbous arteriosus. Untreated larvae displayed an average chamber area of approximately 981 ±30 μm^2, and perimeter of 112 ±2 μm. Treated larvae showed an average chamber area of 675 ±9 μm^2, with an average perimeter of 99 ±2 μm. Treated larvae showed approximately a 300 μm (31.12%) decrease in area when compared to untreated control larvae. A difference of 13 μm (11.67%) in perimeter is observed when comparing O+D larvae to controls (Table 8 & 8.1). The bulbus arteriosus can be seen to be reduced in size, with a concomitant change in shape from a characteristic 'onion-like' morphology to a more elongated structure, with less definitive boundaries between the preceding ventricular chamber (Figure 25). The outflow tract, or bulbus arteriosus in untreated larvae is 2-3 cells thick in most regions, compared to the 1-2 cell thickness in experimentally treated embryos (Figure 25.1). Corresponding with the aberration of the outflow tract, a malformation in organization and distribution of endocardial cells that form the cardiac cushions can be observed at the boundary of the ventricle and bulbus arteriosus in O+D treated larvae. The ventriculo-bulbar cushions (VBc) in untreated larvae are 2-cell layers thick, are arranged compactly into two leaflets present at the ventriculo-bulbar junction (VBJ), and are organized uniformly along chamber lumen. In contrast, the VBc in O+D treated larvae are 1-cell thick arranged at the VBJ. These cardiac cushions lack the leaflet-like organization of endocardial

cells that was seen in VBc of untreated controls, and are sparsely distributed around the lumen. In many cases, cardiac cushions in treated larvae were unable to be identified histologically.

Morphometric comparison of histological images representative of the ventricular chamber in embryos at 72 hpf showed significant reductions in all four categories of measurement in larvae exposed to oil and dispersant. Control larvae displayed a ventricular area of 6579 ±83 μm^2, perimeter of 304 ±2 μm, ventricular length of 108 ±2 μm, and chamber width of 81 ±1 μm. Morphometric analysis of a comparable section in O+D treated larvae showed a chamber area of 3485 ±200 μm^2, perimeter of approximately 244 ±8 μm, length of 87 ±2 μm and width of 53 ±2 μm. Treated larvae displayed a reduction of ventricular area of 3100 μm^2 (47.04%) when compared to controls. This dramatic reduction in area was accompanied by a significant decrease of approximately 70 μm (23.01%) in perimeter, 21 μm (19.86%) decrease in length, and 28 μm (34.05%) in width (Table 5 & 5.1). This data is consistent with the reduction of overall size of the heart in treated larvae, and the thinning and narrowing of cardiac chambers in experimental larvae. Comparatively, untreated larvae exhibit an overall rounder and thicker structure marked by more clearly defined boundaries between chambers (Figure 22 & 22.1).

By 3 days (72h hpf), stereoscopic observation of gross morphology of larvae in control and O+D treated specimens revealed unequivocal morphological differences characterized by pronounced pericardial and yolk sac edema; hemorrhaging in the forebrain, midbrain and hindbrain; reduction in the number of the caudally developing pharyngeal arches, as well

as changes in the shape and structure of the heart from a simple elongated tube-like organ to a more compact, complex, and specialized organ following completion of cardiac looping (Figure 35). In contrast to the untreated controls that display normal cardiac looping and associated S-shaped heart, hearts from oil and dispersant treated larvae showed defective looping, appearing elongated and tube-like. Whereas the normal looping process in untreated larvae result in positioning of the atrium and ventricle in a side by side orientation such that these chambers overlap when viewed from a lateral perspective, the phenotype expressed by larvae exposed to oil and dispersant shows altered positioning of the chambers, resulting in ventricles that are rostral to the atrium (Figure 30).

Quantitative analysis of area and perimeter of the embryonic eye and otic vesicle was measured at 72 hpf (Figure 35). Comparison between the area and perimeter of the embryonic eye of untreated controls and O+D treated larvae shows a statistically significant reduction in both the area and perimeter of O+D treated larvae. The average area and perimeter of the eye in untreated larvae is 56,085 ±1370 $\mu m^2$and 843 ±10 μm respectively. In contrast, O+D larvae had an average of area of 42,739 ±862 μm^2, and perimeter of 736 ±8 μm (Table 1 & 1.1). Comparison of area and perimeter of the otic vesicle in zebrafish embryos shows a statistically significant reduction of both parameters when comparing O+D embryos to untreated control larvae. Control larvae showed an average area of 22, 799 ±694 μm^2 and perimeter of 537 μm in untreated controls. O+D treated larvae showed an area and perimeter of 16,069 ±667 μm^2 and 452 ±10 μm respectively (Table 2.2)**.** The heart beat rate of untreated larvae averaged 88 ±2 bpm as compared to 65 ±2 bpm in the oil-treated larvae, which is indicative of a significant change

in the physiological function of the developing heart in control and experimental larvae (Table 3 & 3.1)(Supplemental video 4 & 4.1).

Effects of Crude Oil Exposure on Heart Development at 96 hours post-fertilization

Due to the dramatic oil and dispersant induced effects by this stage of embryonic development, quantitative morphological comparisons between sections of untreated and treated larvae were limited to regions and structures that were able to be identified between comparable sections of treatment groups and their related untreated controls (Figure 31).

Quantitative histological comparison and analysis of a section representative of the atrium at 96 hpf show an statistically significant decrease in atrial area and width, but not perimeter and length. Untreated larvae showed an average atrial area of approximately 5,763 ±94 μm^2, perimeter of 302 ±4 μm, length of 99 ±1 μm and width of 65 ±1 μm. Comparatively, treated larvae had an average chamber area, perimeter, length, and width of 3,488 ±382 μm^2, 265 ±22 μm, 103 ±14 μm and 47 ±4 μm respectively. (Table 4 & 4.1) The collective data shows a dramatic and statistically significant 37.55% decrease in atrial area when comparing atrial area from O+D to untreated control larvae. When comparing the chamber width of treated larvae to their control counterparts, a statistically significant reduction of 27.95% (18.156 μm) is observed (Table 4 & 4.1). The dramatic reduction in atrial area coupled with a significant reduction of atrial width in treated larvae observed by morphometric analysis can be confirmed by visual inspection of histological preparations.

When compared to the clearly defined deltoid shape of the atrial section in control larvae, O+D treated larvae are, characterized by an elongated and narrow tube consisting of loosely organized cardiomyocytes (Figure 18 & 18.1).

Qualitative comparisons between treatments show a similar yet more dramatic phenotype than what was observed at 72 hpf of development. The untreated control larvae exhibited progressive cardiac development. Histological examination of sections in series displays a well-developed inflow tract, or sinus venosus, extending from the common cardinal vein. The sinus venosus of untreated control larvae is clearly defined and displays a clear division from the atrial chamber. The atrial myocardium remains one cell layer thick, displaying a well-defined chamber with compact cardiomyoctye organization and uniform distribution of cells around the chamber periphery (Figure 18 & 18.1). Although a definitive boundary between the sinsus venosus and atrium can be observed in oil and dispersant exposed larvae, chamber formation and positioning is defective when compared to untreated controls. Histological comparison of treated larvae to untreated controls show a dramatic alteration in the position of the atrium and its emergence from the sinus venosus and the common cardinal vein. In oil and dispersant treated larvae, the atrium is positioned much lower, towards the ventral aspect of the larvae, anterior to the yolk sac, and traveling in a dorso-rostral direction. Likewise, the common cardinal vein appears to dramatically elongated and circumflexed along the anterior portion of the yolk sac, which likely reflects the shift in atrial positioning. Although one cell thick as seen in untreated control larvae, the vascular structures of treated larvae are severely compromised, indicative of vascular thinning throughout the cardinal vein, sinus venosus, as well as the

atrium. Endocardial and myocardial cells appear more loosely organized and distributed in O+D treated larvae, suggesting an effect on cell-cell adhesion. In comparison, untreated larvae display a deltoid shaped atrial chamber emerging from the sinus venosus, and histological sections of untreated control larvae show continuity of the sinus venosus from the common cardinal vein anterior to the yolk sac, but positioned dorsally. In contrast to that of treated larvae described above, the vasculature, and cellularization of control larvae is compact, and distributed amongst the chamber margins uniformly. Endocardial and myocardial cells appear to be robust and abundant (Figure 18 & 18.1).

At the AVC in untreated control larvae, the cardiac cushions are very well defined, and can be differentiated from endocardial cells lining the lumen of the chambers by the fact that they are two to three cells thick, have a clear 'leaflet' type configuration, and are physically located at the atrio-ventricular and ventriculo-bulbar boundaries. The progressive development of the cardiac cushions leading to mature valve formation can be observed when compared to its cellular structure and arrangement at earlier time points of control larvae (Figure 26. & 26.1). The presence of cardiac cushions clearly marks the boundary between major chambers. In contrast, cardiac cushions from oil and dispersant treated larvae are one cell layer in thickness and are organized in a circular fashion, lining the lumen of the AVC. In addition to reduced cellularization associated with the cardiac cushions, a dramatic malformation of valve structure can be observed in histological preparations as evident by histological review of sections. Comparisons of serial sections concentrating on the AV valve system from experimentally treated larvae revealed a structure characteristic of that seen at earlier stages of development (48 hpf) in untreated

larvae i.e. the endocardial cells of cardiac cushions assume a circular conformation along the perimeter of the canal lumen, and are not arranged in leaflet orientation characteristic of untreated control larvae. This alteration of cellular structure and arrangement of the cardiac cushions appear to reflect the deterioration of the heart as reflected by incomplete looping of the zebrafish heart, elongation and narrowing of the chambers, regurgitation of blood during cardiac systole, and ultimate cessation of beating. In concert, these aberrations contribute to the tubular structure of the AVC and progressive string-like structure of the elongated cardiac chambers in treated embryos. Due to the dramatic difference in the structure and organization of the AVC in treated larvae, comparable measurements were unable to be taken and results were limited to qualitative analysis (Figure 26).

Measurement of the ventricle in the same section and plane as that of the AVC, showed an average of 6,391 ±156 μm^2, and its perimeter, 367 ±9 μm. In contrast, O+D treated larvae showed a chamber area of 2454 ±51 μm^2, and perimeter of 208 ±8 μm. Comparing measurements of treated larvae to those of untreated controls, a significant 61.61% decrease in chamber area and 43.22% decrease in perimeter of treated larvae is evident(Table 7 & 7.1). As the data, suggests, there is a change in chamber development and morphology, leading to a reduced ventricular size in treated larvae (Figure 26 26.1).

The bulbus arteriosus of untreated control larvae appears as an onion-shaped thick-walled chamber composed of 2-3cell layers, which extend from the ventricle to the ventral aorta. Endocardial cells forming robust cardiac cushions are easily identified by their distinct

leaflet organization at the boundary between the ventricle and bulbus arteriosus. Vasculature associated with the outflow tract and the ventral aorta is well defined and the associated endocardial cells appear uniformly distributed at the inner boundaries of the chamber walls. Qualitative comparison of treated larvae show the walls of the bulbus arteriosus is comprised of 1-2 cell layers and lack the characteristic onion-like shape(Figure 26 & 26.1). The bulbus arteriosus of treated and untreated larvae can be clearly differentiated from the ventricle in histological preparations, as defined by a constriction of the lumen at chamber boundaries. Although a constriction between segments defines the boundary between successive chambers, we were unable to definitively identify the presence of cardiac cushions at the ventriculo-bulbar junction by histological examination of endocardial cells in experimentally treated larvae due the lack of characteristic leaflet appearance and similar appearance to the endocardial cells lining the chamber lumens.

Quantitative analysis of the bulbus arteriosus at 96 hpf, shows the area and perimeter of the chamber is significantly reduced in O+D treated larvae when compared to untreated controls. Control larvae showed an average chamber area and perimeter of 1373 μm^2 and 132 μm respectively. Oil and dispersant treated larvae had an average chamber area of 517 μm^2 larvae with the 1,373 μm^2 area of comparable controls, the significant reduction in area by 62.36% of untreated controls values is indicative of a dramatic change in chamber morphology. Comparison of chamber perimeter shows a 37.53% reduction of treated larvae when compared to controls (Table 8 & 8.1).

Quantitative analysis of the area, perimeter, length and width of a section deeper into the ventricle showed significant reductions of all parameters in treated larvae when compared to untreated controls. Control larvae displayed a ventricular area of 7218 ±41 μm^2, perimeter of 331 ±6 μm, and length and width of 127 ±3 μm and 84 ±1 μm respectively. In contrast, oil and dispersant treated larvae had an average area, perimeter, length and width of 3668 ±83 μm^2, 236 ±8 μm, 89 ±6 μm, and 56 ±4 μm respectively. When comparing the 3,668 μm^2area of O+D larvae with the 7,218 μm^2area of untreated control larvae, a dramatic 49.18% decrease in ventricular area is observed. Similarly, there is a 28.50% reduction in ventricular perimeter, 29.73% reduction in length, and a 32.93% decrease in chamber width (Table 5 & 5.1). The changes in chamber dimension, leading to a shorter, thinner, and smaller ventricle in treated larvae, is representative of the progressive and teratogenic effects of exposure to crude oil and chemical dispersant at early embryonic stages of development.

Qualititive analysis of histological sections from untreated larvae at 96 hpf reveals a multicellular myocardial layer, reaching up to three cell layers in thickness. The myocardial wall is well defined, consists of a sponge-like meshwork of interwoven muscle fibers, and trabeculation can be observed. The endocardial cells can be seen lining the ventricular chambers and are distributed along the perimeter of the ventricular lumen. In comparison to untreated controls, the ventricle of crude oil treated larvae is elongated and narrower in size as evident by morphometric analysis of tissue dimensions (Figure 23 & 23.1). Upon microscopic histological analysis of the ventricle, trabeculation of the myocardium is also observed in treated larvae at 96 hpf. The myocardium of the ventricular chamber in treated

larvae is 1-2 cells thick. Endocardial cells can be identified in O+D treated larvae and can be distinguished from myocardial cells by their organization about the perimeter of the chamber lumen deep to the myocardium. The overall and progressive effects of oil and dispersant on the development of the embryonic zebrafish heart is most pronounced by 4 days post fertilization. The tube-like cardiac phenotype observed in crude oil and dispersant emulsion exposed larvae by 96 hpf represents the culmination of the progressive teratogenic effects chemical exposure plays on the development of the zebrafish heart (Figure 23.1).

The changes and defects observed in treated larvae at 72 hours post fertilization are more progressive and pronounced by 96 hpf. Qualitative morphological analysis of whole mount treated and control larvae under a stereomicroscope at 4x and 10x magnification show severe and advanced pericardial edema, yolk sac edema, hemorrhaging in the brain, reduction of cartilaginous structures, as well as changes in the shape and structure, and orientation of the heart and its associated chambers (Figure 36). Cardiac morphology of affected larvae can be characterized by incomplete cardiac looping and extreme narrowing of the cardiac chambers, causing the organ to take on a filamentous or string-like appearance. Defective heart formation and cellular patterning is associated with elongation of the atrium (Figure 18 & 18.1) and ventricle (Figure 23 & 23.1). Flawed looping of the cardiac chambers was observed (Figure 26 & 26.1). Defective cardiac cushion and valve function was observed in treated larvae by gross examination of whole mount larvae as evident by the regurgitation of blood from the bulbus arteriosus to the preceding ventricle,

and from the ventricle to the preceding atrium during cardiac diastole (Supplemental video 5 & 5.1).

The area and perimeter of the embryonic eye and otic vesicle was measured in untreated control and experimental larvae at 96 hpf (Figure 36). Similar to results observed at 72 hpf, comparison between the area and perimeter of the embryonic eye of untreated controls and O+D treated larvae shows a statistically significant reduction in both the area and perimeter in O+D treated larvae. The average area and perimeter of the eye in untreated larvae is 66,883 ±1850 $\mu m^2$and 917 ±13 μm respectively, compared to an average area of 52,133 ±728 μm^2, and perimeter of 813 μm in experimental larvae (Table 1 & 1.1). Comparison of area and perimeter of the otic vesicle in zebrafish larvae at 96 hpf shows a statistically significant reduction of both parameters when comparing O+D larvae to untreated control larvae. Control larvae showed an average area of 33,302 ±671 μm^2 and perimeter of 648 ±6 μm in untreated controls. O+D treated larvae showed an area and perimeter of 18,809 ±1249 μm^2 and 489 ±17 μm respectively (Table 2 & 2.2). Untreated larvae showed an average heart rate of 99 ±3 beats/minute, and as a result of the effects of oil and dispersant on treated specimen at 96 hpf, exposed larvae showed no cardiac contractility and exhibited cardiac arrest (0 bpm) (Table 3 & 3,1).

Discussion

Oil spills such as the 1989 Exxon Valdez spill and the more recent 2010 Deepwater Horizon spill have posed disastrous threats to marine and terrestrial ecosystems. Since, a tremendous amount of research efforts have been catalyzed to discern the teratogenic effects of crude oil and chemical dispersant in a variety of teleost species. The most vulnerable organisms are those encountering these pollutants during their early life stages (De Soysa et al., 2012). Exposure to polycyclic aromatic hydrocarbons as ubiquitous contaminants in aquatic habitats has been studied in significant detail using the zebrafish (Danio rerio) as a model, and has been shown to cause morphologic and physiologic aberrations including but not limited to growth retardation, defective cardiac development and reduced blood flow, yolk sac edema, malformation of craniofacial structures, impaired locomotive behavior and muscle patterning, as well as a host of other defects compromising the health and vitality of pink salmon (*Oncorhynchus gorbuscha*) and Pacific herring (*Clupea pallasi*) populations in the gulf waters. 'In aquatic species, PAH's are generally accepted as acting through either of two mechanisms of action: (1) "dioxin-like" toxicity mediated by activation of the aryl hydrocarbon receptor (AHR), which controls a battery of genes involved in PAH metabolism, such as cytochrome P4501A (CYP1A) and (2) "non-polar narcosis", in which tissue uptake is dependent solely on hydrophobicity and toxicity and is mediated through non-specific partitioning into lipid bilayers' (Incardona et al., 2006). It has been shown in pervious studies using the Pacific herring that the developing heart is the primary target of crude oil exposure, causing aberrations through a pathway that does not require activation of the ARH. Although many studies have been conducted in an effort to characterize the nature and developmental origins of crude oil

induced defects on teleost species, previous crude oil exposure studies using zebrafish and Pacific herring embryos focused on the teratogenic effects observed at relatively late in embryonic development. As a consequence, the earliest time post-fertilization at which defects in cardiac form and function can be observed remained largely unknown.
In the current study, a gross and histological assessment of exposure to MC252 crude oil and chemical dispersant emulsions at 150-250 ppm during early embryonic development (from 30-96 hpf) resulted in high level reproducible teratogenesis leading to an elongated atrium, compact ventricle, and overall string like cardiac morphology characterized by defective chamber looping which was observed early in development.

Results from previous studies have not investigated changes in embryonic heart development of zebrafish as early as 30 hpf in development. Morphometric data collected from analysis of histological preparations and gross morphological data acquired by whole mount imaging and videography of zebrafish embryos from 30 to 96 hpf shows the effects of crude oil and dispersant on the morphology as well as function of the developing zebrafish heart is onset by 48 hpf, and is characterized in this study by yolk sac edema, cardiac edema, defective and reduced looping of the cardiac chambers, alteration in chamber morphology and positioning, reduction of cardiac function and circulation, as well as reduction in size of the eye and otic vesicle. These effects are comparable to and correlate with those observed in previous studies assessing the effects of PAH exposure during embryonic development, and become more apparent as development progresses.

Taken together, a progressive decrease in the size of the embryonic heart coupled with reduced cardiac contractility will have a substantial impact on circulation, hence, the viability of zebrafish embryos.

Effects of O+D on Cardiac Morphology and Function

These data are the first histological analysis of cardiac structure and function in developing zebrafish as early as 30 hpf. The early differentiation of chamber boundaries is best demonstrated by specific antibody staining, as the usual morphological markers (cardiac cushions and trabeculae) are not developed yet (Hu et al., 2000). Due to the lack of chamber specific antibody staining of whole mount specimen to definitively identify chamber boundaries, a more holistic morphometic analysis of cardiac structures at 30 & 36 hpf using chamber specific antibody staining in whole mount specimen is needed to reinforce data presented in this study. Due to limitations of the experimental design; it is plausible that the differences observed in morphometric analysis of histology at 30 and 36 hpf are due to comparison of measurements from non-comparable sections resulting from slight variations in cardiac orientation and positioning during embryonic development, or embedding and sectioning samples, despite best efforts to normalize sections selected for analysis. The lack of identifiable differences in gross morphology by wholemount stereoscopic analysis could suggest a possible discrepancy in chamber morphometrics obtained from histological analysis of single sections. Therefore, a more complete analysis

of cardiac structures at 30 and 36 hpf using antibody staining in whole mount specimen would supplement data presented in this study.

30 hpf

Concurrent with previous findings by Stainier, Lee, and Fishman; the embryonic heart has begun looping which leads to the formation of distinct chambers demarcated by narrowing of the lumen at the junctions. Looping of the heart tube to the embryo's right hand side is known to be a conserved feature amongst vertebrates (Stainier et al., 1993). Consistent with the composition of the definitive heart tube as desrcribed by Staintier et al., 1993, the embryonic heart at 30 hpf was seen in this analysis to consists of an outer myocardial layer, and an inner endocardial layer of cells as evidenced in histological sections.
Quantitative histological analysis of zebrafish embryos exposed to O+D suggests potentially altered chamber morphology beginning as early as 30 hpf. A significant reduction in atrial perimeter, and significant increase of atrial width in O+D treated embryos is observed. Despite no statistical significance, we note an increase in average atrial area by 306 um2 in O+D embryos, coupled with a slight decrease in atrial length. This data is suggestive of a difference in shape but not size, i.e. wider and more compact atrial chamber in treated embryos when compared to untreated controls. Despite significant morphometric differences, no gross or cellular aberrations were detected in O+D treated embryos when compared to controls.

Statistically significant increase in the ventricular area and width, coupled with significant decreases in chamber length of O+D treated embryos is suggestive of altered ventricular morphology. Unlike the atrium, the significant increase in area of the ventricle in treated embryos along with increased width and decreased chamber length, is potentially representative of a change in both size and shape of ventricles leading to a wider and more compact chamber. This could be the start of a general trend towards a malformed cardiac organogenesis as a result of embryonic exposure to O+D. In contrast, and similar to previous findings by Incardona et al., these data suggest altered cardiac morphology independent of changes in cardiac function. 'The genetics of heart development in zebrafish has established the inseparable relationship between cardiac form and function during early stages of cardiac morphogenesis. Mutations affecting heart structure impact its function, whereas mutants with impaired function concomitantly experience impacts to form of the chambers or valve structure says Hicken et al., (2011).

Results of this study show no observable differences between untreated controls and experimental larvae in cardiac function in whole mount specimen, with an average heart rate of 60 bpm for untreated controls and 57 bpm in O+D treated embryos. It is of interest to note that the heart rate of untreated control embryos in this study had a much lower than the 140 bpm observed in a previous study by Didier et al., 1993. While it is unlikely that the difference encountered results from differences in staging and growth rate, this discrepancy is most likely due to differences in instrumentation or techniques.

36 hpf

Comparable to observations made by Stainier et al., gross analysis of chamber morphology in both untreated and treated embryos at 36 hpf, shows clear indentations marking the boundaries of chambers, and the looped heart tube leaves the atrium sitting on the left and brings the ventricle to right side of the embryo. The two minor chambers, the sinus venosus and the bulbus arteriosus can also be distinguished at the extremities of the heart tube (Stainier and Fishman, 1992). Cardiac chambers of both untreated and treated embryos are made up of a myocardial and endocardial layer of cells, similar to described previously in 30 hpf embryos.

Histological analysis of zebrafish embryos exposed to O+D also shows potential evidence of altered chamber morphology in embryos at 36 hpf. A significant increase in atrial area, coupled with a significant increase in chamber width of O+D treated embryos is observed. Despite the lack of statistical significance, the slight 34 μm^2 increase in average atrial perimeter in O+D embryos, along with the slight increase of atrial length and be noted. Unlike the data observed at 30 hpf suggesting a change in atrial shape but not overall size, this data suggests altered shape and size of the atrium, i.e. longer, and wider and larger atrial chamber in treated embryos when compared to untreated controls. The dilation of the atrium in experimental embryos evident in this study is similar to the effects of retene (7-isopropyl-1-methyl-phenanthrene), a class of compounds present in crude oil and toxic to developing fish, on zebrafish embryos at the same stage of development as described by Scott and colleagues (Scott et al., 2011). In Scott's study focusing on the effects of toxicity on zebrafish embryos, he found that retene embryotoxicity was first observed at 36 hpf,

with pericardial edema and reduction of blood flow as the obvious signs of toxicity (Scott et al. 2011). They found that the atria in exposed embryos were slightly dilated with a reduction of cardiac jelly between the myocardium and endocardium, even noting smaller ventricular chambers in some retene-exposed embryos.

Though no statistically significant differences were observed by histological comparisons of treated and untreated controls, quantification of the ventricle at 36 hpf displayed a reduction of area, perimeter, length and width in O+D treated embryos. The reduction in all parameters of the ventricular chamber of treated embryos is suggestive of a slightly, shorter, and narrower ventricular chamber, unlike that which was observed and described at 30 hpf. These results suggest that exposure of embryos to crude oil and dispersant affect both the atrial and ventricular chambers at different time points in development.

Heart rate data collected at 36 hpf showed no statistical difference when comparing the 78 bpm average of untreated controls to the 76 bpm heart rate of experimental embryos. It is of interest to note that just as in embryos at 30 hpf, the heart rate data collected for untreated control embryos in this study are much lower than the 180 bpm recorded by Stainier et al., 1993. Despite no observable differences in cardiac function, qualitative analysis of the heart and its chambers in videos recorded for whole mount specimen shows a reduction in overlap of the atrial and ventricular chambers. This suggests a subtle delay or disruption of cardiac looping evident as early as 36 hpf in embryos exposed to crude oil.

48 hpf

By 48 hpf, there are clearly observable differences in cardiac form and function. Consistent with previous findings, the zebrafish heart at 48 hpf consisted of a smooth-walled tube divided into four definitive regions including the sinus venosus, atrium, ventricle, and bulbus arteriosus in succession. The myocardium is observed to be one cell layer thick in each segment except for the ventricle, which reached up to two cell layers in thickness. Analysis of atrial tissue in histological sections of zebrafish larvae exposed to O+D also shows evidence of altered chamber morphology compared to control larvae at 48 hpf.

There was no statistically significant differences observed in atrial area, perimeter or length when comparing treated larvae to untreated controls. Chamber width however, showed a significant decrease in treated larvae. The significant reduction in chamber width is suggestive of a slightly longer and much narrower atrial chamber in O+D treated larvae, compared to controls.

In analyzing the AVC canal in larvae at 48 hpf, no significant differences were observed in area and perimeter, compared to untreated controls. Cardiac cushion formation in O+D treated larvae can be observed in histological preparations to be defective as the endocardial cells contributing to cardiac cushion formation in treated larvae are largely indistinguishable from endocardial cells lining the lumen of the chambers in most larvae. In contrast, endocardial cells contributing to cardiac cushion formation in control larvae can be seen as thickenings and aggregation of cells along the dorsal and ventral aspects of the atrio-ventricular junction . The aberrations in cardiac cushion formation suggest an effect

on the EMT of endocardial cells, consistent with previous studies on the effects of TCDD on migration and proliferation of endocardial cells at the boundaries between chambers. TCDD is a liopophillic, halogenated, aromatic hydrocarbon that persists in the environment and causes cardiovascular malformations in mammalian, avian, and aquatic species (Vatsal et al. 2008). Its molecular mechanisms of action are similar to those of PAH's of crude being mediated by the ligand activated transcription factor aryl hydrocarbon receptor (AHR) (Dagmara et al. 2005). In a 2008 study by Vatsal et al., testing the effects of TCDD on the embryonic zebrafish heart, it was shown that the activation of the AHR through exposure to TCDD produces alterations in valve formation. The defective heart valve formation was attributed to disruption of cellular patters associated with normal cardiac cushion formation. Unlike like aforementioned study where the localized clusters of endothelial cells normally observed at the AV and BV junctions were clearly present and formed normally despite the presence of TCDD at 48hp; we note that zebrafish O+D exposure at 48 hpf does show changes in cardiac cushion malformation, suggesting a disruption of the regulatory mechanism governing endothelial cell localization at the AV and BV junction.

Results from the measurement of area, perimeter and length of histological sections representative of the ventricle of experimentally treated larvae at 48 hpf showed significant differences were observed in histological comparisons of treated and untreated controls, and quantification of the ventricle at 48 hpf displayed an increase in area, perimeter, and length of O+D treated larvae, while chamber width was significant reduced in treated larvae. This data is indicative of the narrowing and elongation the ventricle in O+D treated larvae when compared to untreated controls, consistent with the results

reported for atrial chambers. The bulbus arteriosus showed an increase in cross sectional area and perimeter when comparing O+D larvae to that of untreated controls.

Comparing the average heart rate of 48 hpf untreated larvae (82.2 bpm) to that recorded in O+D exposed larvae (65 bpm), a significant reduction in cardiac function is observed. The average heart rate of untreated larvae recorded in this study was significantly less than that observed in previous studies, most likely due to differences in experimental technique. A qualitative assessment of reduction in overlapping of the atrial and ventricular chambers seen in whole mount images and videos at 48 hpf, is indicative of progressive defective cardiac looping, and is observed to be more severe than previously observed at 36 hpf (Figure 29). The degree of looping corresponds with the number of sagittal sections in which both the atrium and ventricle can been seen side by side.

In contrast to studies assessing the malformations associated with early exposure to TCDD (2,3,7,8-tetrachlorodibenzo-p-dioxin) in embryonic zebrafish where there was no distinguishable difference in the heart structure or function between treatments at 48 hpf, we observe altered morphology and physiology in hearts of larvae exposed to O+D by stage in development. TCDD is a highly lipophilic environmental pollutant, producing effects of toxicity, immunotoxicity, neurotoxicity, cardiotoxicity and lethality. Similar to the molecular mechanisms of PAH's of crude oil, most of the toxic endpoints seen in TCDD-exposed vertebrates are mediated by the ligand activated transcription factor aryl hydrocarbon receptor (AHR) (Dagmara et al. 2005).

72 and 96 hpf

By 72 hpf and 96 hpf, defects associated with embryonic exposure to oil and dispersant are easily identifiable by gross and histological analysis of the heart and its chambers and results of this study are consistent with previous research on the effects of crude oil exposure on zebrafish embryogenesis. Unlike data collected from earlier time points (30-48 hpf) time points, the data obtained from analysis of 72 and 96 hpf larvae displayed a consistent trend of reduction in almost all parameters. As expected based on previous research, gross morphological analysis, and preliminary results (Stellwag, personal communication), larvae at the later time point studies (72-96 hpf) exhibited poorly developed cardiac chambers characterized by a reduction of myocardial and endocardial cell layers, as well as defective cardiac cushion remodeling. In control larvae, we observe a normal looping process, such that atrium and ventricle overlap each other from the lateral perspective. In O+D exposed larvae, the chambers can easily be distinguished with little to no overlap. The degree of looping corresponds with the number of sagittal sections in which both the atrium and ventricle can been seen side by side. Likewise, the hearts of O+D treated larvae were stretched; such that the ventricle is positioned anterior to the atrium in a similar configuration is that representative of earlier embryonic stages of development. In contrast to the S-shaped hearts observed by gross and histological examination of untreated fish, O+D exposed larvae exhibited an elongated and string like appearance. The change in cardiac morphology, specifically the defective looping of the heart chambers observed at 30-48 hpf is of particular interest, and mechanism by which cessation of normal cardiac looping occurs should be a major focus of study in follow up studies.

Histological comparison of sections shows a significant reduction in area and width of the atrial chambers in O+D treated larvae at 72 and 96 hpf. Chamber length was roughly the same across treatments and time points. This data corresponds with previously observed malformations associated with PAH induced cardiac toxicity in zebrafish, showing atrial chambers that were thin and elongated but in which the perimeter was unchanged likely because a reduction in width of the atrium was compensated by an increase in the length, as reflected by an overall morphological shift from an ovoid to an elongated tubular structure.

A similar significant reduction in area and perimeter of the AVC and bulbus arteriosus is observed by quantitative histological comparison between control and treated larvae at 72 hpf suggesting a widespread effect on all cardiac chambers by this stage of development compared to the more limited and in many instances insignificant differential and chamber specific effects observed in embryos examined from 30-48 hpf.

Comparable to the results of the atrial chambers; quantification of area, perimeter, length, and witdh of the ventricular chamber shows a reduction of all measurement sin both 72 and 96 hpf larvae exposed to O+D compared to untreated control specimens. These changes in chamber dimension are representative of a smaller and more compact ventricle than in normal fish at a comparable time point as evident by gross and histological comparison of embryonic hearts between treatments (Figure 22 & Figure 23).

Associated with defective organ formation and function, qualitative analysis of histological sections show an alteration of cellular organization of cardiomyocytes and endocardial cells in O+D treated larvae as described in the results of this study, leading to a reduction in the size of chambers, leading to an elongated tubular cardiac structure, compared to the robust and well defined hearts of control larvae.

Although histological data suggests a potential effect on the morphology of the developing zebrafish heart as early as 30 and 36 hpf, changes in cardiac structure as evident in gross and quantitative measurement of defined heart structures from histological sections are statistically significantly different by 48 hpf. These effects include yolk sac and pericardial edema, defective cardiac looping coupled leading to continued narrowing and elongation of all the heart chambers, and a thin and elongated heart with virtually indistinguishable chambers that ultimately ceases beating and is incapable of sustaining blood flow through the developing vasculature.

Comparative Effects of Crude Oil and chemical dispersant treatment on non-heart organ primordia.

In order to compare the changes in heart morphology to those of other organ primordia to understand whether the effects of crude oil and chemical dispersant treatment were general for all organs, or specific to the heart developmental compartment; the embryonic eye and otic vesicular compartments were measured in histological tissue sections over the time course evaluated for the heart.

Measurements of area and perimeter of the embryonic eye and otic vesicle from 30 hpf - 96 hpf showed statistically significant differences between control and experimental groups in the area or perimeter of the eye at 36, 48, 72, & 96 hpf. A statistically significant difference between control and experimental groups in the area or perimeter of the otic vesicle was seen at 48, 72, & 96 hpf. These results are consistent with those reported by de Soysa et al. (2012) for similar developmental periods, and mirror the results obtained for the heart.

Cardiac priomordia are characteristically different from cells that form the eye and otic vesicle as they are derived from the mesodermal germ layer of the gastrula. During cardiac organogenesis, the heart undergoes morphogenetic changes like chamber differentiation and looping that is a specific and non-parallel to the morphogenetic regulatory process governing development of the embryonic zebrafish eye and otic vesicle, which arise from the ectoderm. These factors limit comparison, however, they do suggest that some effects of embryonic exposure to crude oil and chemical dispersant may have a more general effect, i.e. reduction in overall size, while other effects such as the failure to complete cardiac looping and chamber compartmentalization, thinning of the myocardium, malformation of cardiac cushions, and overall elongation and deterioration of the heart.

At 30 hpf, there were no statistically significant differences between control and experimental groups in the area or perimeter of the eye and otic vesicle. Despite the lack of significance in comparing means between treatments, we notice a reduction of area and

perimeter of the eye and otic vesicle in O+D treated fish. Although the difference observed could potentially arise from differential staging of zebrafish embryos, this data suggests a possibility of a slight delay in development, potentially leading to differences observed in cardiac morphology described previously. This data is concurrent with the 2012 study by de Soysa et al., where it was determined that embryos exposed to a water accumulated fraction of Macondo crude oil and chemical dispersant showed an overall reduction of the brain, jaw, and eyes.

At 36 hpf, a significant reduction in area and perimeter of the embryonic eye is observed. Despite a the lack of significance, it is important to note that as in 30 hpf embryos, there was a slight reduction of area and perimeter of the otic vesicle. This data indicates that the embryonic eye is affected prior to significant reductions of area and perimeter of the otic vesicle. At 48 hpf however, a significant reduction in area and perimeter of the otic vesicle is observed. Similar to the reduction observed at 36 hpf, zebrafish embryos exposed to oil and dispersant at 48 hpf show significant reductions in area and perimeter of the eye. Starting at 48 hpf, a trend in the significant reductions of eye and otic vesicle can be seen. A linear relationship between embryonic stage and the degree of defects observed in craniofacial organs can be seen in when comparing means of area and perimeter of associated structures between treatments. Area and perimeters of both the eye and otic vesicle is observed leading up 96 hpf. These results appear to parallel the effects of high concentrations of retinoic acid as seen in a study conducted by Didier and Fishman, during which they determined RA treatment of zebrafish embryos at high concentrations leads to the progressive deletion of anterior structures. It was observed that the embryonic heart

tube was truncated at doses of RA that clearly do not visibly perturb surrounding tissues (Didier et al., 1992).

Similar to oil induced aberrations described in previous literature, qualitative whole mount comparison between control and experimental larvae show no strikingly obvious malformations in the general shape and size of the zebrafish embryo. However, by 48 hpf, the time point representative of aberrations in gross morphology at which we observed significant differences in both the eye and otic vesicle, we witness an array of morphological phenotypes including cardiac and yolk sac edema, hemorrhaging in the forebrain, midbrain and hindbrain, dorsal tail curvature, craniofacial defects, as well as cyst formation at the caudal aspect of the tail. The observed phenotypes are progressively observed through development up to 96 hours. By this time, larvae exposed to O+D begin to die presumably because of truncated blood flow related to defects in cardiovascular development and function.

These results are consistent with well-documented literature detailing phenotypes that result from exposure to crude oil and PAHs at early embryonic stages of development; however, the caveat here is that the treatment regimen described in this study results in a much higher frequency and degree of reproducibility of teratogenic effects than reported previously.

In conclusion, this study supports the hypothesis that exposure to crude oil and chemical dispersant leads to specific defects in cardiac development marked by a change in chamber

morphology and positioning, coupled with a reduction of cardiac function; leading to cardiac stasis and embryonic death. Embryonic exposure to Macondo crude oil and chemical dispersant causes teratogenic effects in cardiac development of zebrafish embryos with phenotypic abberations in form and function evident as early as 48 hpf. Specifically, there is progressive yolk sac and cardiac edema, defective and reduced looping of the cardiac chambers, alteration in chamber morphology and positioning, reduction of cardiac function and circulation, and even a reduction in size of the eye and otic vesicle.

These results aim to shed a new light on the timing of these effects, in hopes to refine our understanding of the toxicokinetic and toxicodynamic mechanisms through which exposure to crude oil and dispersant cause developmental toxicity. Integrating the results of this study with gene expression profiles obtained from genome-wide transcriptomics at comparable time points promotes the formulation of future hypotheses aiming to more thoroughly understanding the pathways and genetic mechanisms though which PAH toxicity effects the zebrafish heart. Understanding the nature and mechanisms of oil exposure is especially critical for assessing toxicity of PAH contaminated environments. Implications of this study extend to the future assessment of oil spills in lakes, rivers, and well coastal marine ecosystems where storm water runoff, carrying pryogenic PAH mixtures can be a source of toxicity.

Figure 1: Gross morphological deformations in zebrafish embryos exposed to crude oil and dispersant (de Soysa et al., 2012)

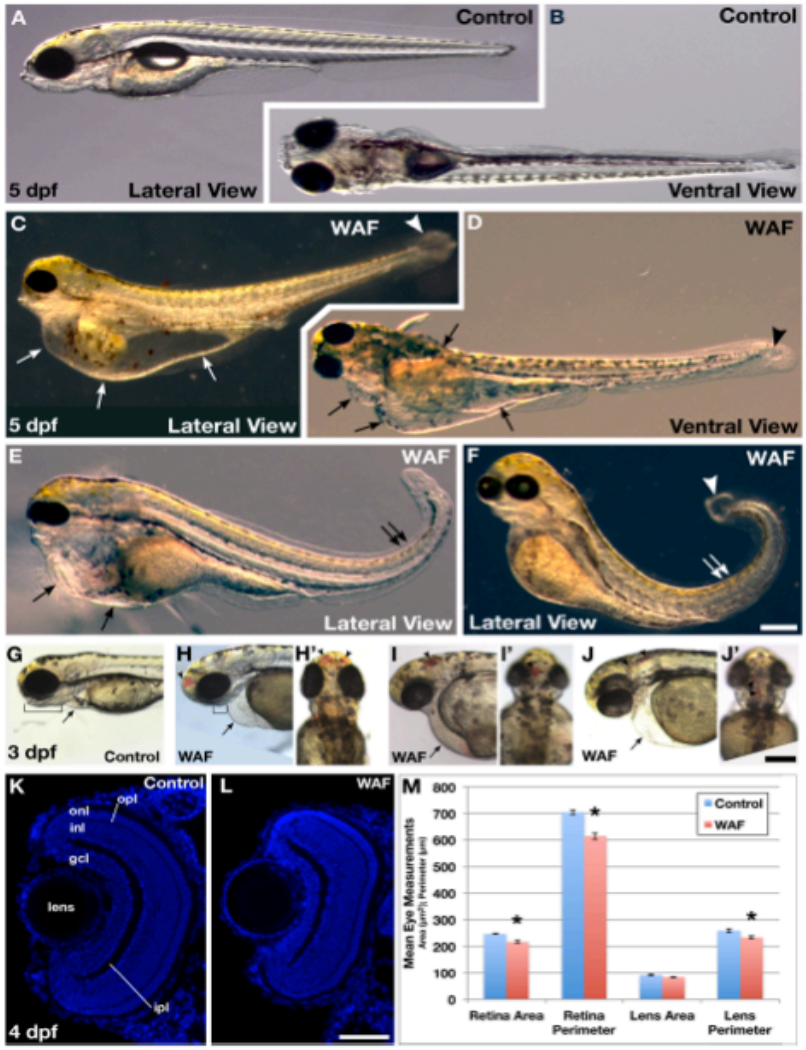

Figure 1 Exposure to Macondo crude oil-derived WAFs induced diverse gross morphological deformations in zebrafish embryos. (**A-F**) Lateral and ventral views of live untreated control (A, B) and WAF-treated embryos (C-F) at 5 dpf. Severe cardiac and yolk edema (C, D, E, arrows), dorsal tail curvature (E, F, double arrows), and cysts at the tip of the tail (C, D, F, arrowhead) were visible. (**G, H**) WAF-treated embryos (H) had reduced jaws compared to controls (G, brackets). (G-**J**) At 3 dpf cardiac edema was evident in WAF-treated embryos (arrows), and 28% of embryos had hemorrhaging in the forebrain, midbrain and hindbrain (arrowheads). Lateral (G, H, I, J) and dorsal views (H', I', J'). (**K-M**) Retinal architecture appeared normal in control and WAF-treated embryos (K, L) but there was a slight reduction in the area and perimeter of WAF-treated retinas (M). Except for lens area, the size reductions were statistically significant (M, asterisks; *t*-tests: lens area, $P = 0.015$; lens perimeter, $P = 0.007$; retina area $P < 0.0005$; retina perimeter, $P < 0.0005$). Scale bars: 200 µm, F, J'; 50 µm, L. Abbreviations: gcl, ganglion cell layer; ipl, inner plexiform layer; inl, inner nuclear layer; opl, outer plexiform layer; onl. outer nuclear layer.

Figure 2: Cell proliferation vs. Apoptosis in zebrafish (de Soysa et al., 2012)

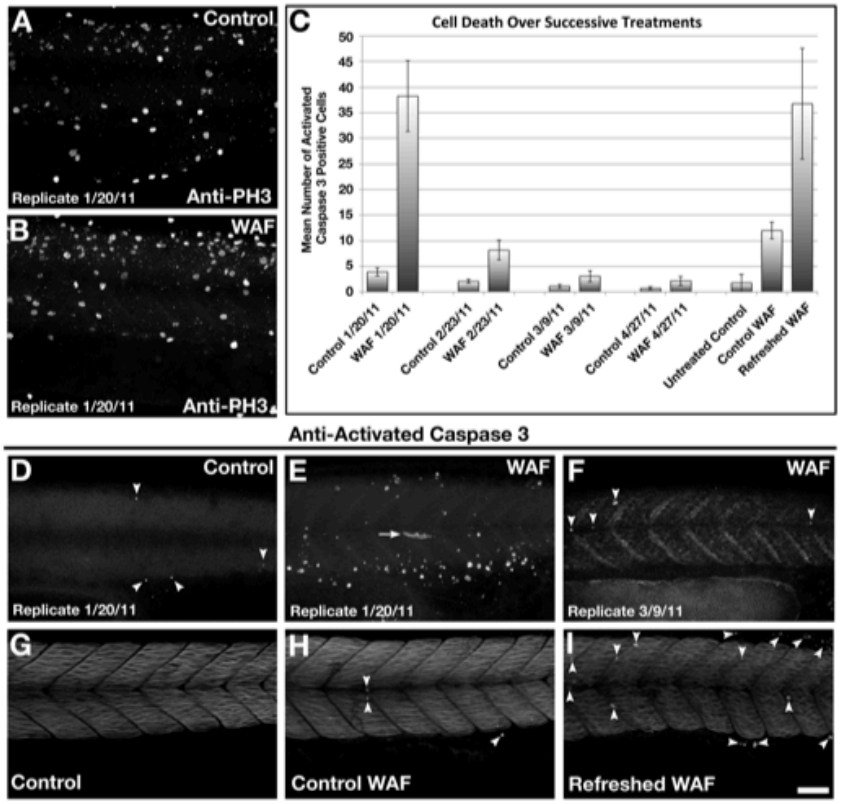

Figure 3 Macondo crude oil exposure did not affect cell proliferation but did induce programmed cell death. (**A**, **B**) Phospho-Histone H3 labeling of cells in mitosis were unaffected in 30 hpf WAF-treated embryos (B). (**C**) Quantification of anti-Activated Caspase 3-positive cells in 30 hpf control and WAF-treated embryos over 4 replicates and a WAF-refreshing procedure. The number of apoptotic cells decreased with each successive replicate, but increased following application of freshly-mixed WAF. (**D-F**) Activated caspase-3 labeled 30 hpf control (D, arrowheads) and WAF-treated embryos (E) from experiments in January 2011, and a WAF-treated embryo from an experiment in March 2011 (F, arrowheads). There was a significant decrease in the number of apoptotic cells in WAF-treated embryos between January (E) and March (F). (**G-I**) Representative images from the refreshed WAF experiments (arrowheads denote positive anti-Caspase 3 cells). Embryos were either untreated (G), exposed to the same WAF from 3.5 hpf to 30 hpf (H), or exposed to WAF from 3.5 hpf to 15 hpf and then exposed to a fresh WAF solution from 15 hpf to 30 hpf (I). Embryos in the refreshed WAF group (I) partially recovered the cell death phenotype of earlier replicates (E). (A, B, D-I) Lateral trunk views centered on somites 14 to 21. Scale bar 50 μm, A, B, D-I.

Figure 3: Growth of the adult heart by hypertrophy and dilation (Olson and Schneider, 2003)

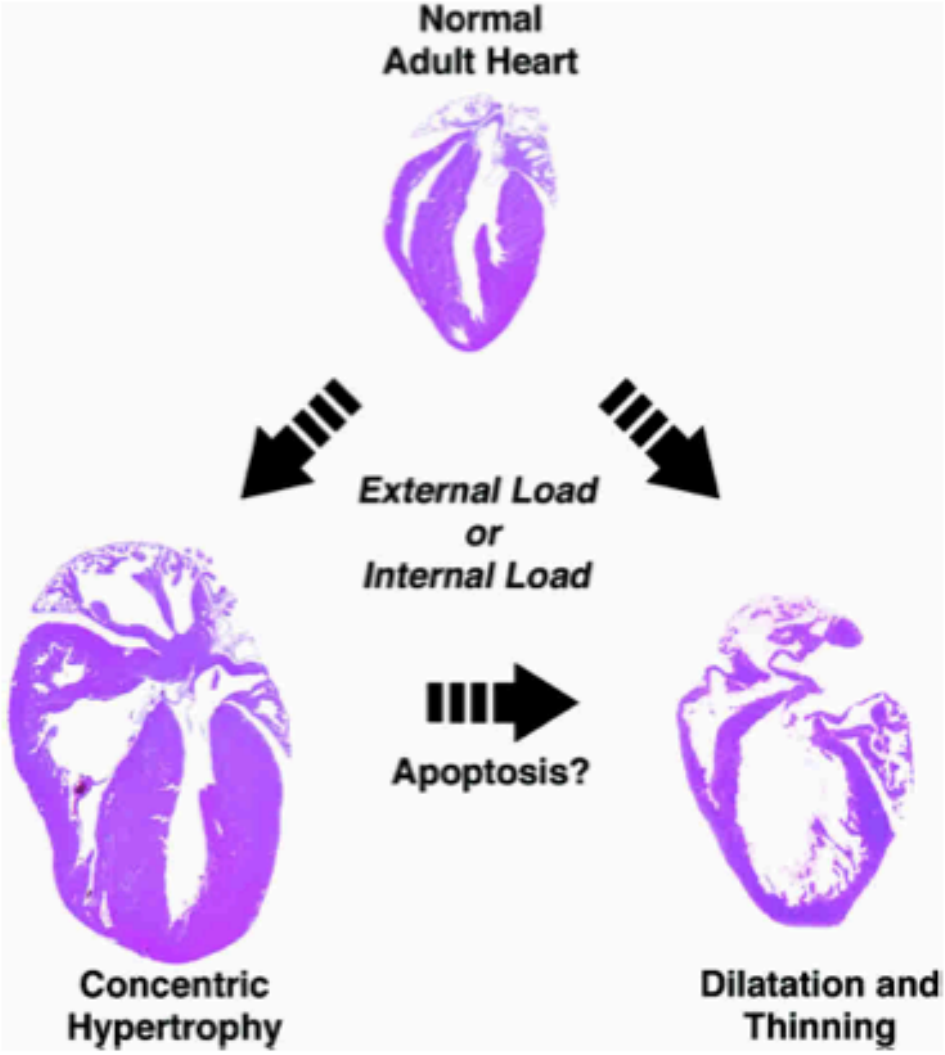

Figure 3. Growth of the adult heart by hypertrophy and dilation. The adult heart can undergo concentric hypertrophic growth that progresses to dilated cardiomyopathy or it can undergo dilatation directly through the actions of pathological signaling pathways that impose external or internal load.

Figure 4: Correlation of craniofacial defects with defective neural crest development (de Soysa et al., 2012)

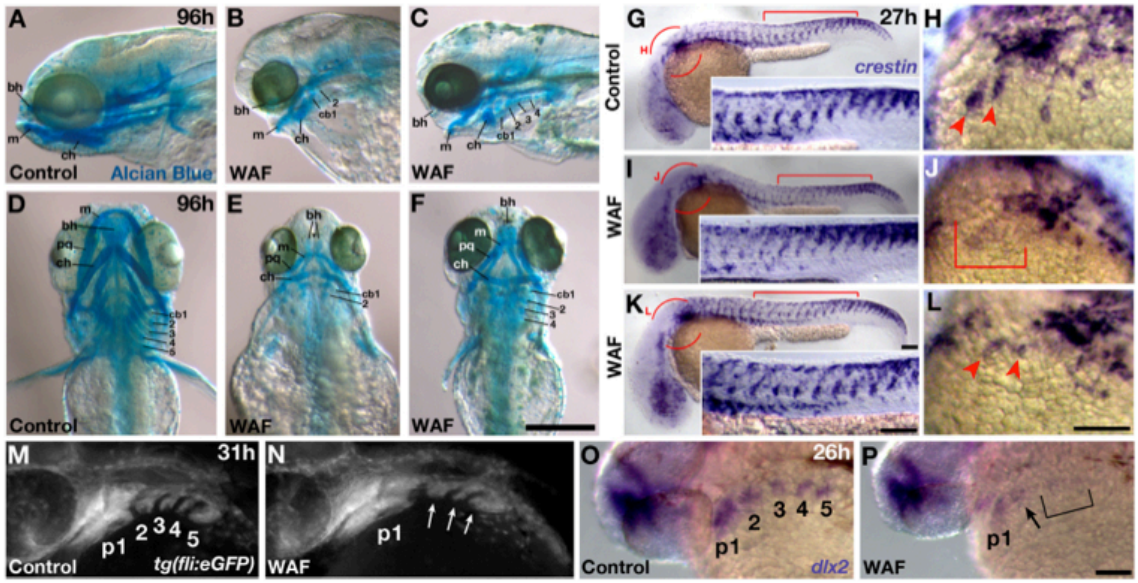

Figure 5 Craniofacial defects induced by Macondo crude oil exposure were correlated with defects in neural crest development. (**A-F**) Alcian blue staining of head and jaw cartilage in 4 dpf control (A, D) and severely (B, E) or moderately (C, F) affected WAF-treated embryos. WAF-treated embryos had a variable reduction in the size of all cartilage components, notably a lack of anterior extension of jaw elements and a dramatic reduction in posterior pharyngeal arches (B, C, E, F). (**G-L**) Whole mount *in situ* hybridization of *crestin* expression in neural crest cells. *crestin* expression is normal in the trunks of control and WAF-treated embryos (G, I, K, bracket; circles in G, I, K represent magnified view in H, J, L). However, *crestin* expression was variably reduced specifically in the anterior migratory streams, an area of cells that will populate the pharyngeal arches (H, J, L, arrowheads and bracket). (**M, N**) Cranial neural crest forming pharyngeal arches (p1-5) at 31 hpf as visualized by *fli* driven expression of GFP. One of the posterior-most pharyngeal arches is missing in WAF treated embryos (N, arrows) as compared to controls (M, 3, 4, 5). (**O, P**) *dlx2* expression in the region of pharyngeal arches is reduced in 26 hpf WAF-treated embryos (P, p1, arrow, bracket) as compared to controls (O). *dlx2* expression is nearly lost in the most posterior regions of the presumptive pharyngeal arches (P, bracket) despite robust expression still seen in the forebrain. Abbreviations: bh, basihyal cartilage; cb1-5, ceratobranchial branches; ch, ceratohyal; m, Meckel's; pq, palatoquadrate. Scale bars = 200 μm, A-F; 100 μm, G-L.

Figure 5: Position and migration of cardiac progenitor cells in Danio rerio (Stainier and Fishman, 1994)

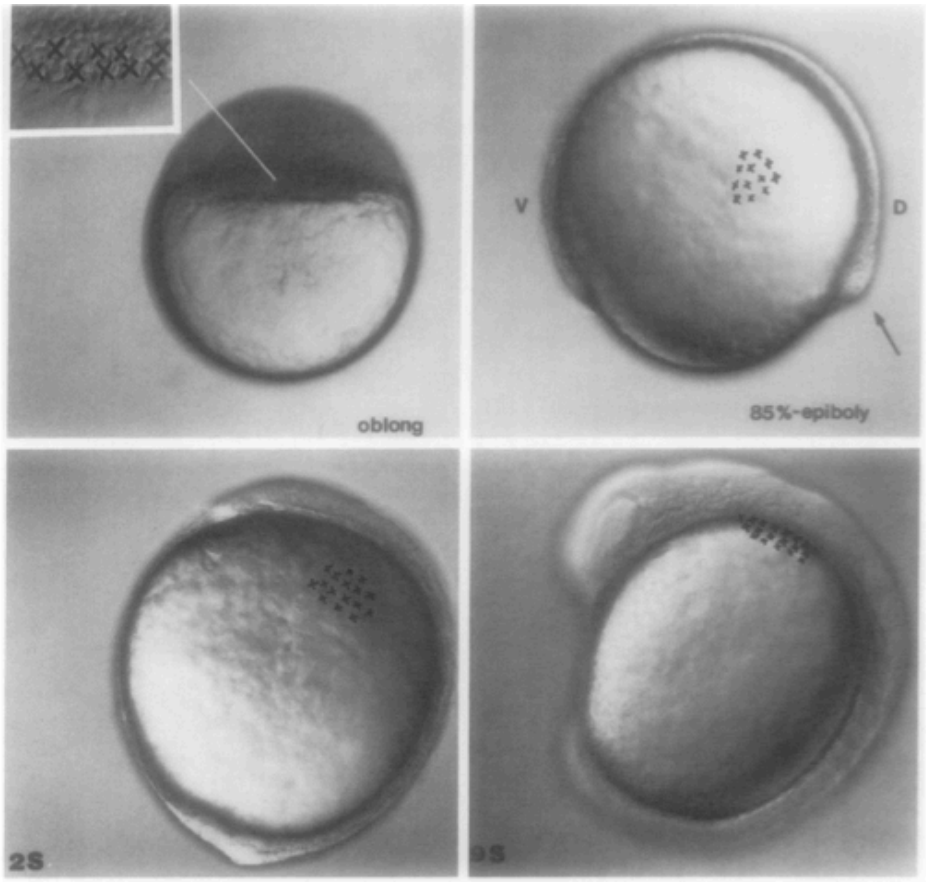

FIG. 1. Schematic representation of the position and migration of cardiac progenitor cells at early developmental stages. After a period of rapid cleavages during early development, the blastoderm thins and spreads to cover the yolk cell in a process termed epiboly (Kimmel, 1990; Warga and Kimmel, 1990). During gastrulation (which starts at 50% epiboly), deep cells involute and move anteriorly. As cells converge toward one side of the gastrula, a local thickening appears along the margin, the embryonic shield (arrow), which marks the dorsal side of the embryo (D). Single cells located at or near the margin of blastula embryos were labeled with rhodamine–dextran and their progeny followed until 24 hr postfertilization to determine their contribution to the beating heart tube. Some of the data for this figure were originally collected by Warga and Kimmel (1990) and later by Warga, Stainier, and Kimmel (unpublished). Cells from this marginal region at 90° longitude also contribute to the outflow tract and possibly to pharyngeal endoderm. From the 2000-cell stage to the 9-somite stage, cardiac progenitors divide once or twice. Time table of development at 28.5°C: oblong, 3.75 hr; 50% epiboly (onset of gastrulation), 5.2 hr; 85% epiboly, 8.5 hr; 2-somite, 10.6 hr; 9-somite, 13.5 hr. V, ventral.

Figure 6: Migrating anterior lateral plane mesoderm gives rise to tubular primordial in Danio Rerio (Stainier and Fishman, 1994)

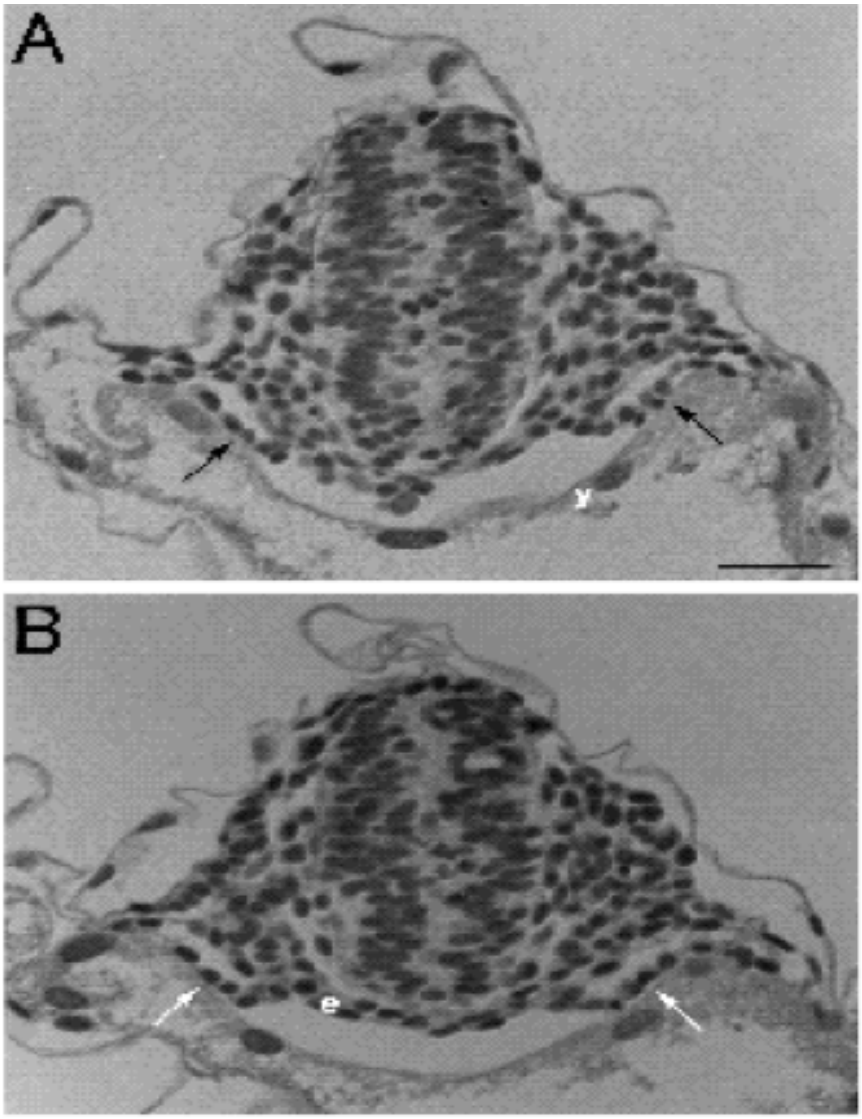

Fig. 4. The migrating anterior lateral plate mesoderm gives rise to 2 tubular primordia. Transverse sections of a 15-somite stage embryo at the level of the cardiac primordia. Embryos were stained with HNK-1 to determine the location of the trigeminal ganglia which approximates the anterior extent of the cardiac primordia (data not shown). Bilateral tubular primordia (arrows) are in direct contact with the yolk syncytial layer (y) ventrally. Dorsally, a thin endodermal (e) layer spans the width of the embryo. (A) Rostral section; (B) caudal section. Scale bar, 50 μm.

Figure 7: Location of the heart at 20-somite stage & Tropomyosin immunoreactivity of cardiac tubes in Danio Rerio (Stainier and Fishman, 1994)

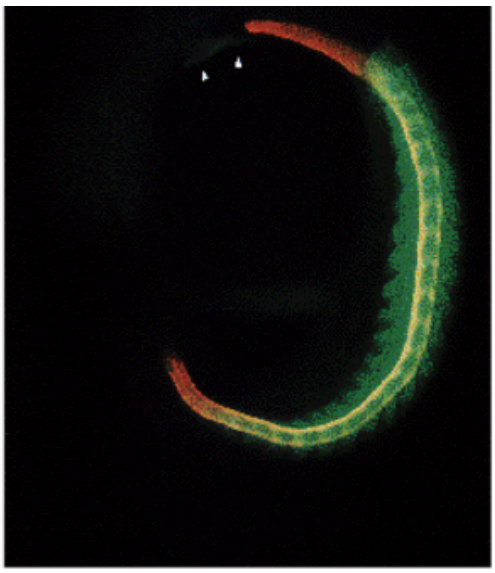

Fig. 5. Location of the heart at the 20-somite stage. The heart (arrowheads; CH1-positive, in green), which at this stage consists of bilateral tubes, lies adjacent to the yolk sac. The posterior extent of the cardiac tubes corresponds closely to the anterior extent of the notochord (CC8-positive, in red). Somitic muscles are also CH1-positive.

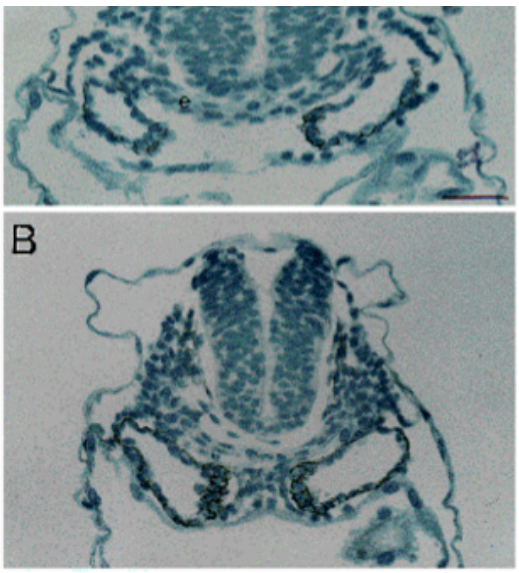

Fig. 6. Tropomyosin immunoreactivity outlines the bilateral cardiac tubes. Transverse sections of a 21-somite stage embryo stained with CH1, at the level of the cardiac primordia. Medially (B), and between the CH1-positive cardiac tubes lies a group of CH1-negative cells called the *portion moyenne du mésoblaste* (Swaen and Brachet, 1901) that gives rise to the endocardium. This group of cells is not present rostrally (A) or further caudally (not shown). The endodermal layer (e) is 2-3 cells thick. Scale bar, 50 μm.

Figure 8: Model for definitive heart tube formation (Stainier and Fishman,1994)

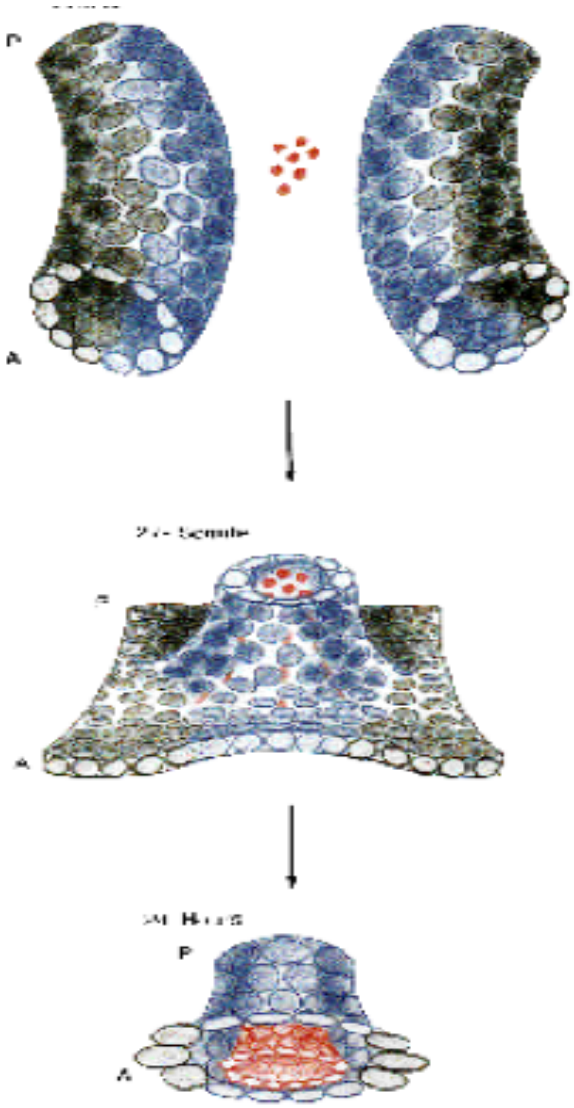

Fig. 10. Model for the formation of the definitive heart tube from two bilateral cardiac tubes. At the 21-somite stage (top), the bilateral tubular primordia form complete tubes that sit on either side of the endocardial progenitor cells (in red). By the 27-somite stage (middle), a cone is formed, with its (venous) base sitting on the yolk. Medially, the myocardial cells surrounding the endocardial cells form the apex of the cone. As the head lifts dorsally, the cone is rotated so that by 24 hpf (bottom), its (venous) base sits anteriorly. At this stage, an outer myocardial layer and an inner endocardial layer form the definitive heart tube.

Figure 9: CH1 staining in the positioning of the heart tube in Danio rerio (Stainier and Fishman, 1994)

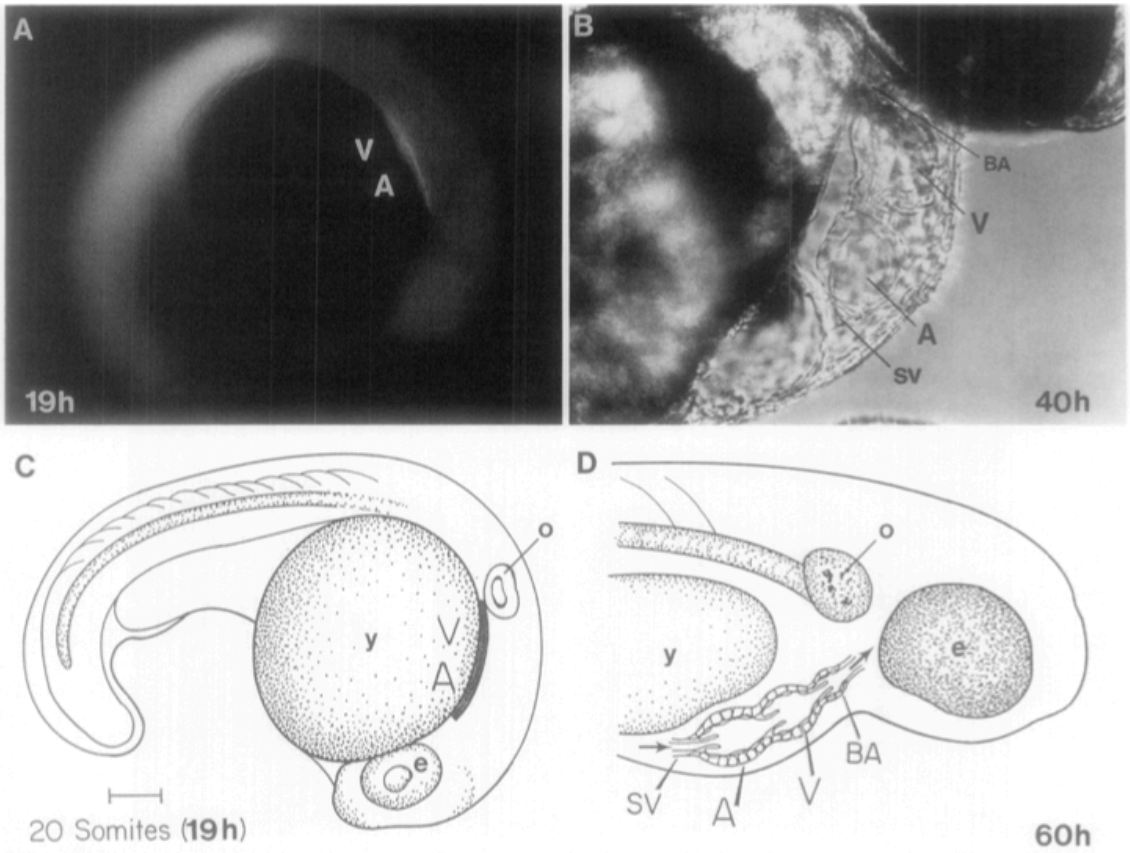

FIG. 2. Position of the zebrafish heart tube. (A, C) The early embryonic heart tube, revealed by CH1 staining (for tropomyosin), lies under the embryonic axis, adjacent to the yolk sac. At the 20-somite stage (19 hr), the atrium (A) lies anteriorly and the ventricle (V) lies posteriorly. scale bar in C is 100 μm; e, eye; o, otic vesicle; y, yolk. (B, D) At 40 hr (B) (and at 60 hr (D)) of development at 28.5°C, the head has lifted dorsally, the yolk is partially depleted, and the heart comes to lie with the atrium posterior and the ventricle anterior. In order to better illustrate the finer structure and position of the heart, B is a photograph of a mutant embryo in which the heart develops normally, although without a beat. In the wild type, the heart structure and position are as shown in B. SV, sinus venosus; BA, bulbus arteriosus.

Figure 10: Cardiac patterning and development in early embryonic stages of danio rerio (Bakkers, 2011)

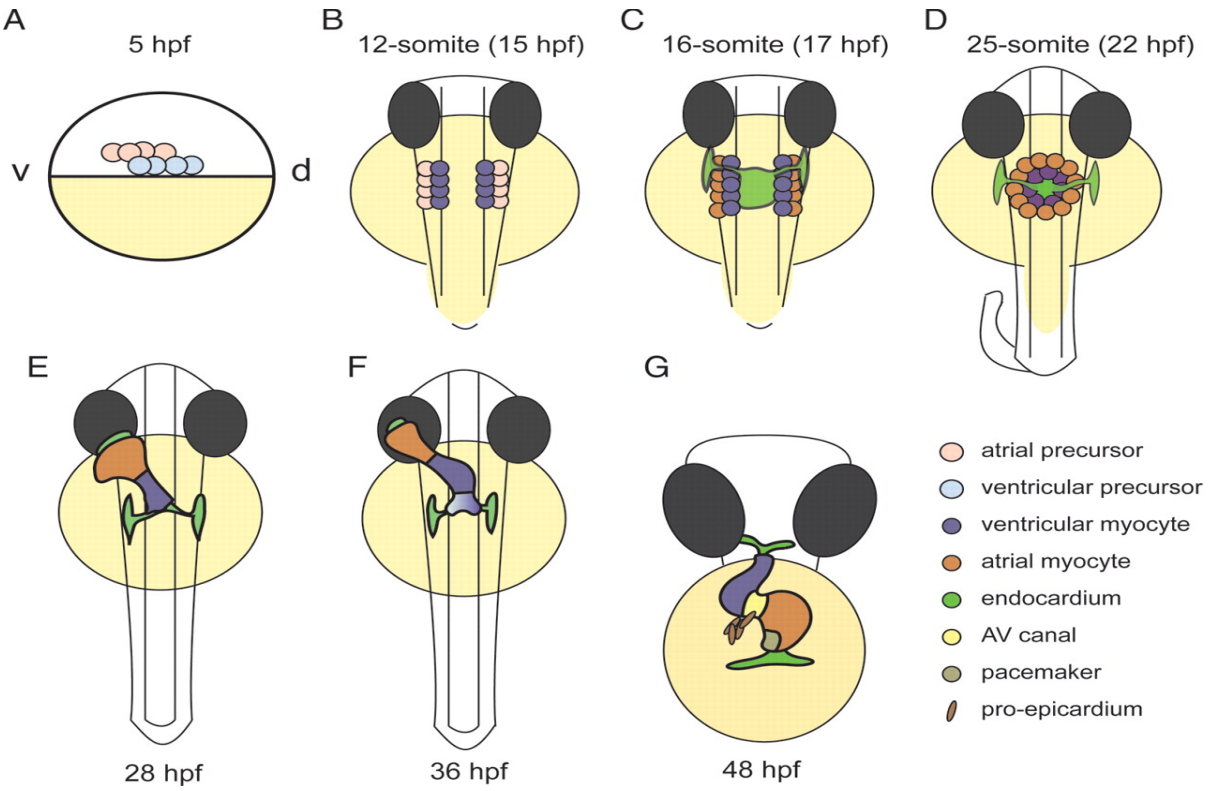

Figure 11: Transverse sections of 48 hpf zebrafish heart (Hu et al., 2000)

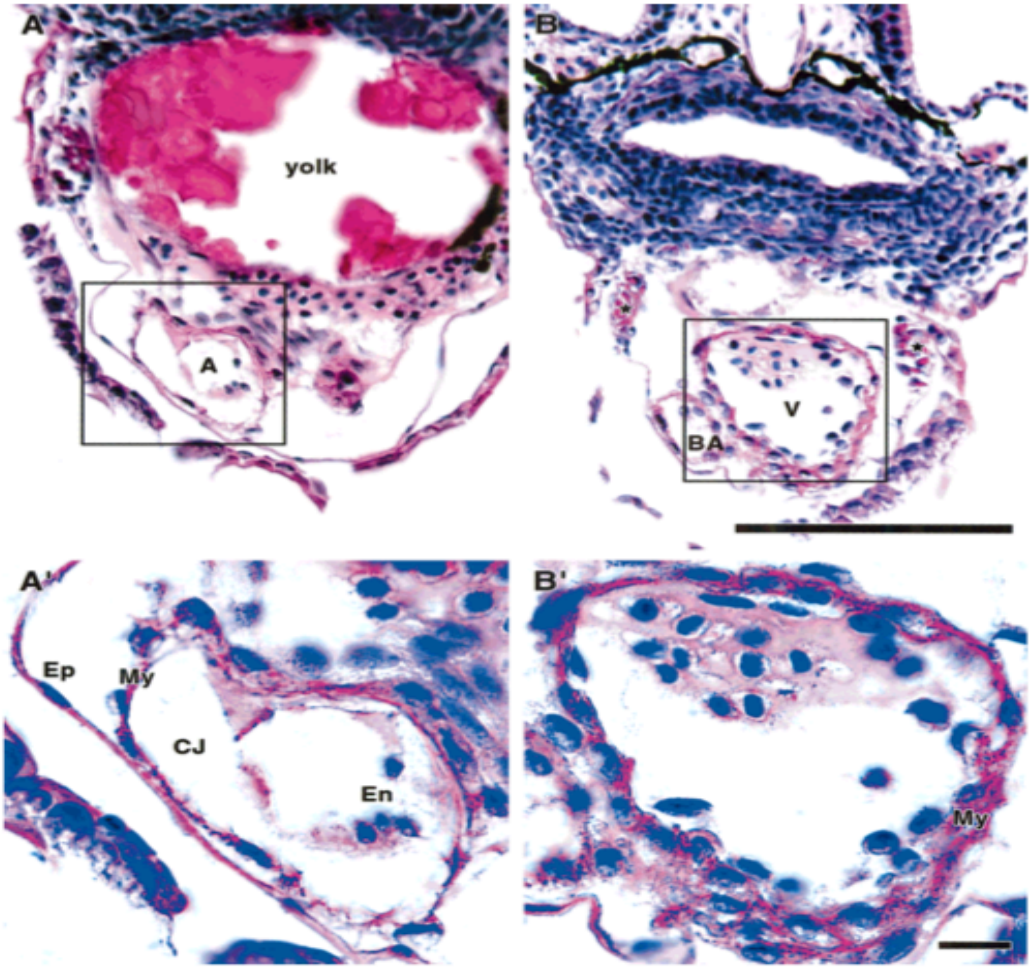

Fig. 2. Transverse sections through a 48-hr post-fertilization zebrafish heart. **A**: The yolk sac is most prominent at the caudal heart region. **A'**: High power view of the atrial wall shows the epicardium (Ep), and the single cell layer myocardium (My) separated from the endocardium (En) by acellular cardiac jelly (CJ). **B**: Inner surface of the entire heart is smooth, and the chambers can be distinguished only on the basis of their relative position in the serial sections. **B'**: High power view of the ventricle shows the myocardium reaches two cell layers in some areas. Hematoxylin-eosin staining. A, atrium; BA, bulbus arteriosus; ★, pericardial muscles; V, ventricle. Scale bar = 100 microns in A, B; 10 microns in A', B'.

Figure 12: Transverse and sagittal sections through 120 hpf zebrafish heart (Hu et al., 2000)

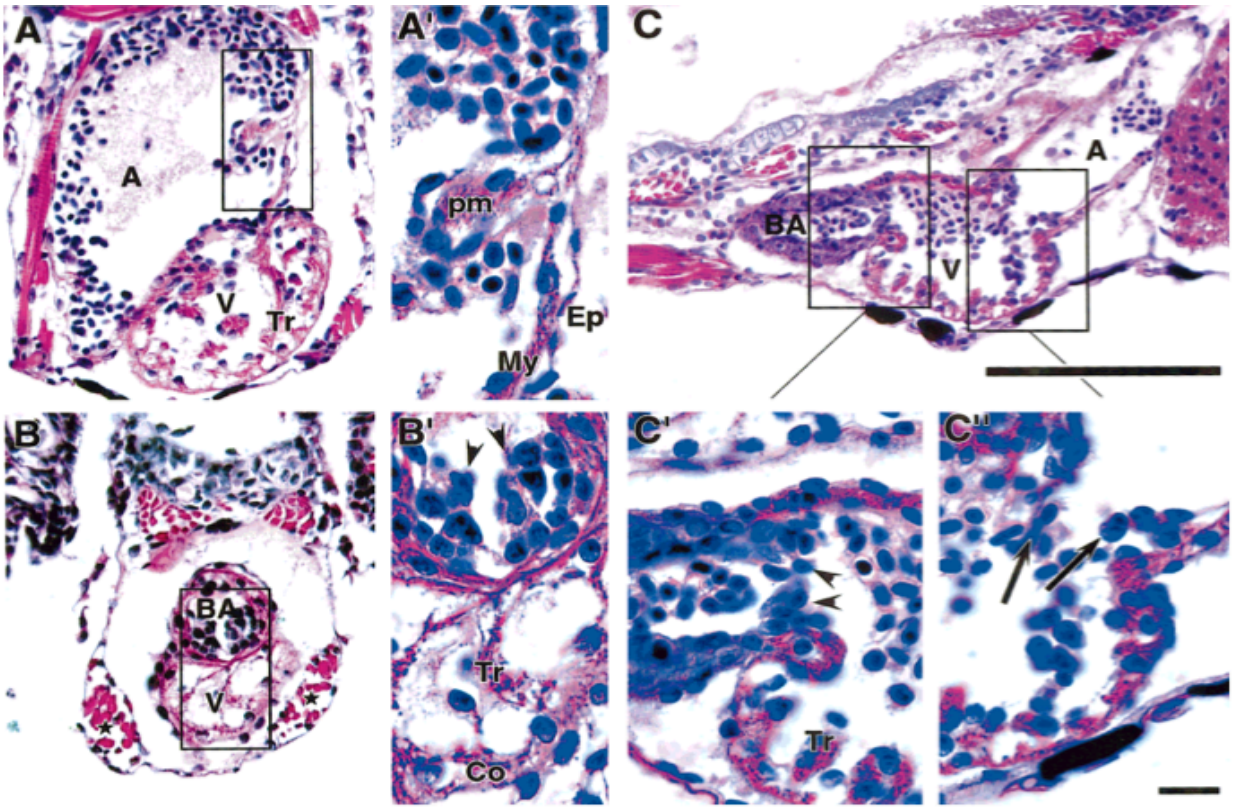

Fig. 3. Transverse (A,B) and sagittal (C) sections through a 5-days post-fertilization zebrafish heart. **A**: Caudal cross-section shows the atrium (filled with blood) and the ventricle with prominent trabeculation. **A′**: High power view of the atrial wall with its single cell layer myocardium (My) covered by epicardium (Ep), and the first forming pectinate muscle (pm) protruding into the lumen. **B**: Cranial section of the same specimen shows the myocardial character of the bulbus arteriosus, and the cushion-like character of the developing valves. **B′**: High power view of the ventricular wall structure. The compact layer (Co) is two cell layers, while the trabeculae (Tr) are single-cell thick. Arrowheads point to the ventriculo-bulbar valve leaflets. **C**: All chambers are encountered on the sagittal section. Note the spouting of the trabeculation in the outer curvature of the ventricle (partly filled with blood). Boxed areas show the character of the ventriculo-bulbar (arrowheads, **C′**) and atrioventricular (arrows, **C″**) valves. Hematoxylin-eosin staining. A, atrium; BA, bulbus arteriosus; ★, pericardial muscles; V, ventricle. Scale bar = 100 microns in A–C; 10 microns in A′–C′, C″.

Figure 13: Frontal and sagittal sections through an adult zebrafish heart (Hu et al., 2000)

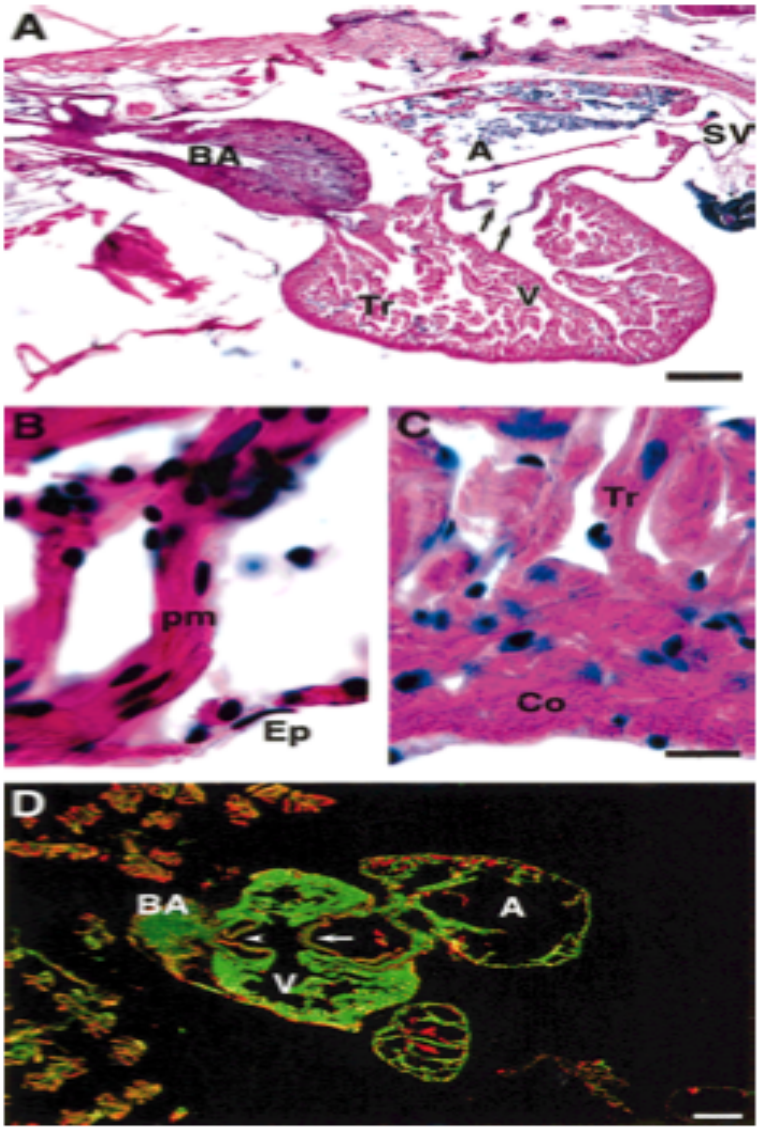

Fig. 6. Sagittal (A–C) and frontal (D) sections through an adult (3-months post-fertilization) zebrafish heart. **A:** All four chambers have their unique characteristic shape and morphology. Note the abundant pectinate muscles in the atrium. **B:** High power view of the atrium. While some areas of the myocardium are single-cell thick, the pectinate muscles (pm) can reach to three cell layers. Ep, epicardium. **C:** High power view of the ventricular wall. Increase in cell size is apparent from comparison with sections in earlier stages at the same magnification (100×). Compact myocardium (Co) reaches up to four cell layers. The trabeculae (Tr) are considerably thicker than at the earlier developing stages. Hematoxylin-eosin staining. **D:** MF-20 (green) staining shows the continuity between the atrial and ventricular myocardium, and loses the MF-20 staining in the bulbus arteriosus and the valves (arrowhead points to ventriculo-bulbar valve, and arrow to atrioventricular valve). Nuclei (red) are counterstained with propidium iodide. A, atrium; BA, bulbus arteriosus; SV, sinus venosus; V, ventricle. Scale bars = 100 microns in A, D; and 10 microns in B, C.

Figure 14: Comparison of atrial chamber morphology in control and oil+dispersant treated 30 hpf embryos

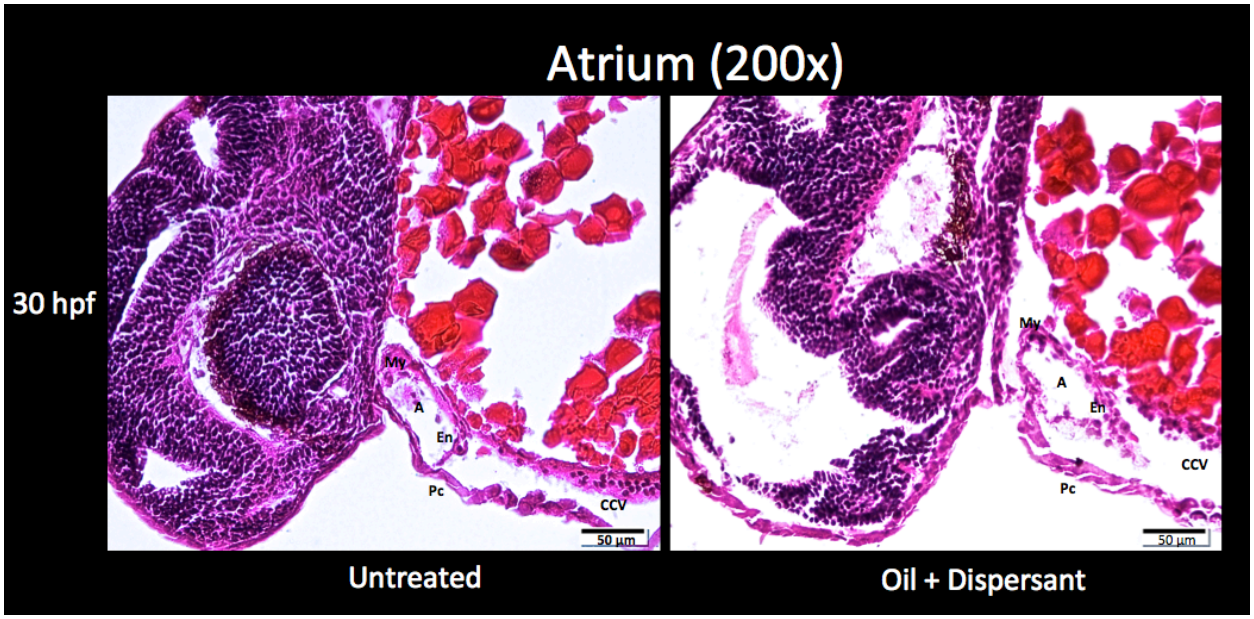

Figure 14.1: Comparison of atrial chamber morphology in control and oil+dispersant treated 30 hpf embryos

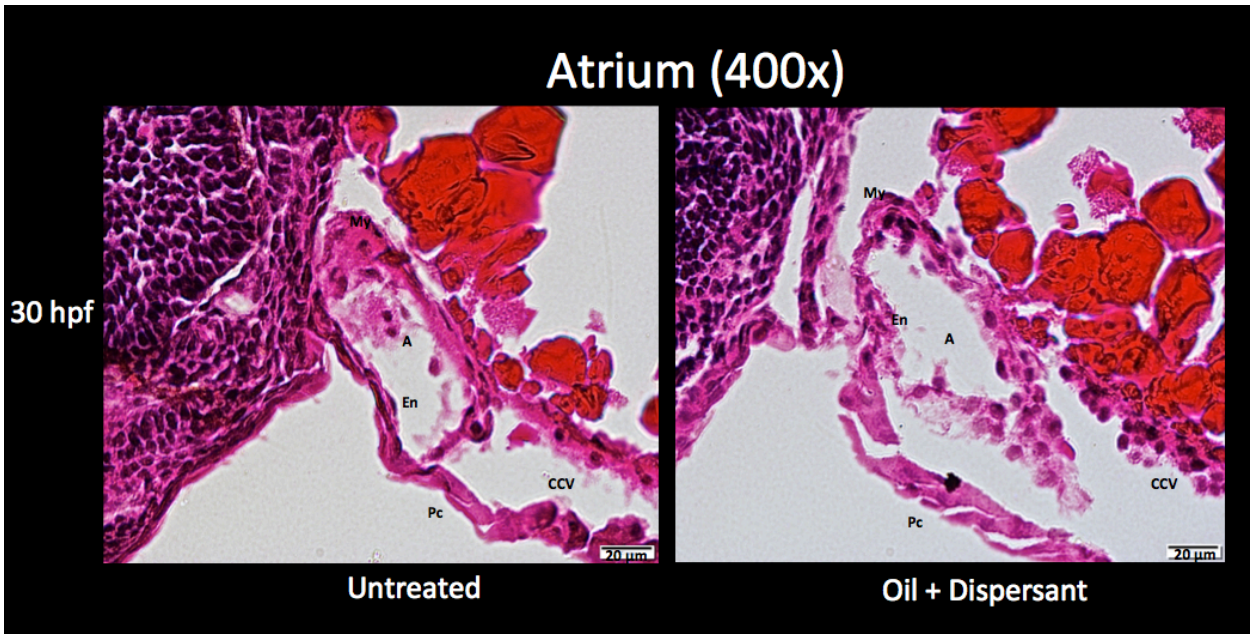

Figure 15: Comparison of atrial chamber morphology in control and oil+dispersant treated 36 hpf embryos

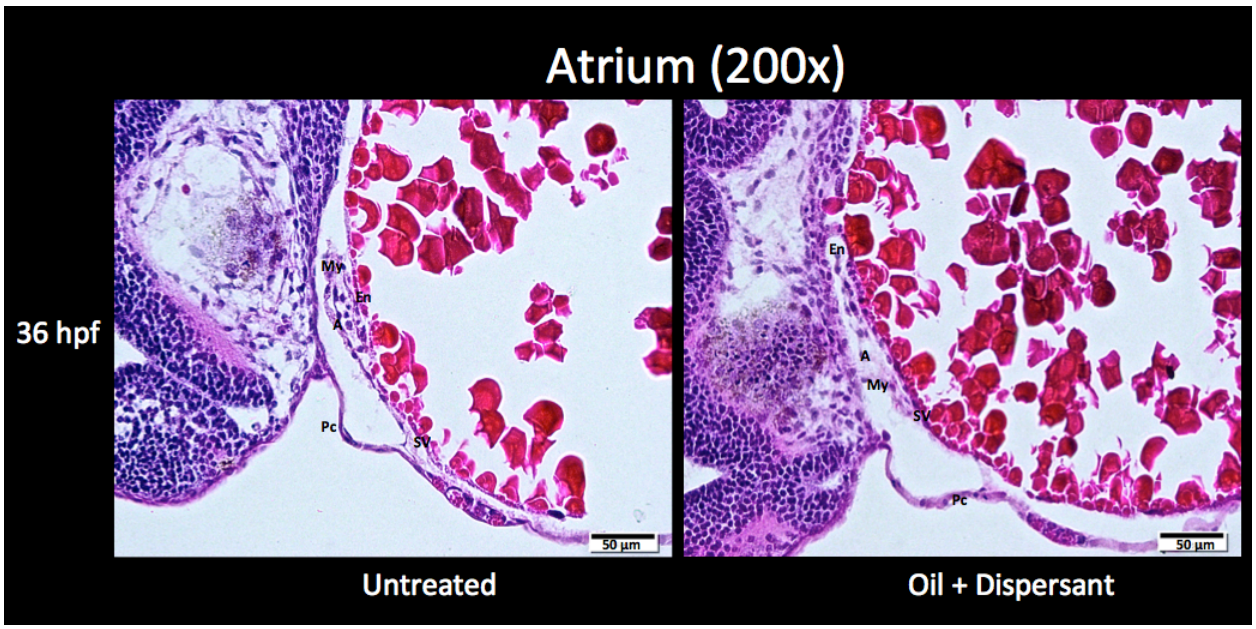

Figure 15.1: Comparison of atrial chamber morphology in control and oil+dispersant treated 36 hpf embryos

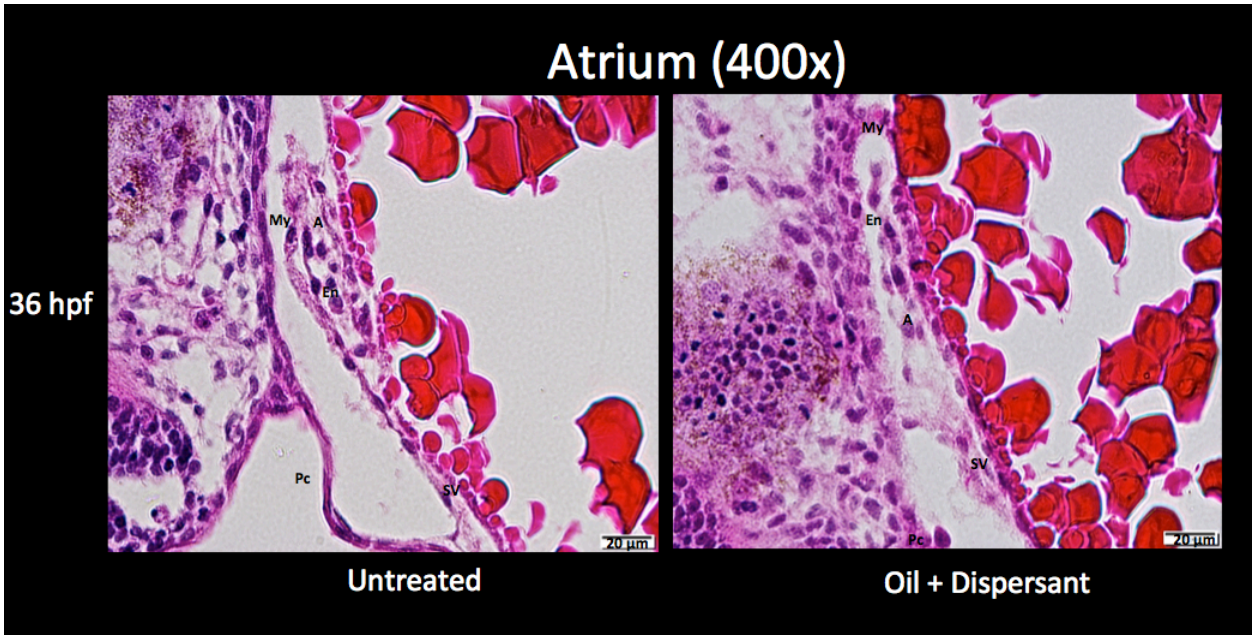

Figure 16: Comparison of atrial chamber morphology in control and oil+dispersant treated 48 hpf larvae

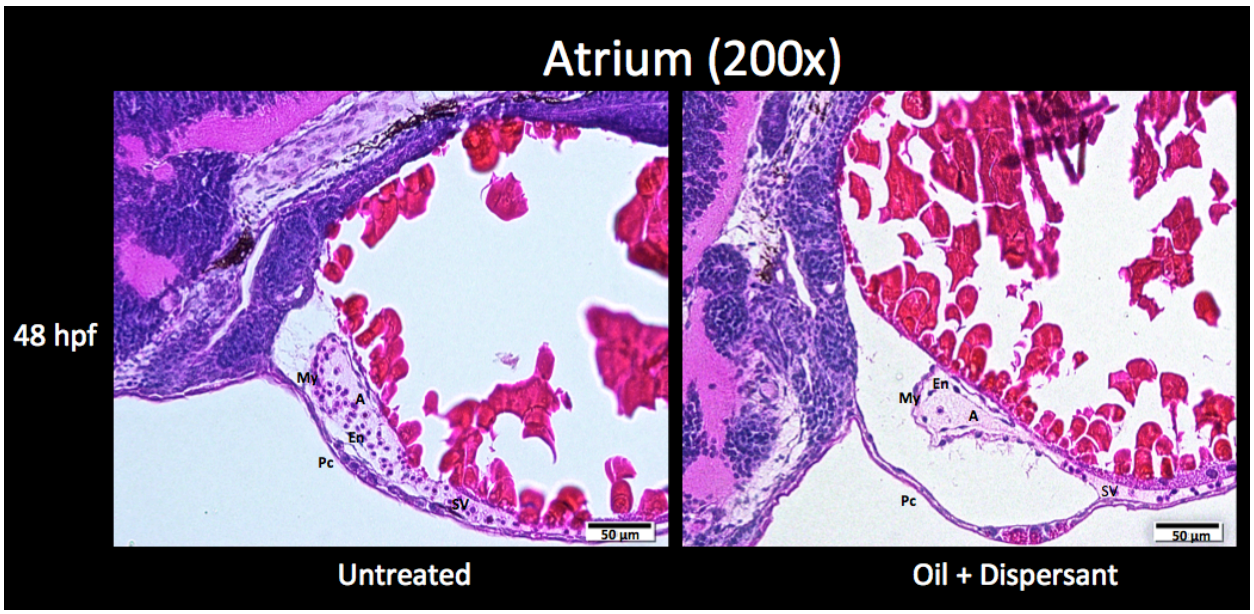

Figure 16.1: Comparison of atrial chamber morphology in control and oil+dispersant treated 48 hpf larvae

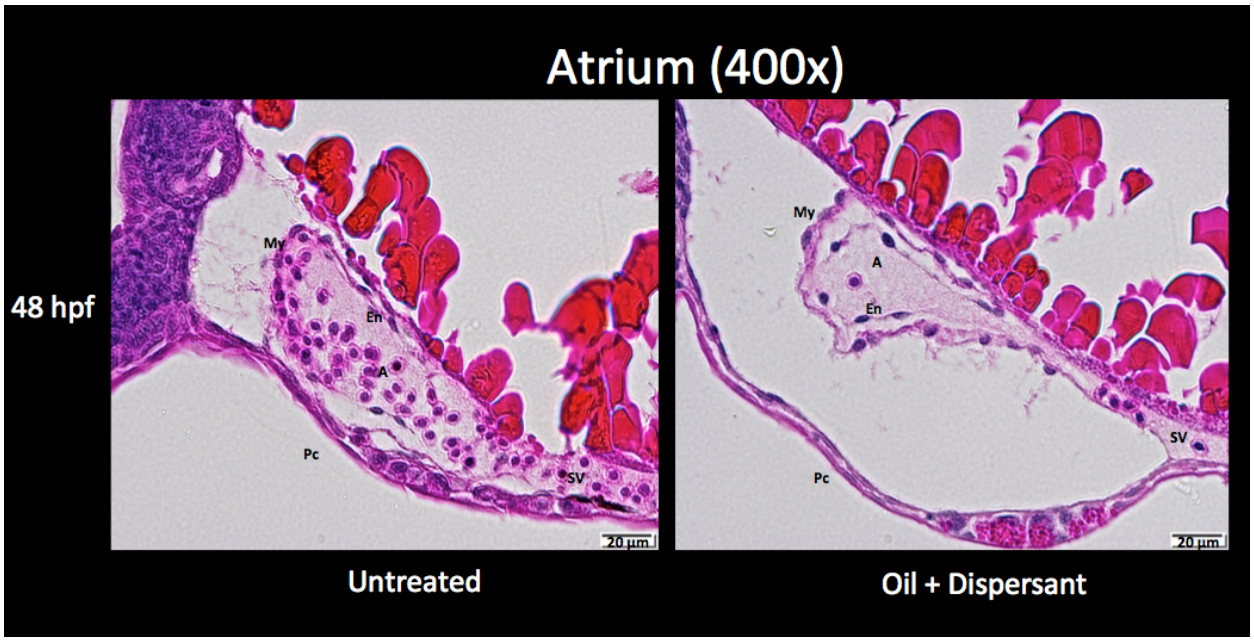

Figure 17: Comparison of atrial chamber morphology in control and oil+dispersant treated 72 hpf larvae

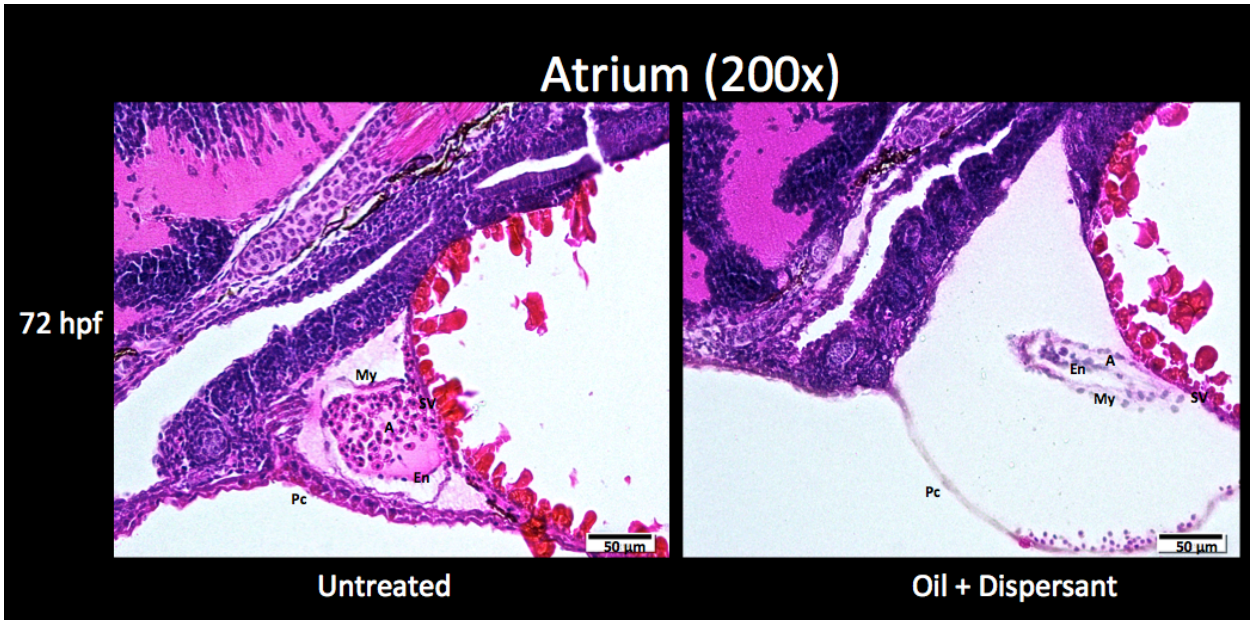

Figure 17.1: Comparison of atrial chamber morphology in control and oil+dispersant treated 72 hpf larvae

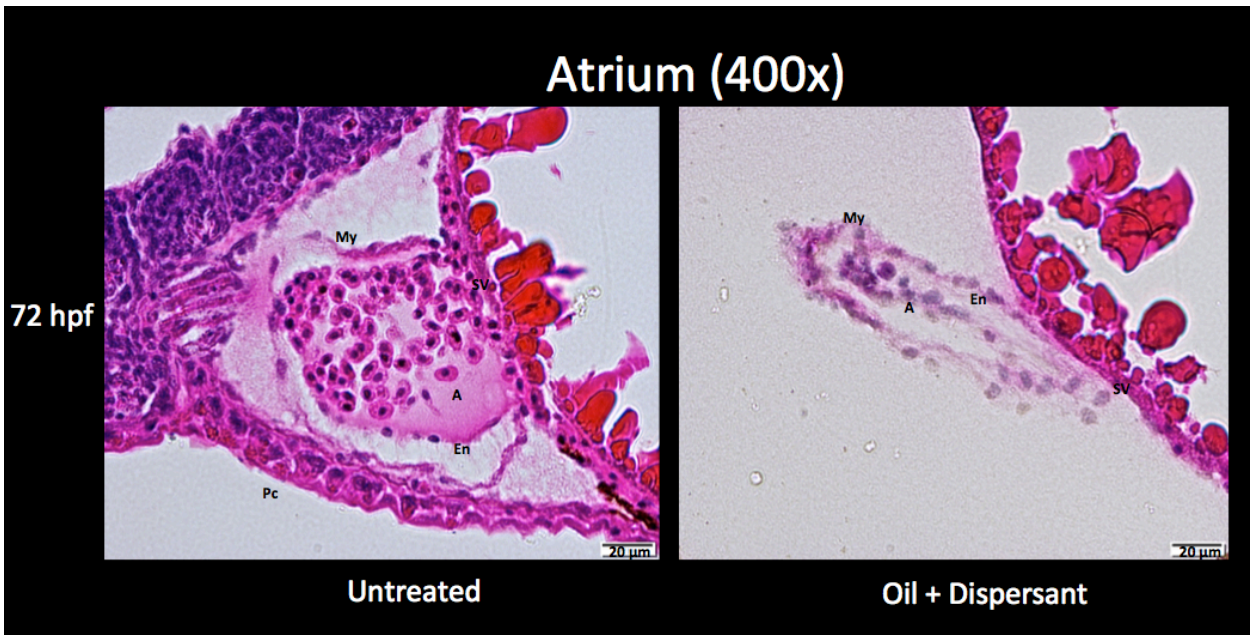

Figure 18: Comparison of atrial chamber morphology in control and oil+dispersant treated 96 hpf larvae

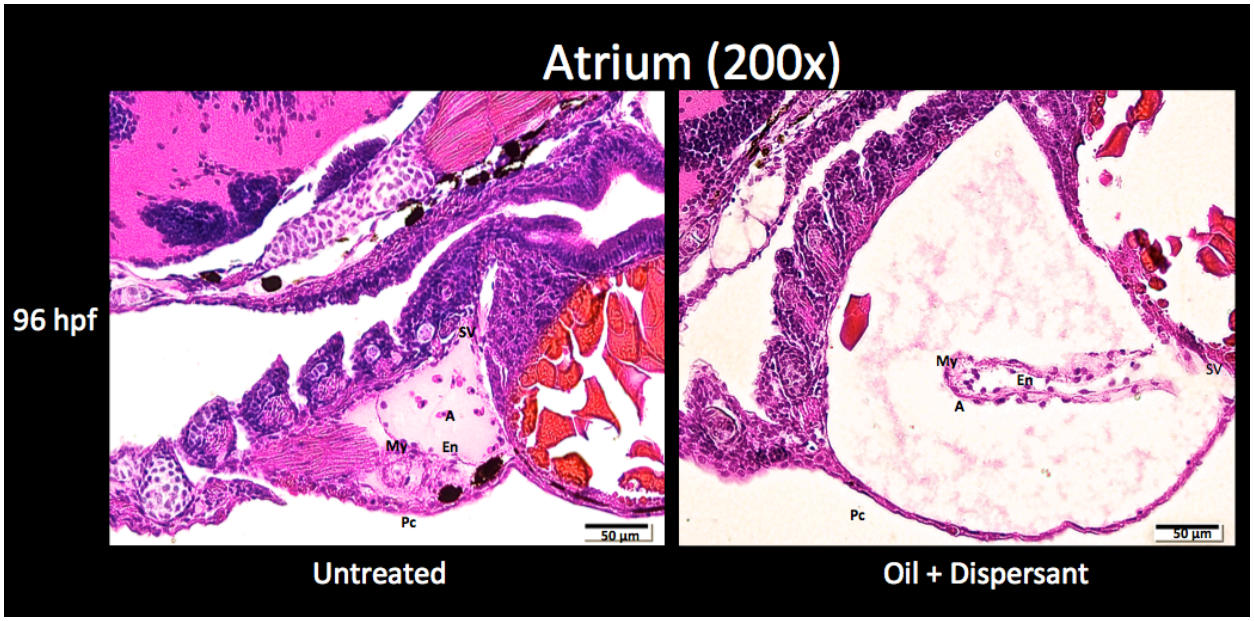

Figure 18.1: Comparison of atrial chamber morphology in control and oil+dispersant treated 96 hpf larvae

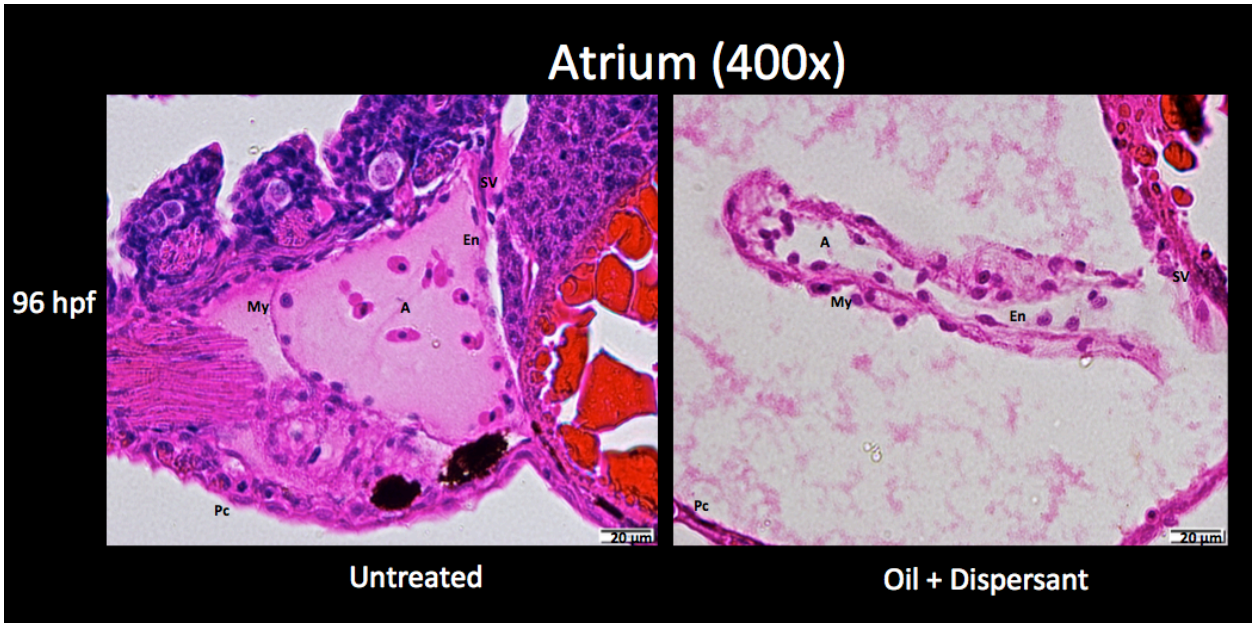

Figure 19: Comparison of ventricular chamber morphology in control and oil+dispersant treated 30 hpf embryos

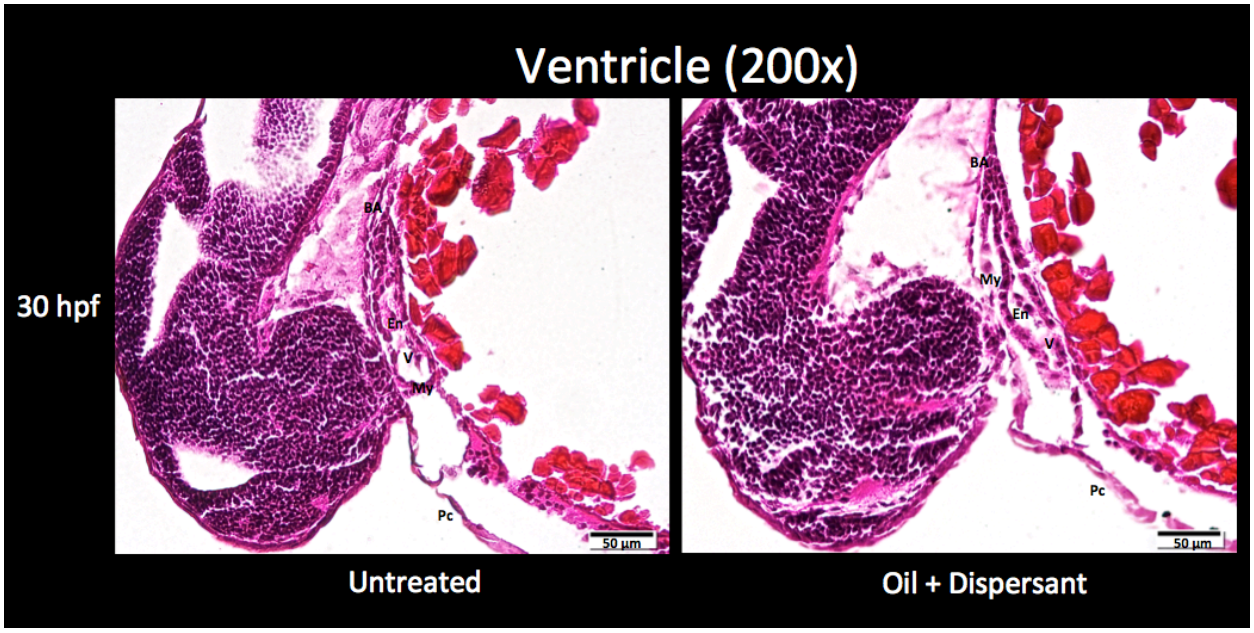

Figure 19.1: Comparison of ventricular chamber morphology in control and oil+dispersant treated 30 hpf embryos

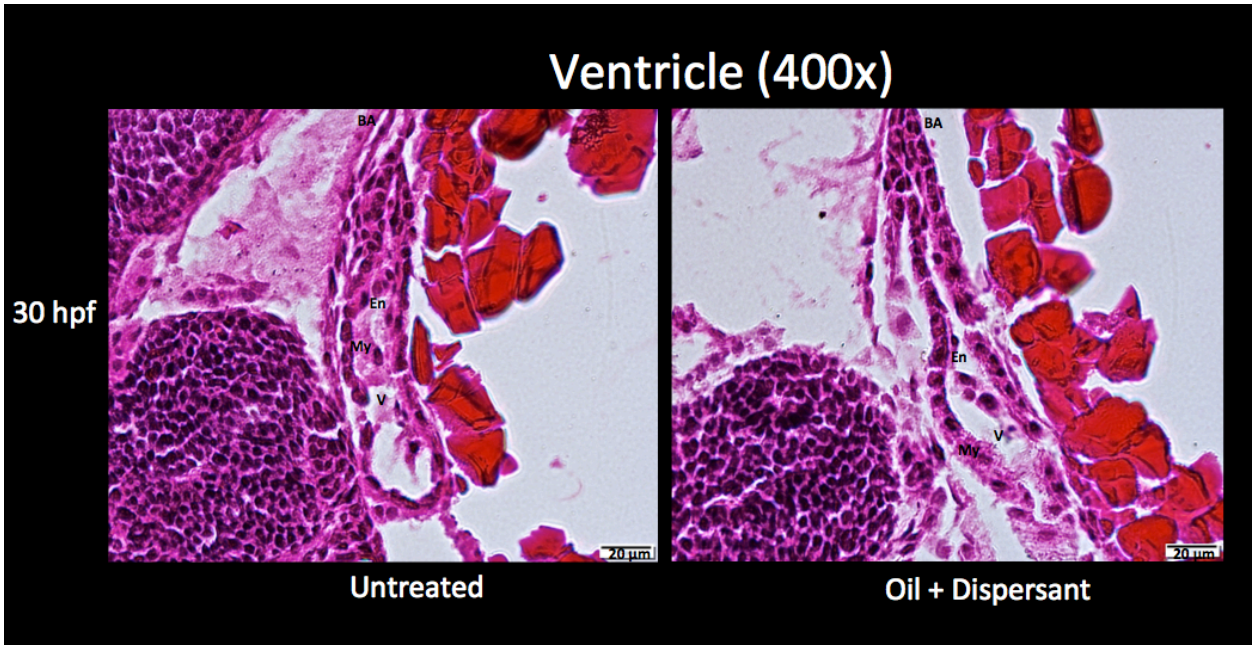

Figure 20: Comparison of ventricular chamber morphology in control and oil+dispersant treated 36 hpf embryos

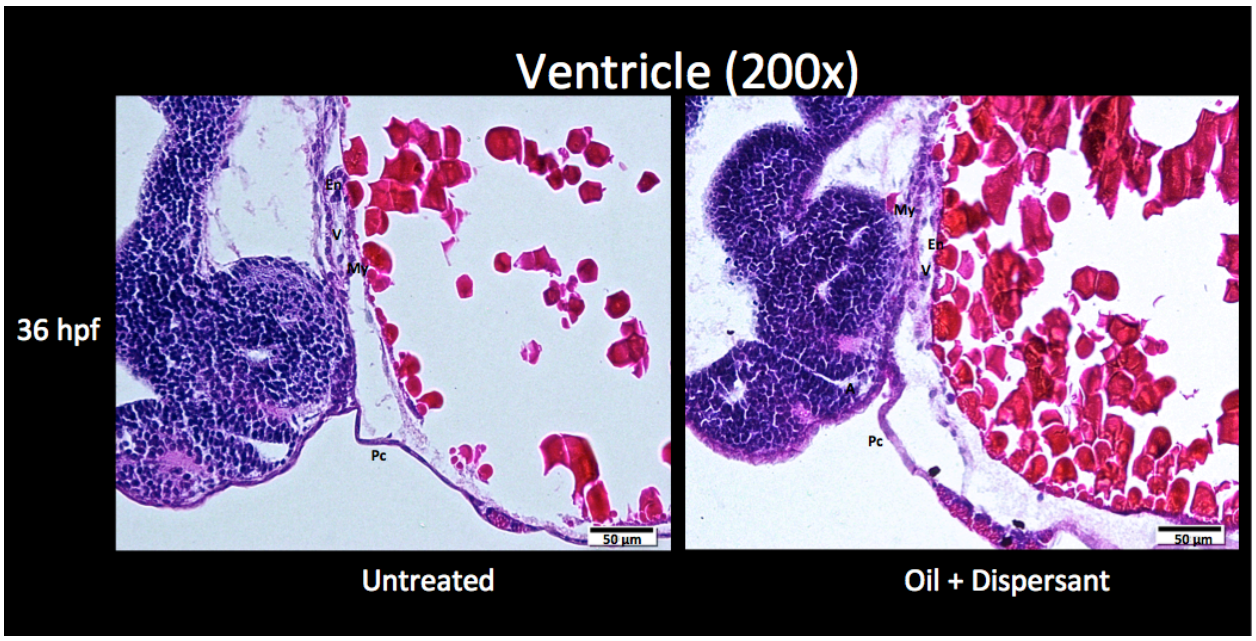

Figure 20.1: Comparison of ventricular chamber morphology in control and oil+dispersant treated 36 hpf embryos

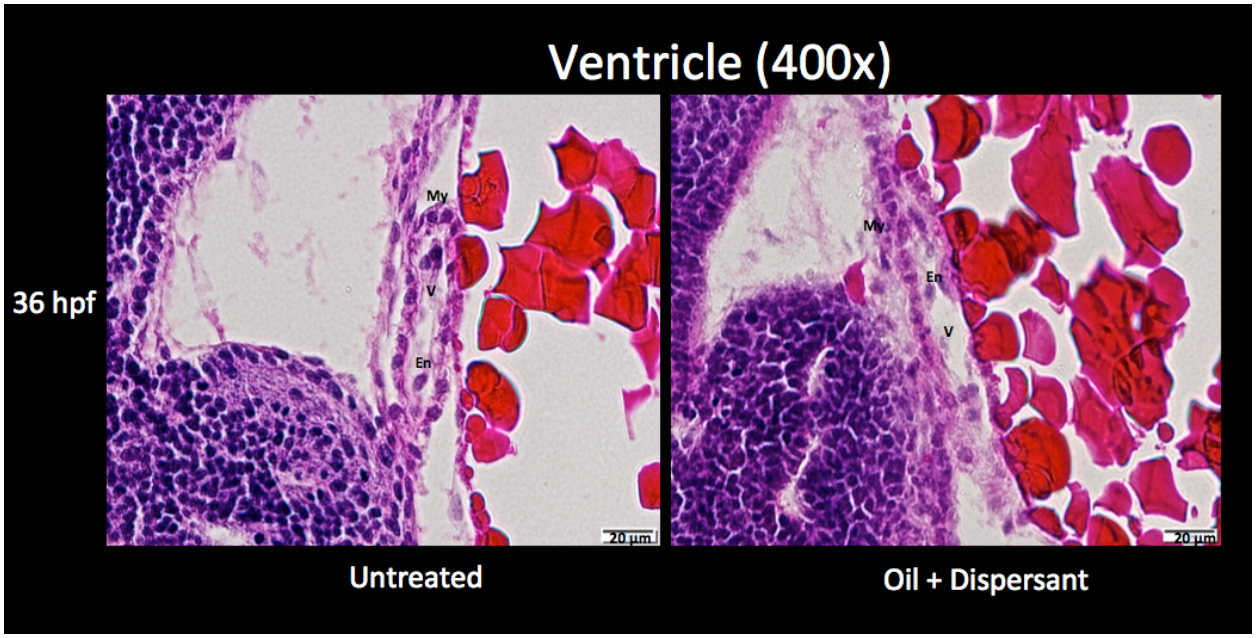

Figure 21: Comparison of ventricular chamber morphology in control and oil+dispersant treated 48 hpf larvae

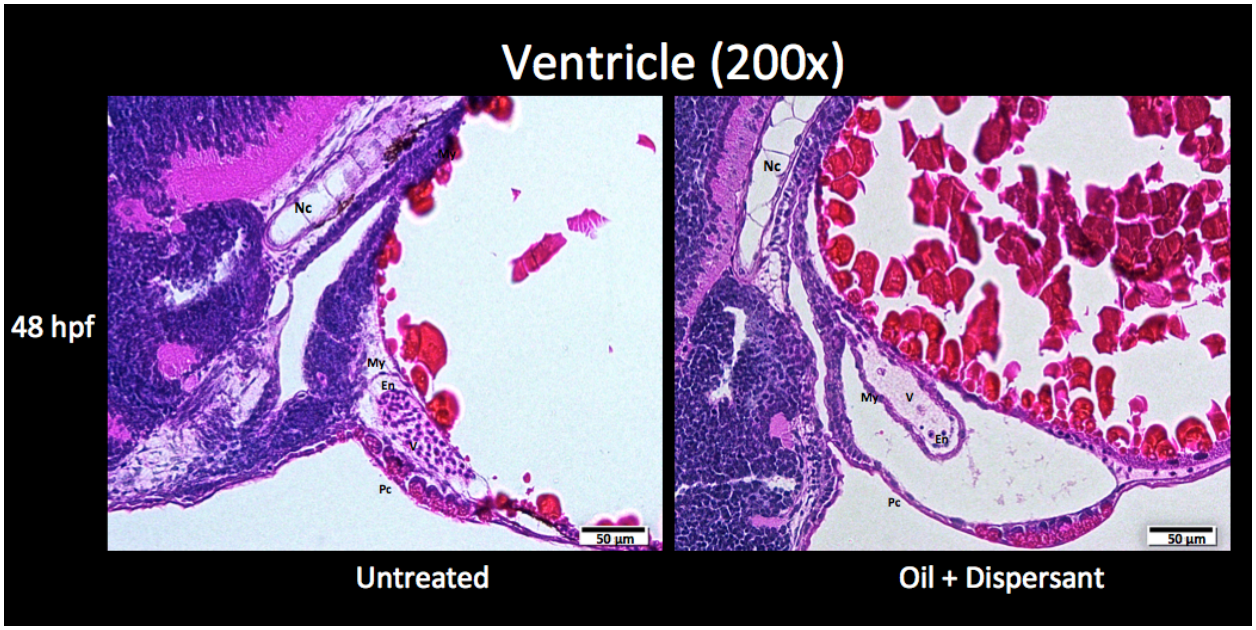

Figure 21.1: Comparison of ventricular chamber morphology in control and oil+dispersant treated 48 hpf larvae

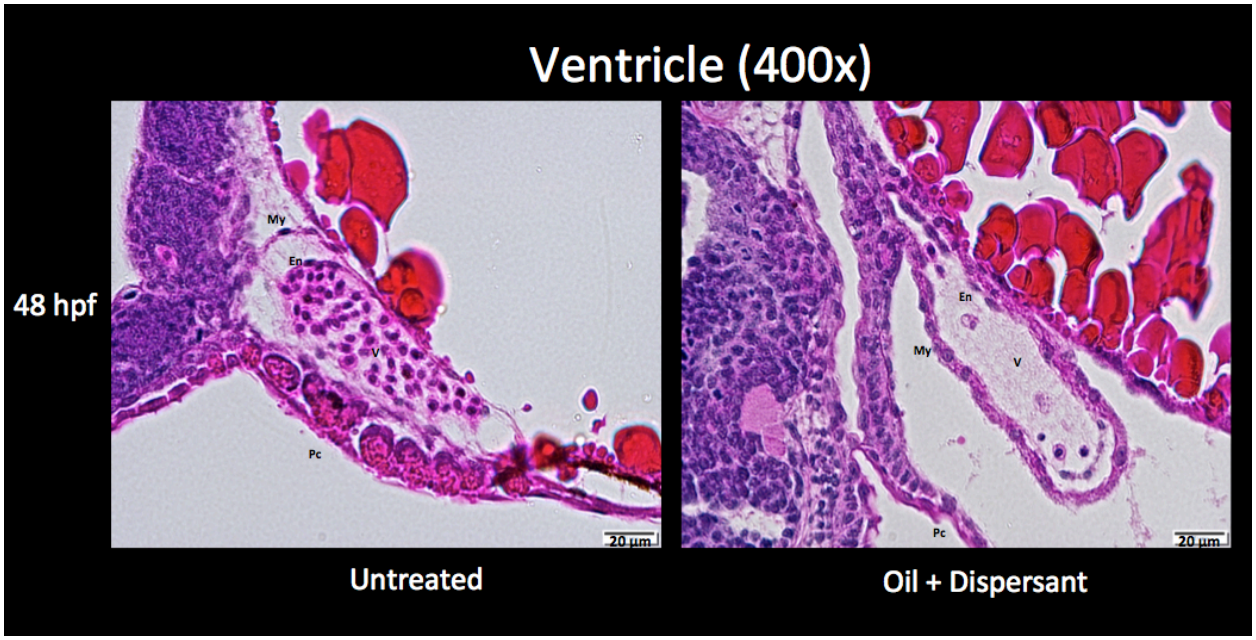

Figure 22: Comparison of ventricular chamber morphology in control and oil+dispersant treated 72 hpf larvae

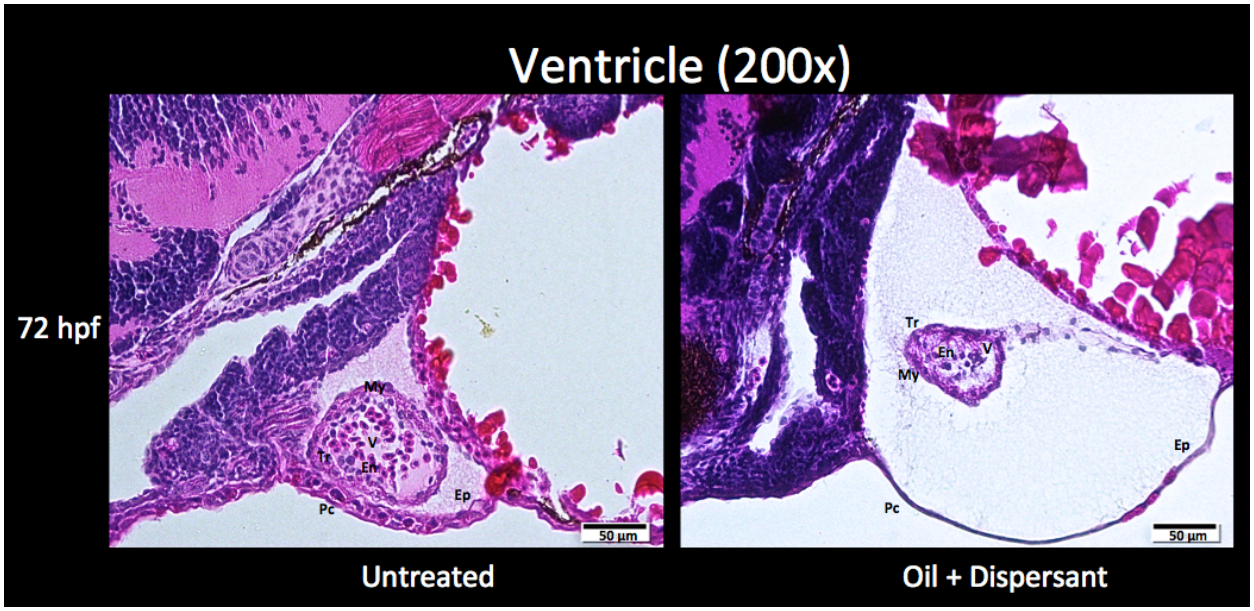

Figure 22.1: Comparison of ventricular chamber morphology in control and oil+dispersant treated 72 hpf larvae

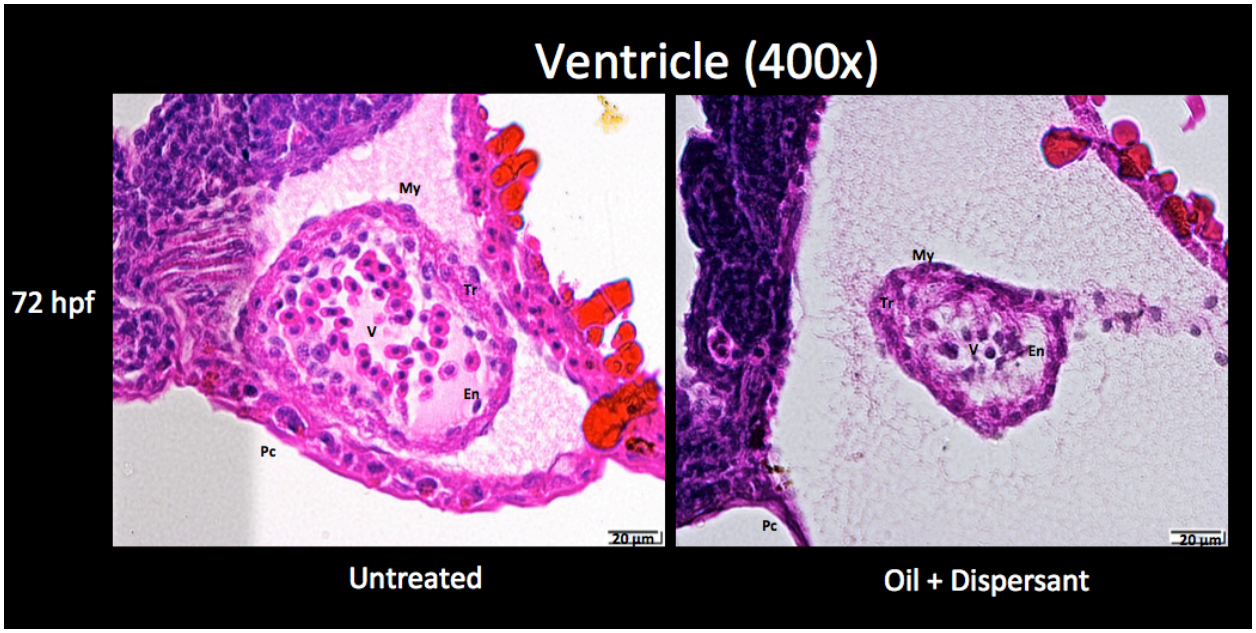

Figure 23: Comparison of ventricular chamber morphology in control and oil+dispersant treated 96 hpf larvae

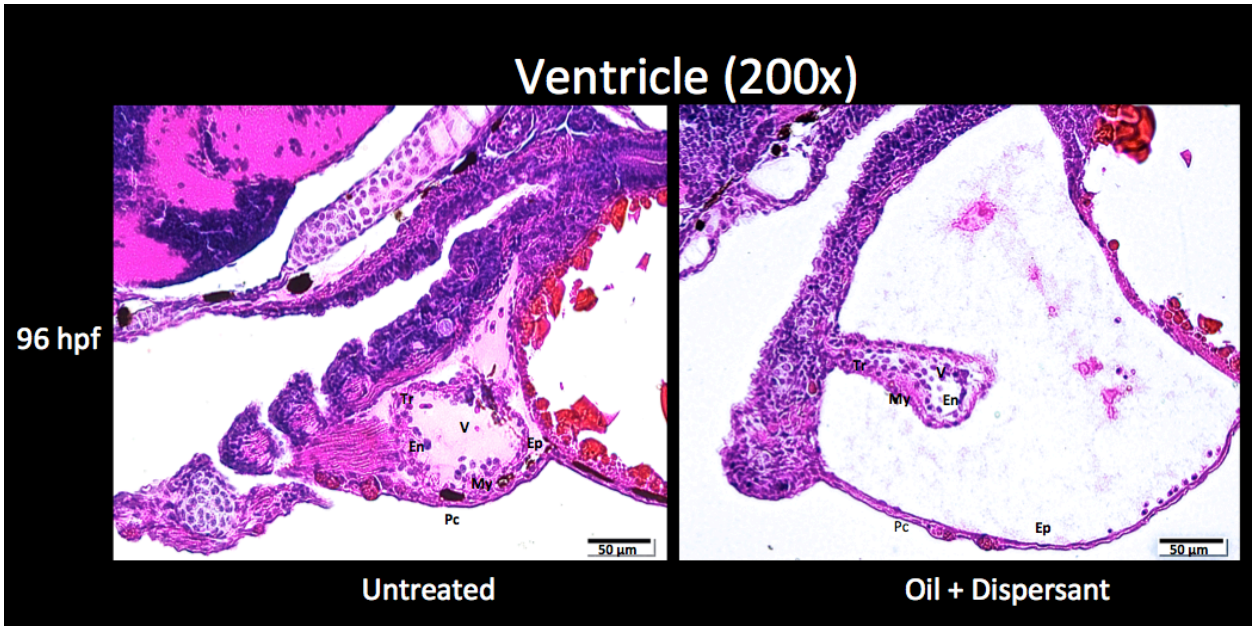

Figure 23.1: Comparison of ventricular chamber morphology in control and oil+dispersant treated 96 hpf larvae

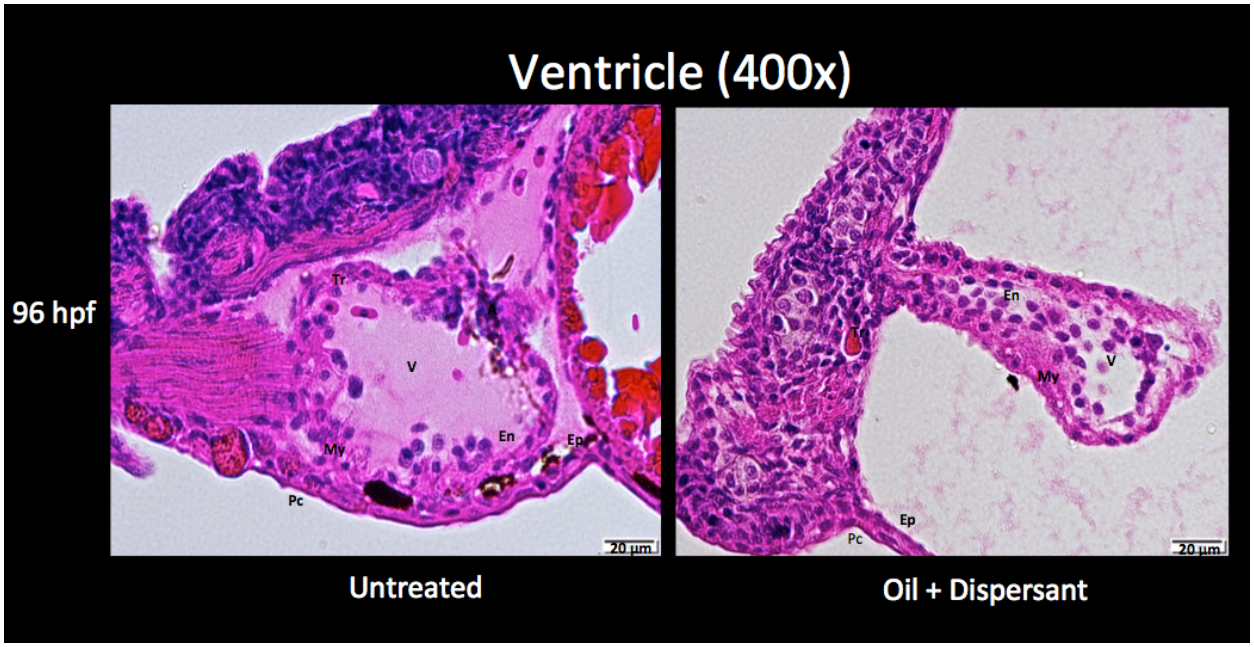

Figure 24: Comparison of AVC morphology in control and oil+dispersant treated 48 hpf larvae

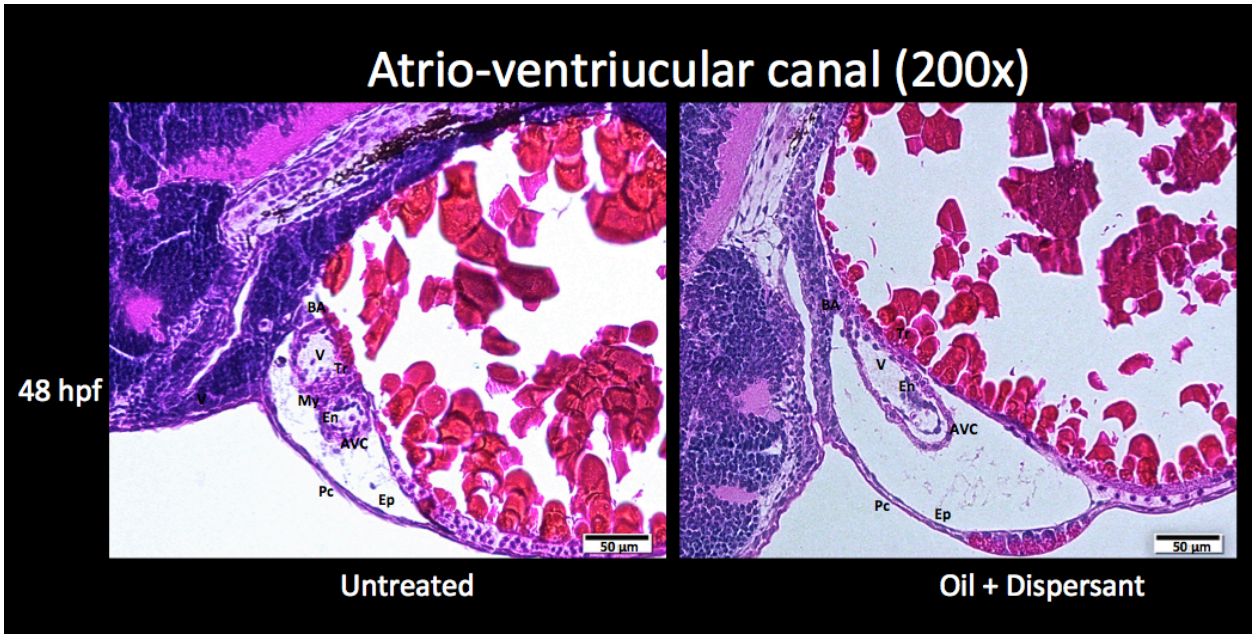

Figure 24.1: Comparison of AVC morphology in control and oil+dispersant treated 48 hpf larvae

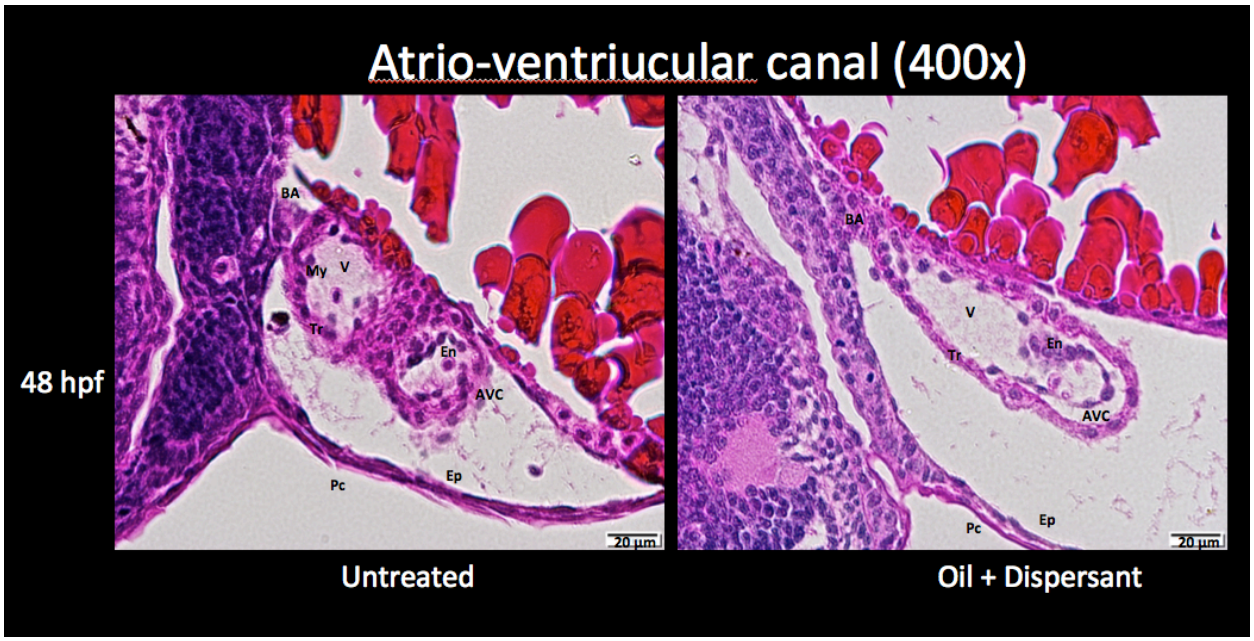

Figure 25: Comparison of AVC morphology in control and oil+dispersant treated 72 hpf larvae

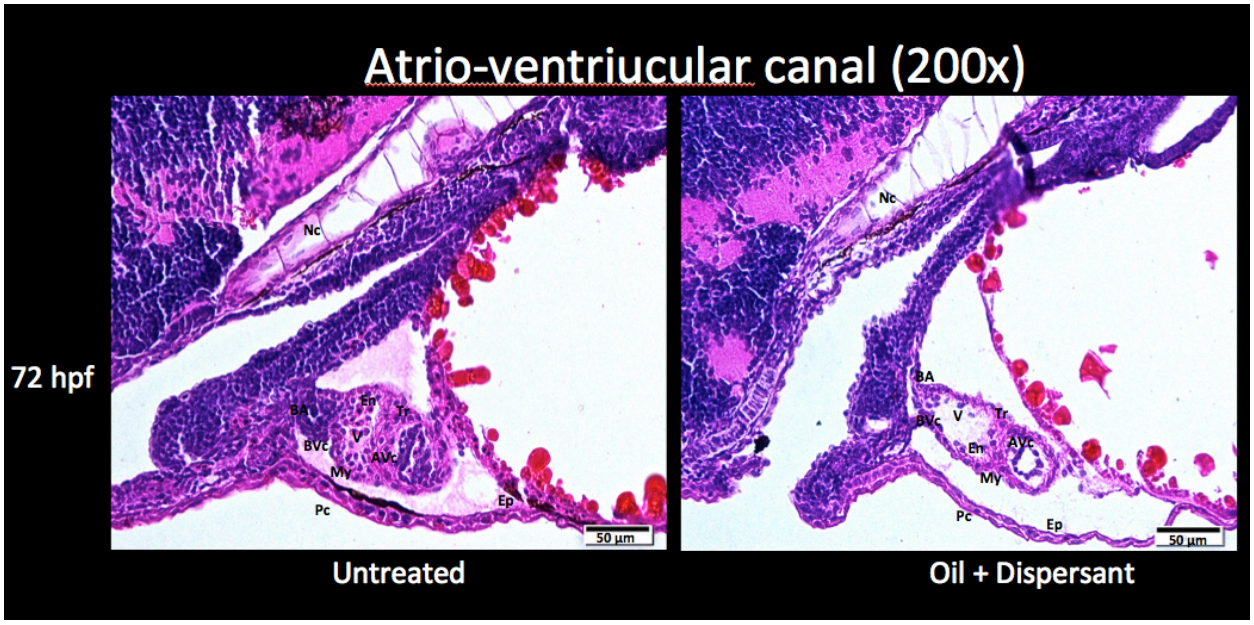

Figure 25.1: Comparison of AVC morphology in control and oil+dispersant treated 72 hpf larvae

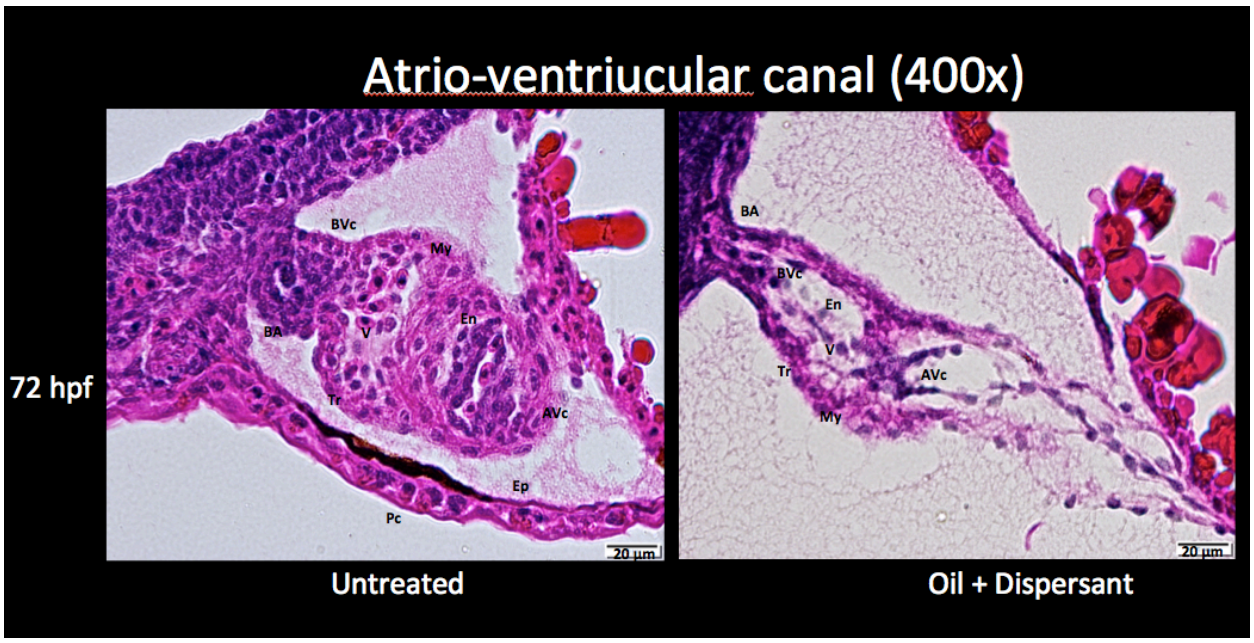

Figure 26: Comparison of AVC morphology in control and oil+dispersant treated 96 hpf larvae

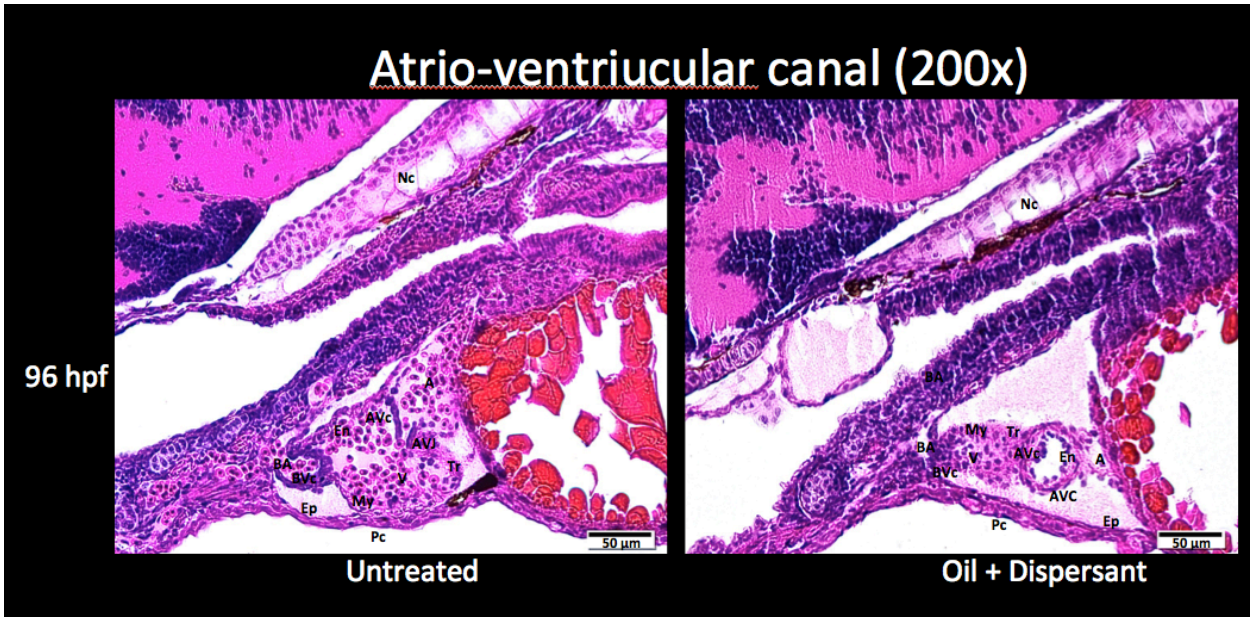

Figure 26.1: Comparison of AVC morphology in control and oil+dispersant treated 96 hpf larvae

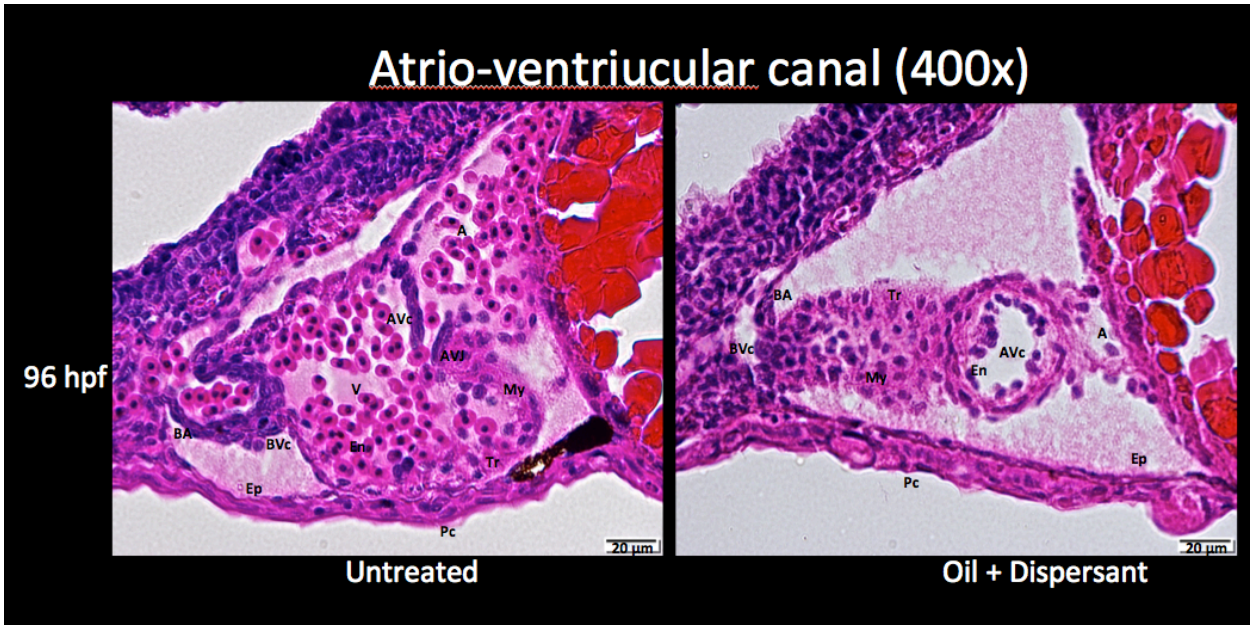

Figure 27: Comparison of gross morphology in control and oil+dispersant treated 30 hpf embryos

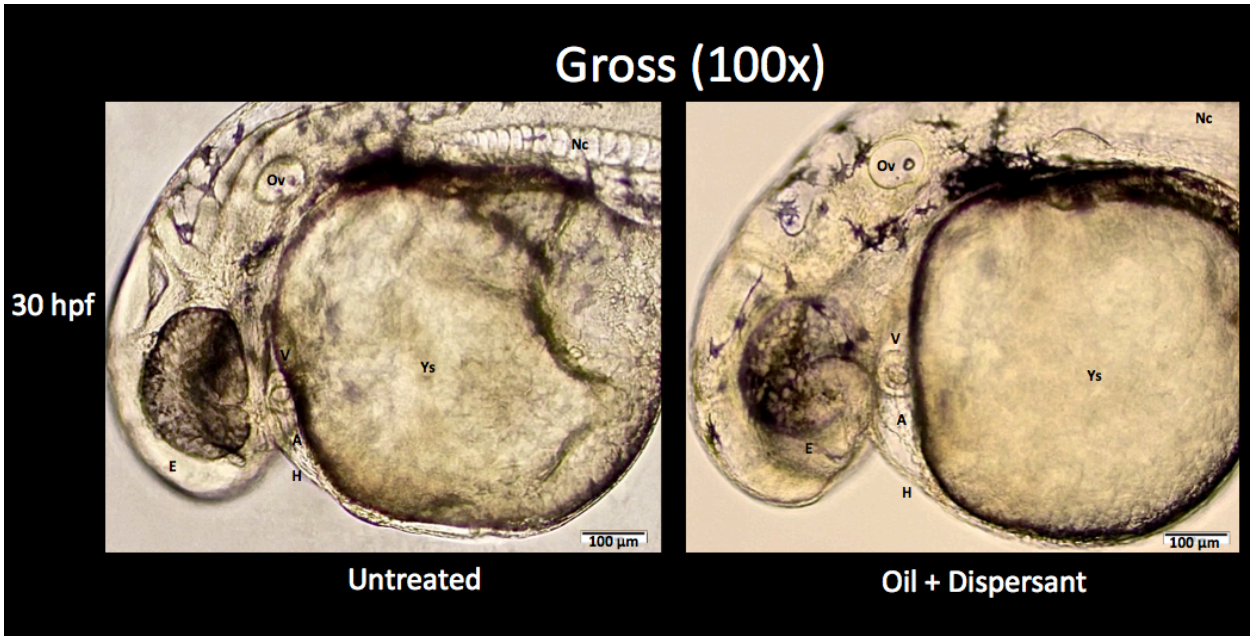

Figure 28: Comparison of gross morphology in control and oil+dispersant treated 36 hpf embryos

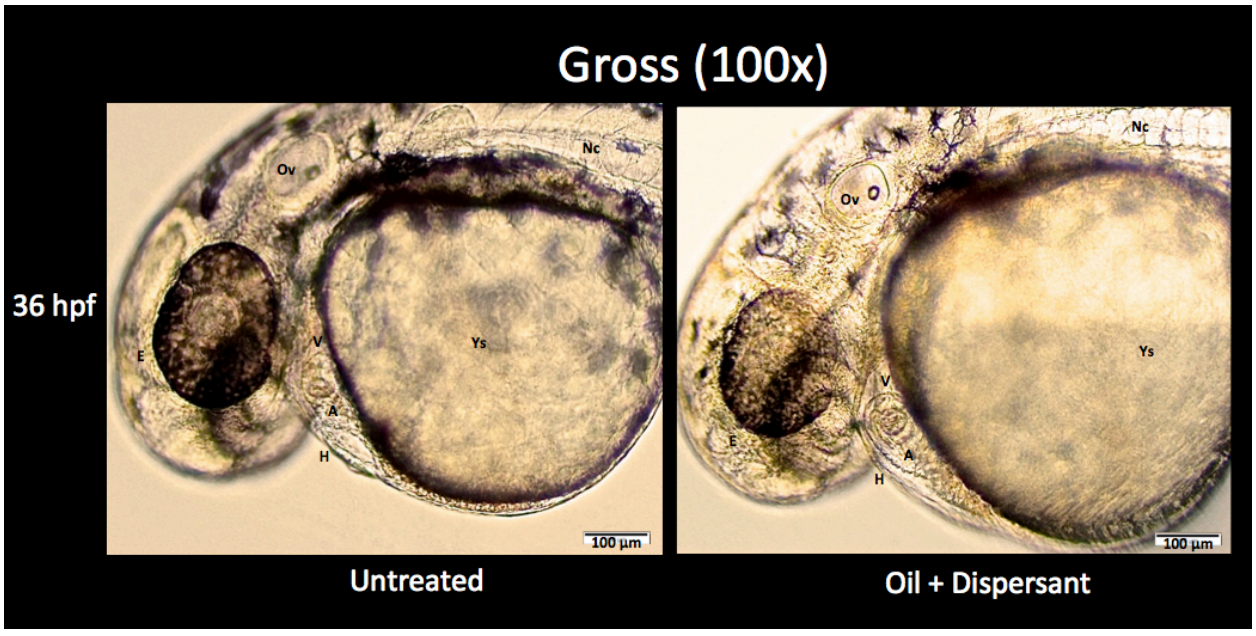

Figure 29: Comparison of gross morphology in control and oil+dispersant treated 48 hpf larvae

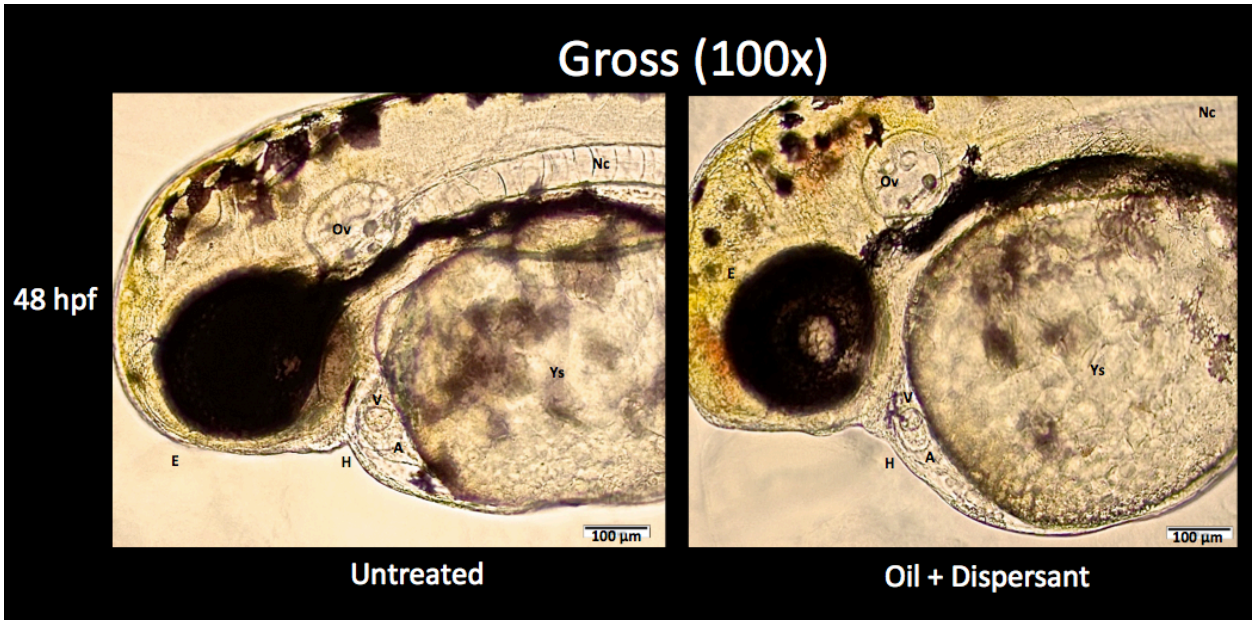

Figure 30: Comparison of gross morphology in control and oil+dispersant treated 72 hpf larvae

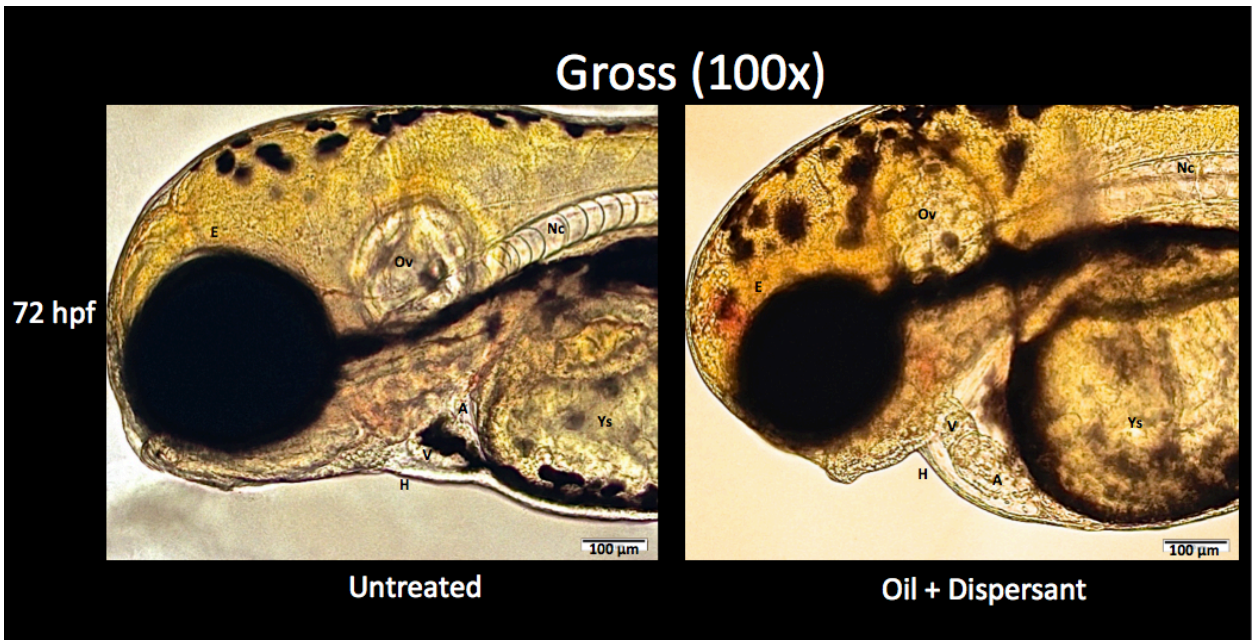

Figure 31: Comparison of gross morphology in control and oil+dispersant treated 96 hpf larvae

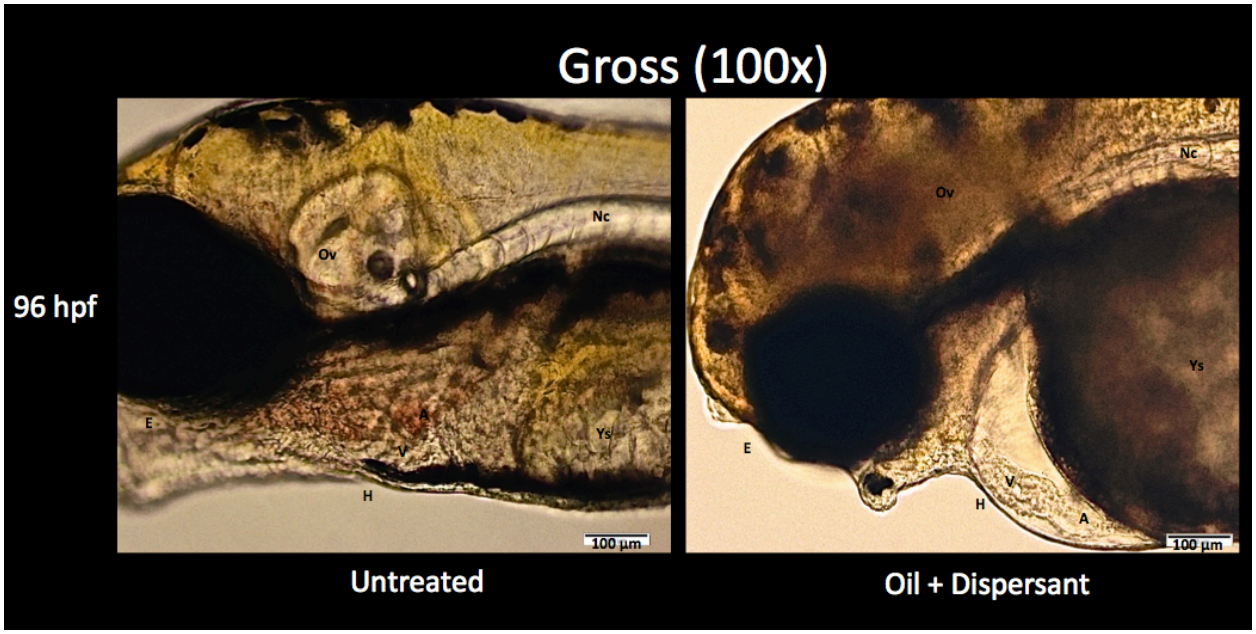

Figure 32: Comparison of gross morphology in control and oil+dispersant treated 30 hpf embryos

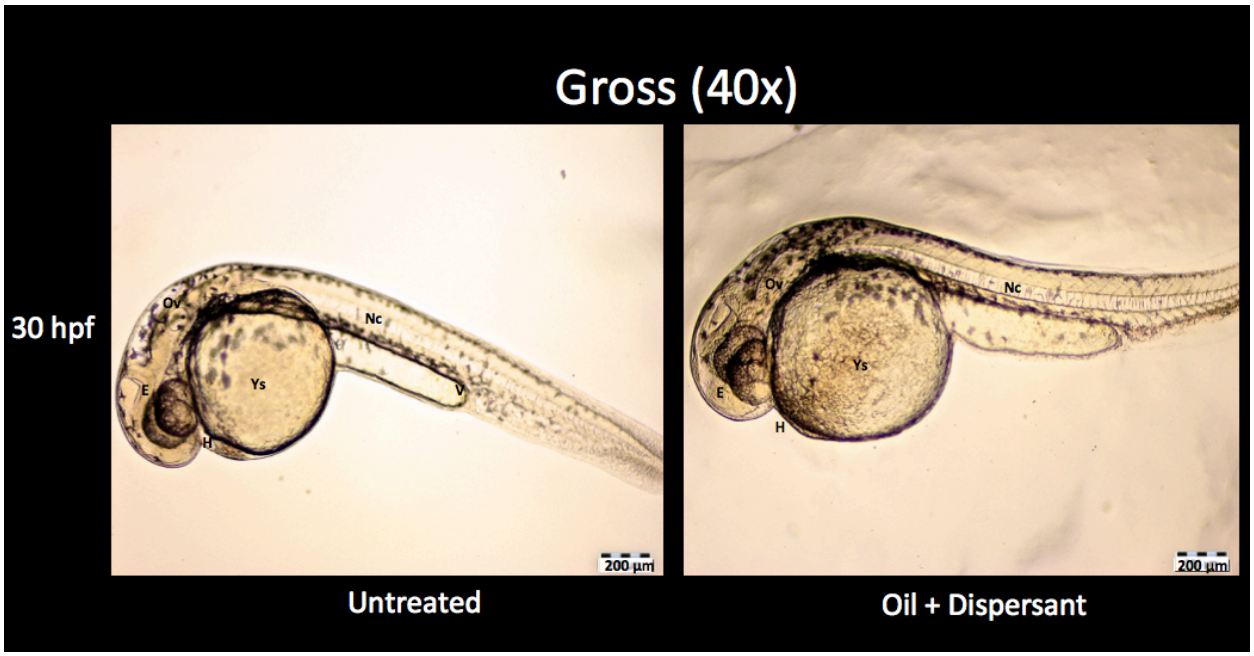

Figure 33: Comparison of gross morphology in control and oil+dispersant treated 36 hpf embryos

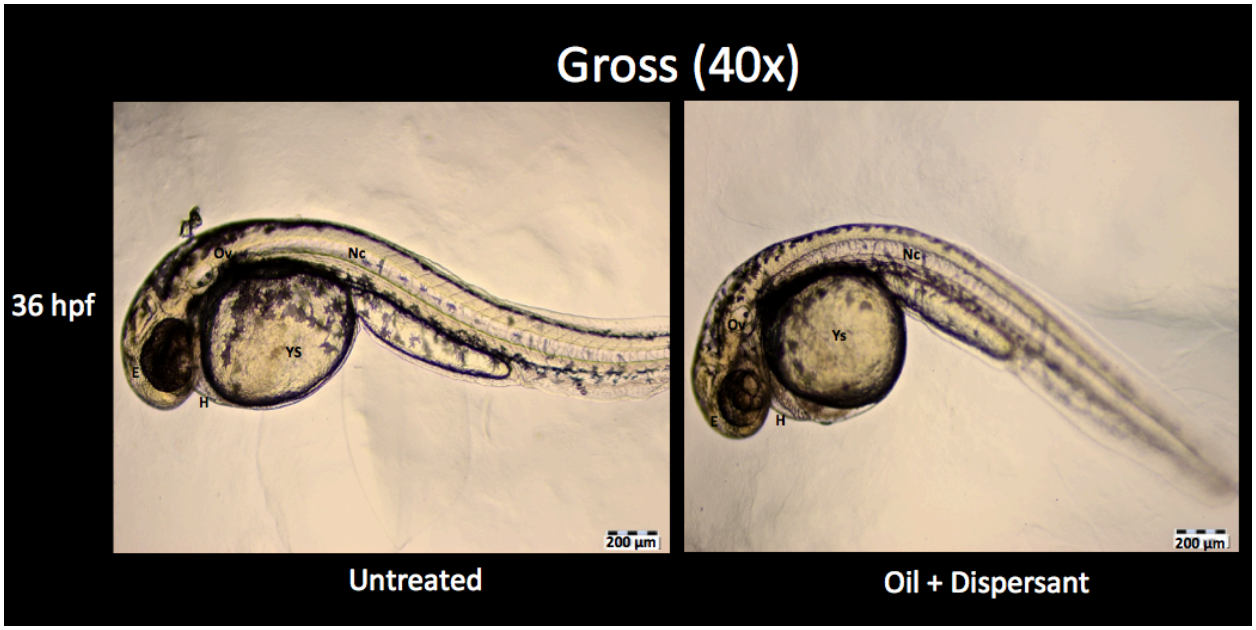

Figure 34: Comparison of gross morphology in control and oil+dispersant treated 48 hpf larvae

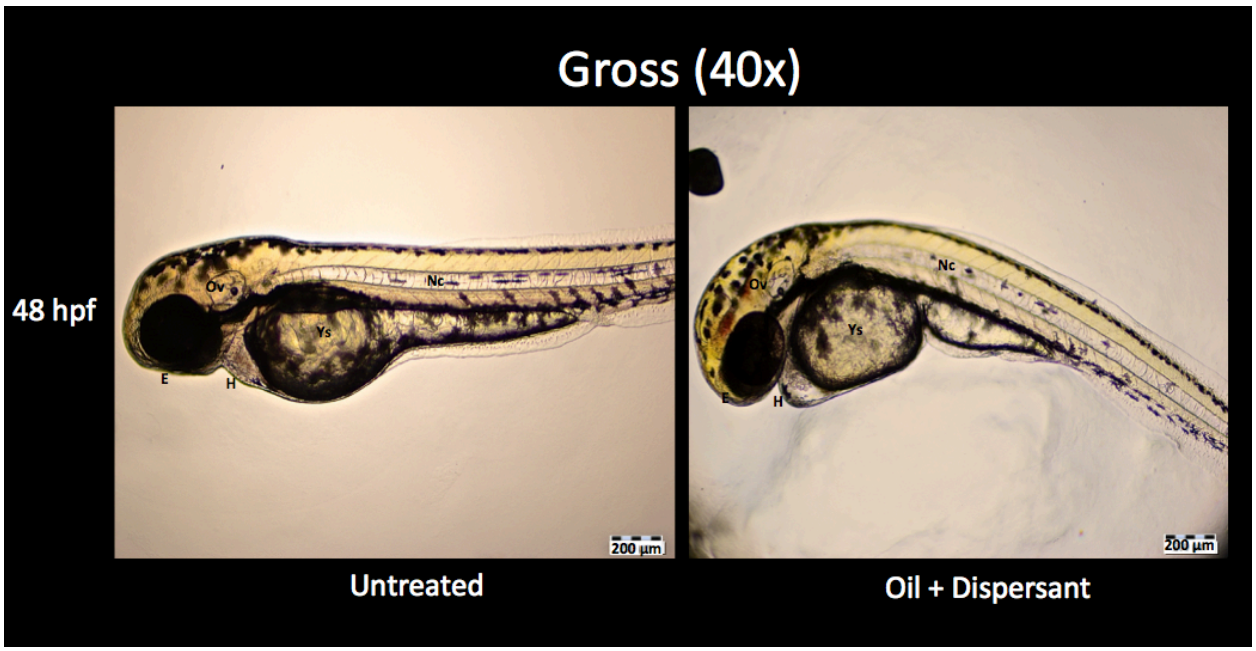

Figure 35: Comparison of gross morphology in control and oil+dispersant treated 72 hpf larvae

Figure 36: Comparison of gross morphology in control and oil+dispersant treated 96 hpf larvae

Table 1: Morphometric analysis of area and perimeter of the zebrafish eye

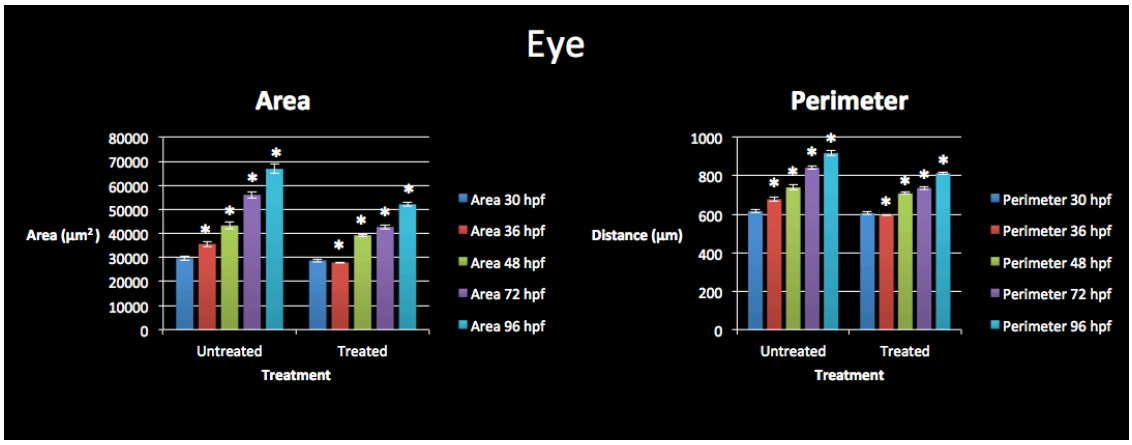

Table 1.1: Descriptive statistics of the zebrafish eye

Descriptives

		N	Mean	Std. Deviation	Std. Error	95% Confidence Interval for Mean		Minimum	Maximum
						Lower Bound	Upper Bound		
Area	Untr 30 hpf	5	29692.8238	2230.77956	997.63495	26922.9451	32462.7025	27389.18	32256.60
	Untr 36 hpf	5	35664.2346	2528.80634	1130.91657	32524.3068	38804.1624	32037.26	38735.47
	Untr 48 hpf	5	43334.8352	3214.09591	1437.38739	39344.0080	47325.6624	39381.38	47964.40
	Untr 72 hpf	5	56084.9264	3064.07974	1370.29812	52280.3689	59889.4839	51681.10	59828.74
	Untr 96 hpf	5	66883.4192	4135.71388	1849.54747	61748.2522	72018.5862	62469.67	73210.85
	O+D 30 hpf	5	28796.7154	1465.09807	655.21177	26977.5559	30615.8749	27058.51	30731.12
	O+D 36 hpf	5	30129.7706	1451.39168	649.08209	28327.6298	31931.9114	28313.36	31670.04
	O+D 48 hpf	5	39247.3462	1175.45566	525.67975	37787.8252	40706.8672	38244.98	41131.71
	O+D 72 hpf	5	42739.1932	1926.83574	861.70714	40346.7106	45131.6758	41096.44	45821.67
	O+D 96 hpf	5	52132.7906	1628.84822	728.44307	50110.3084	54155.2728	50586.59	54715.52
	Total	50	42470.6055	12301.1833	1739.65003	38974.6479	45966.5631	27058.51	73210.85
Perimeter	Untr 30 hpf	5	616.4084	21.25292	9.50460	590.0194	642.7974	595.42	641.41
	Untr 36 hpf	5	678.2902	27.97074	12.50889	643.5599	713.0205	637.68	714.97
	Untr 48 hpf	5	739.8066	28.58160	12.78208	704.3179	775.2953	703.78	780.65
	Untr 72 hpf	5	842.8102	22.93782	10.25811	814.3291	871.2913	807.23	867.24
	Untr 96 hpf	5	917.8022	28.63512	12.80602	882.2470	953.3574	886.23	960.11
	O+D 30 hpf	5	605.9272	15.92900	7.12367	586.1487	625.7057	584.21	626.59
	O+D 36 hpf	5	615.6148	14.97438	6.69675	597.0216	634.2080	596.57	631.66
	O+D 48 hpf	5	708.3038	11.54383	5.16256	693.9702	722.6374	699.05	728.01
	O+D 72 hpf	5	736.3638	16.95566	7.58280	715.3106	757.4170	720.65	762.08
	O+D 96 hpf	5	813.2830	16.02334	7.16586	793.3874	833.1786	797.53	830.55
	Total	50	727.4610	102.60476	14.51050	698.3011	756.6210	584.21	960.11

Table 2: Morphometric analysis of area and perimeter of the zebrafish otic vesicle

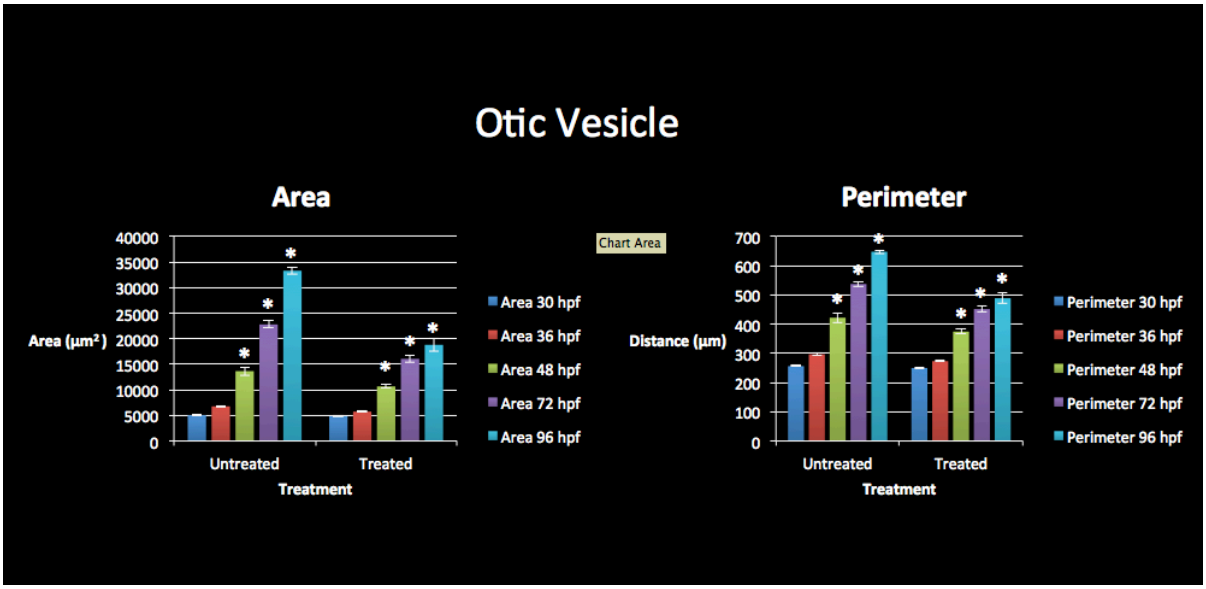

Table 2.1: Descriptive statistics of the zebrafish otic vesicle

Descriptives

		N	Mean	Std. Deviation	Std. Error	95% Confidence Interval for Mean		Minimum	Maximum
						Lower Bound	Upper Bound		
Area	Untr 30 hpf	5	5033.6384	204.26472	91.34996	4780.0103	5287.2665	4715.32	5247.69
	Untr 36 hpf	5	6779.3414	301.19531	134.69864	6405.3580	7153.3248	6511.94	7265.86
	Untr 48 hpf	5	13664.7172	1866.65591	834.79390	11346.9578	15982.4766	12379.08	16896.00
	Untr 72 hpf	5	22799.2920	1552.24891	694.18682	20871.9204	24726.6636	21386.46	24652.35
	Untr 96 hpf	5	33302.3884	1500.85947	671.20476	31438.8252	35165.9516	31234.84	35458.56
	O+D 30 hpf	5	4844.9376	171.27904	76.59832	4632.2666	5057.6086	4699.89	5113.22
	O+D 36 hpf	5	5746.5574	325.82678	145.71416	5341.9900	6151.1248	5436.17	6166.95
	O+D 48 hpf	5	10675.9252	829.49782	370.96270	9645.9676	11705.8828	9808.70	11807.03
	O+D 72 hpf	5	16069.1094	1491.53257	667.03364	14217.1271	17921.0917	14091.94	17631.18
	O+D 96 hpf	5	18808.7984	2792.51475	1248.85056	15341.4334	22276.1634	15578.84	22245.09
	Total	50	13772.4705	8966.08087	1267.99532	11224.3386	16320.6025	4699.89	35458.56
Perimeter	Untr 30 hpf	5	256.2472	4.93360	2.20637	250.1213	262.3731	249.11	262.48
	Untr 36 hpf	5	296.8238	7.88164	3.52478	287.0375	306.6101	287.64	307.62
	Untr 48 hpf	5	421.9464	37.57419	16.80369	375.2919	468.6009	396.50	487.23
	Untr 72 hpf	5	537.3506	18.87103	8.43938	513.9191	560.7821	520.16	559.44
	Untr 96 hpf	5	647.8278	14.09090	6.30164	630.3316	665.3240	628.09	667.84
	O+D 30 hpf	5	249.9618	5.28846	2.36507	243.3953	256.5283	245.30	258.48
	O+D 36 hpf	5	273.3004	6.07635	2.71743	265.7556	280.8452	266.40	281.40
	O+D 48 hpf	5	374.4716	16.83081	7.52697	353.5734	395.3698	355.61	391.54
	O+D 72 hpf	5	451.5534	21.23692	9.49744	425.1843	477.9225	423.72	474.14
	O+D 96 hpf	5	488.5502	38.73358	17.32218	440.4561	536.6443	444.84	540.28
	Total	50	399.8033	129.86336	18.36545	362.8966	436.7101	245.30	667.84

Table 3: Analysis of embryonic heart rates

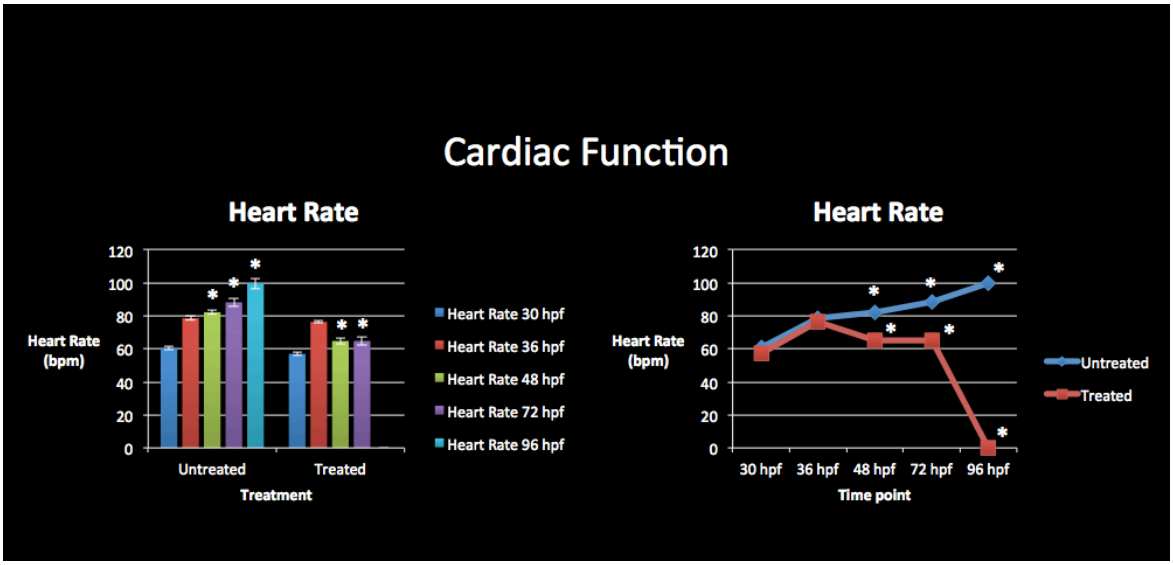

Table 3.1: Descriptive statistics of the zebrafish heart rate

Descriptives

HeartRate

	N	Mean	Std. Deviation	Std. Error	95% Confidence Interval for Mean		Minimum	Maximum
					Lower Bound	Upper Bound		
Untr 30 hpf	5	60.6000	2.50998	1.12250	57.4834	63.7166	57.00	63.00
Untr 36 hpf	5	78.6000	2.50998	1.12250	75.4834	81.7166	75.00	81.00
Untr 48 hpf	5	82.2000	2.68328	1.20000	78.8683	85.5317	78.00	84.00
Untr 72 hpf	5	88.2000	5.44977	2.43721	81.4332	94.9668	81.00	93.00
Untr 96 hpf	5	99.6000	7.16240	3.20312	90.7067	108.4933	90.00	108.00
O+D 30 hpf	5	57.0000	2.12132	.94868	54.3660	59.6340	54.00	60.00
O+D 36 hpf	5	76.4000	2.07364	.92736	73.8252	78.9748	74.00	79.00
O+D 48 hpf	5	64.8000	4.54973	2.03470	59.1508	70.4492	60.00	72.00
O+D 72 hpf	5	64.8000	5.44977	2.43721	58.0332	71.5668	60.00	72.00
O+D 96 hpf	5	.0000	.00000	.00000	.0000	.0000	.00	.00
Total	50	67.2200	26.21208	3.70695	59.7706	74.6694	.00	108.00

Table 4: Morphometric analysis of area, perimeter, length, and width of the atrial chamber

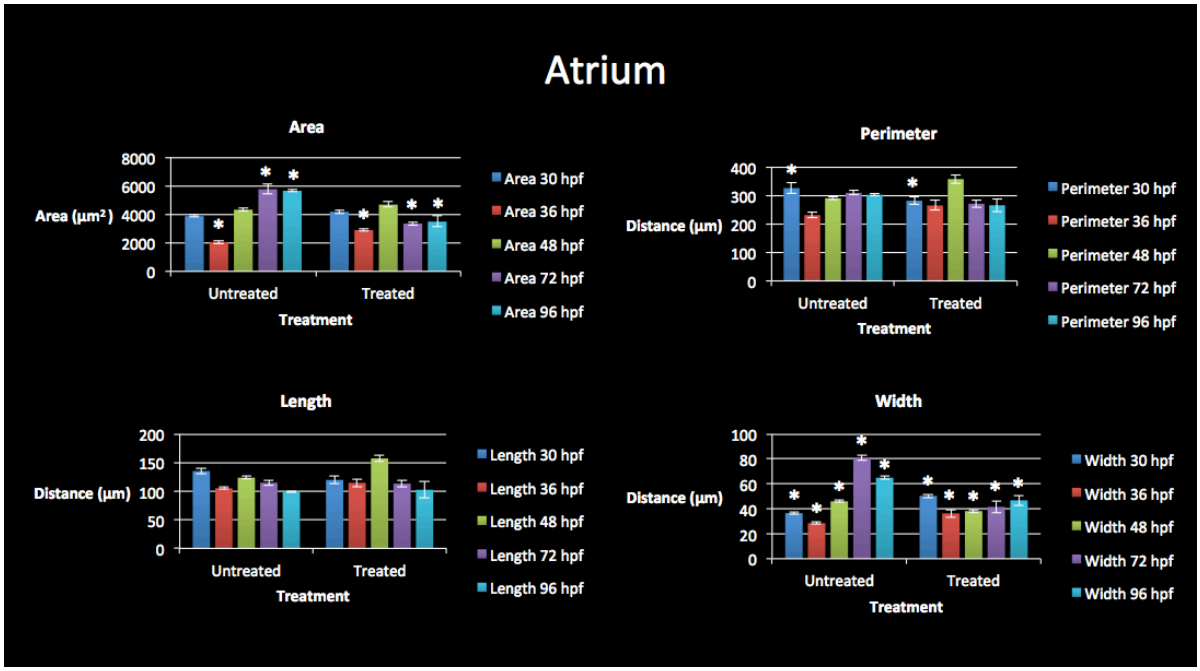

Table 4.1: Descriptive statistics of the zebrafish atrium

Descriptives

		N	Mean	Std. Deviation	Std. Error	95% Confidence Interval for Mean		Minimum	Maximum
						Lower Bound	Upper Bound		
Area	Untr 30 hpf	5	3873.7672	168.32679	75.27803	3664.7619	4082.7725	3608.75	4035.48
	Untr 36 hpf	5	2063.0342	257.38094	115.10426	1743.4535	2382.6149	1803.30	2365.94
	Untr 48 hpf	5	4327.5808	216.43116	96.79096	4058.8460	4596.3156	4092.39	4561.25
	Untr 72 hpf	5	5764.6082	729.46431	326.22636	4858.8586	6670.3578	5069.24	6672.01
	Untr 96 hpf	5	5652.8188	209.21974	93.56591	5393.0382	5912.5994	5440.29	5979.82
	O+D 30 hpf	5	4179.9186	320.32666	143.25444	3782.1805	4577.6567	3830.64	4622.27
	O+D 36 hpf	5	2896.3880	201.41217	90.07426	2646.3018	3146.4742	2562.66	3067.27
	O+D 48 hpf	5	4235.2070	411.50020	184.02849	3724.2620	4746.1520	3735.82	4681.44
	O+D 72 hpf	5	3355.3586	263.25967	117.73330	3028.4785	3682.2387	3030.49	3707.37
	O+D 96 hpf	5	3487.9538	853.40929	381.65624	2428.3062	4547.6014	2153.10	4333.10
	Total	50	3983.6635	1158.96757	163.90277	3654.2886	4313.0385	1803.30	6672.01
Perimeter	Untr 30 hpf	5	325.3164	40.67564	18.19070	274.8109	375.8219	281.68	383.65
	Untr 36 hpf	5	230.7616	20.46401	9.15178	205.3522	256.1710	200.16	252.91
	Untr 48 hpf	5	289.9620	11.18294	5.00116	276.0765	303.8475	277.34	302.69
	Untr 72 hpf	5	308.8282	17.04205	7.62144	287.6677	329.9887	280.89	322.67
	Untr 96 hpf	5	302.0684	8.06089	3.60494	292.0595	312.0773	291.85	313.08
	O+D 30 hpf	5	281.1870	28.66290	12.81844	245.5973	316.7767	239.71	312.29
	O+D 36 hpf	5	264.3940	38.46200	17.20073	216.6371	312.1509	216.99	296.88
	O+D 48 hpf	5	306.8638	33.98732	15.19959	264.6630	349.0646	271.09	357.14
	O+D 72 hpf	5	270.5910	27.93158	12.49138	235.9094	305.2726	241.91	314.29
	O+D 96 hpf	5	265.2352	50.13613	22.42156	202.9830	327.4874	226.78	353.01
	Total	50	284.5208	38.34185	5.42236	273.6241	295.4174	200.16	383.65
Length	Untr 30 hpf	5	135.2346	10.56557	4.72507	122.1157	148.3535	124.25	151.47
	Untr 36 hpf	5	105.0774	3.84449	1.71931	100.3038	109.8510	98.28	107.43
	Untr 48 hpf	5	123.7020	4.66244	2.08511	117.9128	129.4912	118.15	128.76
	Untr 72 hpf	5	114.8300	10.13306	4.53164	102.2481	127.4119	103.29	127.96
	Untr 96 hpf	5	99.2704	2.70543	1.20991	95.9112	102.6296	95.65	101.86
	O+D 30 hpf	5	119.7250	15.10556	6.75541	100.9690	138.4810	95.58	130.80
	O+D 36 hpf	5	114.6388	15.46074	6.91425	95.4418	133.8358	93.00	126.28
	O+D 48 hpf	5	137.0744	11.91204	5.32723	122.2836	151.8652	126.11	157.32
	O+D 72 hpf	5	113.1522	14.70100	6.57449	94.8985	131.4059	101.62	131.81
	O+D 96 hpf	5	102.5578	31.79568	14.21946	63.0782	142.0374	75.12	157.31
	Total	50	116.5263	17.93187	2.53595	111.4301	121.6224	75.12	157.32
Width	Untr 30 hpf	5	36.6222	2.25161	1.00695	33.8265	39.4179	33.39	39.65
	Untr 36 hpf	5	28.5304	1.88331	.84224	26.1920	30.8688	26.31	30.82
	Untr 48 hpf	5	46.0384	1.72255	.77035	43.8996	48.1772	44.16	48.06
	Untr 72 hpf	5	81.0232	4.66691	2.08711	75.2285	86.8179	74.19	85.78
	Untr 96 hpf	5	64.9574	2.55954	1.14466	61.7793	68.1355	62.99	69.23
	O+D 30 hpf	5	50.4048	3.27961	1.46669	46.3326	54.4770	47.57	55.90
	O+D 36 hpf	5	36.3534	6.98641	3.12442	27.6786	45.0282	27.83	46.05
	O+D 48 hpf	5	36.7788	2.82070	1.26146	33.2764	40.2812	34.14	40.91
	O+D 72 hpf	5	41.5492	10.46470	4.67996	28.5556	54.5428	28.67	49.87
	O+D 96 hpf	5	46.8018	9.09927	4.06932	35.5036	58.1000	35.32	57.75
	Total	50	46.9060	15.74241	2.22631	42.4320	51.3799	26.31	85.78

Table 5: Morphometric analysis of area, perimeter, length, and width of the ventricular chamber

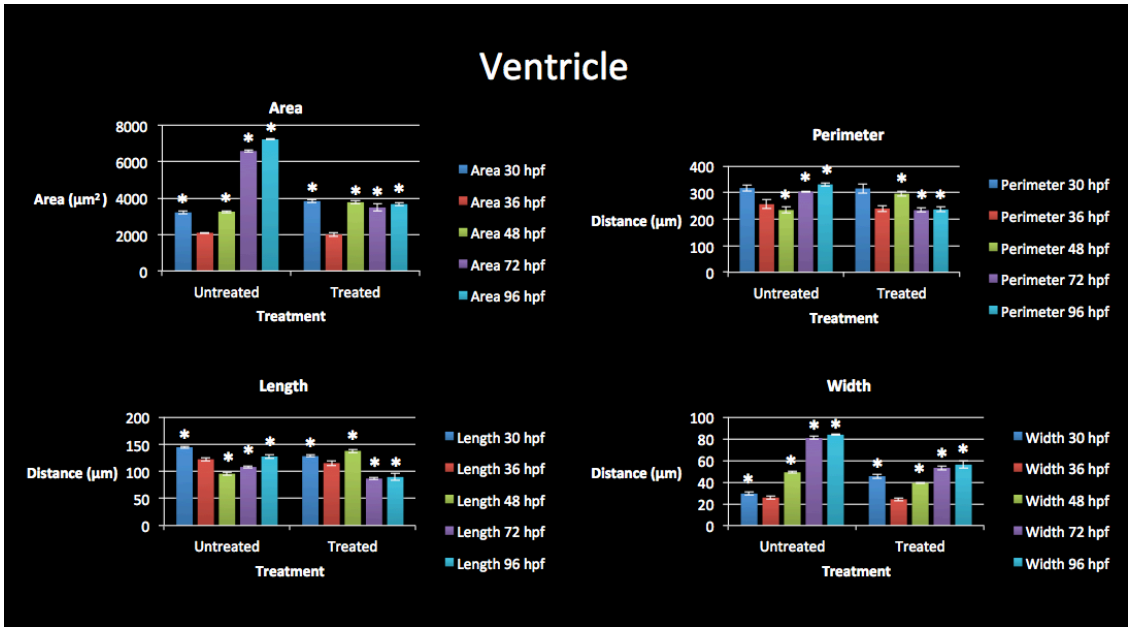

Table 5.1: Descriptive statistics of the zebrafish ventricle

Descriptives

		N	Mean	Std. Deviation	Std. Error	95% Confidence Interval for Mean		Minimum	Maximum
						Lower Bound	Upper Bound		
Area	Untr 30 hpf	5	3212.4014	173.18256	77.44959	2997.3669	3427.4359	3033.16	3434.73
	Untr 36 hpf	5	2095.1884	73.27205	32.76826	2004.2091	2186.1677	2027.66	2199.42
	Untr 48 hpf	5	3254.4790	143.84489	64.32939	3075.8720	3433.0860	3090.59	3404.22
	Untr 72 hpf	5	6579.0598	186.50732	83.40861	6347.4804	6810.6392	6395.36	6878.49
	Untr 96 hpf	5	7218.1540	91.15064	40.76381	7104.9755	7331.3325	7082.92	7339.95
	O+D 30 hpf	5	3831.0526	172.06824	76.95126	3617.4017	4044.7035	3628.16	3993.67
	O+D 36 hpf	5	1994.7610	210.37978	94.08470	1733.5400	2255.9820	1800.83	2336.15
	O+D 48 hpf	5	3769.9706	221.62210	99.11242	3494.7904	4045.1508	3430.72	3971.79
	O+D 72 hpf	5	3484.5292	447.56529	200.15728	2928.8035	4040.2549	3102.50	4192.76
	O+D 96 hpf	5	3668.0794	184.92603	82.70143	3438.4634	3897.6954	3482.24	3891.59
	Total	50	3910.7675	1646.78089	232.88999	3442.7576	4378.7775	1800.83	7339.95
Perimeter	Untr 30 hpf	5	317.1082	25.54067	11.42214	285.3953	348.8211	288.23	354.50
	Untr 36 hpf	5	256.3258	36.03403	16.11491	211.5836	301.0680	211.21	306.00
	Untr 48 hpf	5	234.3668	24.43666	10.92841	204.0247	264.7089	217.85	276.81
	Untr 72 hpf	5	303.5562	4.62326	2.06759	297.8157	309.2967	297.13	308.09
	Untr 96 hpf	5	330.6636	13.63827	6.09922	313.7295	347.5977	309.99	346.72
	O+D 30 hpf	5	315.3722	39.08980	17.48149	266.8358	363.9086	283.06	381.22
	O+D 36 hpf	5	240.0102	25.37759	11.34920	208.4998	271.5206	208.12	277.86
	O+D 48 hpf	5	295.6934	19.85187	8.87803	271.0440	320.3428	266.91	318.28
	O+D 72 hpf	5	233.7146	18.84126	8.42607	210.3201	257.1091	209.02	253.45
	O+D 96 hpf	5	236.4306	18.48277	8.26575	213.4812	259.3800	219.89	267.27
	Total	50	276.3242	43.98304	6.22014	263.8243	288.8240	208.12	381.22
Length	Untr 30 hpf	5	144.2764	8.59508	3.84384	133.6042	154.9486	132.13	155.98
	Untr 36 hpf	5	122.1708	7.07855	3.16562	113.3816	130.9600	114.34	132.31
	Untr 48 hpf	5	95.5042	6.11355	2.73406	87.9132	103.0952	88.09	104.87
	Untr 72 hpf	5	108.0156	4.29443	1.92053	102.6834	113.3478	104.35	114.26
	Untr 96 hpf	5	127.2434	7.52816	3.36670	117.8959	136.5909	115.94	134.01
	O+D 30 hpf	5	127.9076	7.05033	3.15300	119.1535	136.6617	119.31	137.19
	O+D 36 hpf	5	115.0550	10.04977	4.49439	102.5766	127.5334	100.92	127.51
	O+D 48 hpf	5	137.5366	7.32890	3.27758	128.4366	146.6366	130.87	148.42
	O+D 72 hpf	5	86.5652	4.13944	1.85122	81.4254	91.7050	80.50	91.74
	O+D 96 hpf	5	89.4096	13.37055	5.97949	72.8079	106.0113	81.60	113.09
	Total	50	115.3684	20.53690	2.90436	109.5319	121.2050	80.50	155.98
Width	Untr 30 hpf	5	29.4682	3.85471	1.72388	24.6820	34.2544	24.93	35.14
	Untr 36 hpf	5	25.7618	4.00963	1.79316	20.7832	30.7404	21.50	30.54
	Untr 48 hpf	5	49.0536	1.47314	.65881	47.2245	50.8827	47.60	51.06
	Untr 72 hpf	5	80.6902	3.20465	1.43316	76.7111	84.6693	77.16	84.62
	Untr 96 hpf	5	83.7206	1.81068	.80976	81.4723	85.9689	80.56	85.18
	O+D 30 hpf	5	45.4680	4.28341	1.91560	40.1494	50.7866	41.67	51.32
	O+D 36 hpf	5	24.2574	3.26297	1.45924	20.2059	28.3089	21.77	28.79
	O+D 48 hpf	5	39.2310	.87886	.39304	38.1398	40.3222	37.97	40.36
	O+D 72 hpf	5	53.2136	4.33742	1.93975	47.8280	58.5992	46.80	57.08
	O+D 96 hpf	5	56.1550	8.04194	3.59647	46.1696	66.1404	49.51	65.23
	Total	50	48.7019	20.32237	2.87402	42.9264	54.4775	21.50	85.18

Table 6: Morphometric analysis of area and perimeter of the AVC

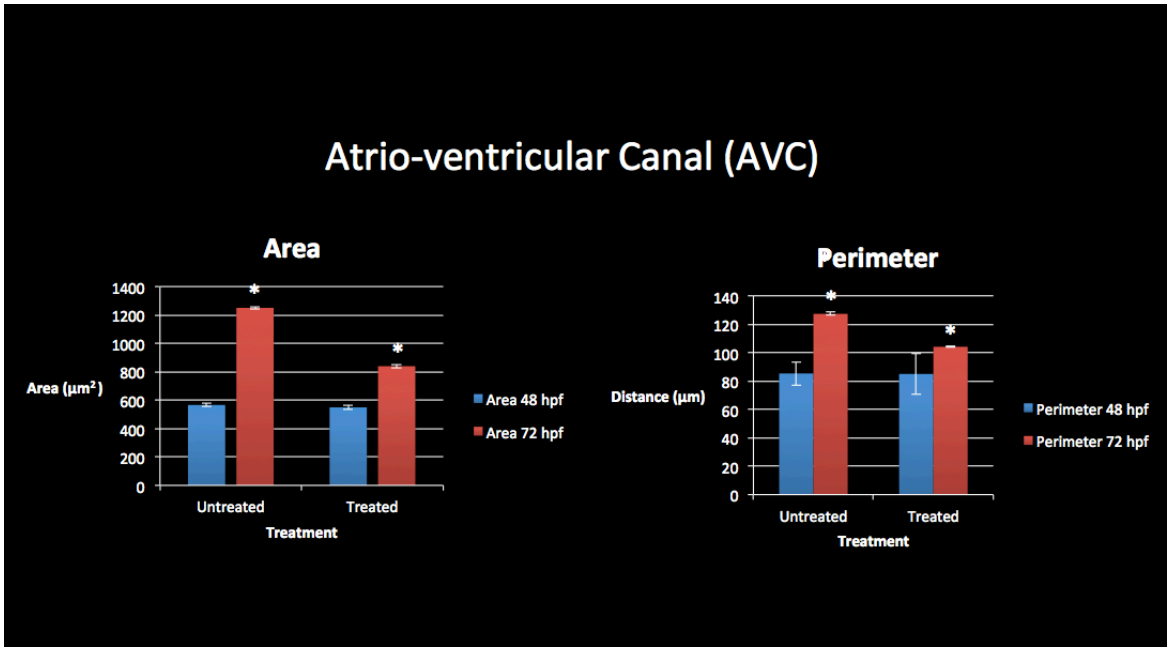

Table 6.1: Descriptive statistics of the zebrafish AVC

Descriptives

		N	Mean	Std. Deviation	Std. Error	95% Confidence Interval for Mean		Minimum	Maximum
						Lower Bound	Upper Bound		
Area	Untr 48 hpf	5	567.1022	24.69721	11.04493	536.4366	597.7678	540.66	597.16
	Untr 72 hpf	5	1252.0956	18.56276	8.30152	1229.0469	1275.1443	1224.22	1275.07
	O+D 48 hpf	5	550.2340	31.39830	14.04175	511.2479	589.2201	517.75	592.74
	O+D 72 hpf	5	840.7298	32.40209	14.49066	800.4973	880.9623	808.68	878.64
	Total	20	802.5404	292.46691	65.39759	665.6617	939.4191	517.75	1275.07
Perimeter	Untr 48 hpf	5	85.4534	2.14981	.96142	82.7841	88.1227	82.61	88.28
	Untr 72 hpf	5	127.5030	2.53947	1.13569	124.3498	130.6562	124.59	131.21
	O+D 48 hpf	5	85.1196	2.37503	1.06215	82.1706	88.0686	82.62	88.22
	O+D 72 hpf	5	104.2894	1.32974	.59468	102.6383	105.9405	103.01	106.00
	Total	20	100.5914	17.92696	4.00859	92.2013	108.9814	82.61	131.21

Table 7: Morphometric analysis of area, perimeter of the ventricle (AVC)

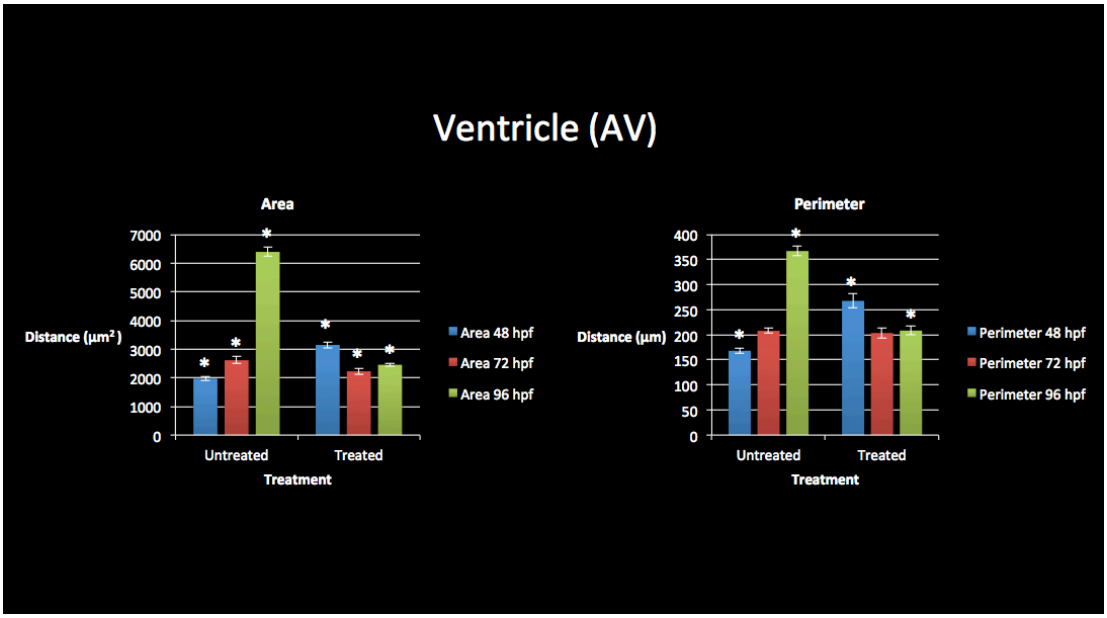

Table 7.1: Descriptive statistics of the zebrafish ventricle (AV)

Descriptives

		N	Mean	Std. Deviation	Std. Error	95% Confidence Interval for Mean		Minimum	Maximum
						Lower Bound	Upper Bound		
Area	Untr 48 hpf	5	1969.9212	148.00888	66.19158	1786.1439	2153.6985	1835.66	2198.49
	Untr 72 hpf	5	2611.1522	269.36567	120.46399	2276.6905	2945.6139	2286.63	2993.51
	Untr 96 hpf	5	6391.3544	348.16883	155.70583	5959.0457	6823.6631	6066.12	6957.39
	O+D 48 hpf	5	3144.3954	231.12935	103.36419	2857.4104	3431.3804	2867.77	3450.86
	O+D 72 hpf	5	2224.0302	235.12434	105.15080	1932.0848	2515.9756	1989.65	2508.22
	O+D 96 hpf	5	2453.7204	113.73130	50.86218	2312.5043	2594.9365	2275.33	2562.24
	Total	30	3132.4290	1542.47817	281.61670	2556.4582	3708.3998	1835.66	6957.39
Perimeter	Untr 48 hpf	5	168.0942	11.68499	5.22569	153.5854	182.6030	156.53	181.01
	Untr 72 hpf	5	207.8408	10.90936	4.87882	194.2950	221.3866	196.96	221.87
	Untr 96 hpf	5	366.9718	20.81602	9.30921	341.1253	392.8183	340.19	389.74
	O+D 48 hpf	5	267.5452	31.36253	14.02575	228.6035	306.4869	224.55	311.26
	O+D 72 hpf	5	203.5194	22.61697	10.11462	175.4367	231.6021	178.07	234.71
	O+D 96 hpf	5	208.3590	18.51383	8.27964	185.3710	231.3470	186.23	232.05
	Total	30	237.0551	68.71555	12.54568	211.3963	262.7139	156.53	389.74

Table 8: Morphometric analysis of the area and perimeter of the bulbus arteriosus

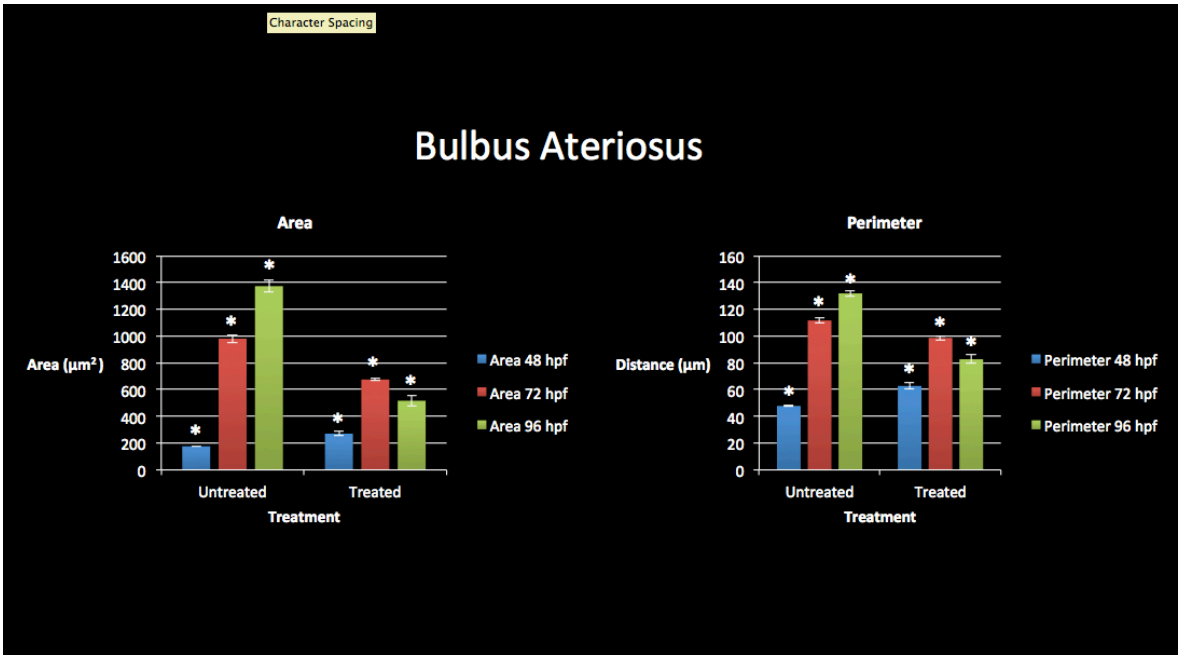

Table 8.1: Descriptive statistics of the zebrafish bulbus arteriosus

Descriptives

		N	Mean	Std. Deviation	Std. Error	95% Confidence Interval for Mean		Minimum	Maximum
						Lower Bound	Upper Bound		
Area	Untr 48 hpf	5	176.4054	3.89112	1.74016	171.5739	181.2369	172.48	181.62
	Untr 72 hpf	5	980.6666	66.40746	29.69832	898.2109	1063.1223	912.33	1065.19
	Untr 96 hpf	5	1373.1920	98.58718	44.08953	1250.7798	1495.6042	1231.30	1480.52
	O+D 48 hpf	5	270.7920	34.94473	15.62776	227.4024	314.1816	224.56	306.34
	O+D 72 hpf	5	675.4396	21.05814	9.41749	649.2925	701.5867	646.06	699.07
	O+D 96 hpf	5	516.9210	87.07569	38.94143	408.8023	625.0397	365.96	589.50
	Total	30	665.5694	422.64630	77.16430	507.7507	823.3882	172.48	1480.52
Perimeter	Untr 48 hpf	5	47.8028	.58868	.26327	47.0719	48.5337	47.23	48.44
	Untr 72 hpf	5	111.6754	4.06428	1.81760	106.6289	116.7219	107.18	116.68
	Untr 96 hpf	5	131.9174	4.81829	2.15481	125.9347	137.9001	124.82	136.44
	O+D 48 hpf	5	62.7322	4.88595	2.18506	56.6655	68.7989	56.20	67.54
	O+D 72 hpf	5	98.6408	3.67115	1.64179	94.0825	103.1991	92.42	101.40
	O+D 96 hpf	5	82.6830	7.18487	3.21317	73.7618	91.6042	71.04	90.25
	Total	30	89.2419	29.29936	5.34931	78.3014	100.1825	47.23	136.44

References

1. Acar, Evrim, George E. Plopper, and Bülent Yener. "Coupled Analysis of In Vitro and Histology Tissue Samples to Quantify Structure-Function Relationship." *PloS one* 7.3 (2012): e32227.
2. Armstrong, Richard A. "Quantitative microscopic analysis of histological sections of brain tissue." (2007): 442-452.
3. Arukwe, Augustine, et al. "Modulation of steroidogenesis and xenobiotic biotransformation responses in zebrafish (< i> Danio rerio</i>) exposed to water-soluble fraction of crude oil." *Environmental research* 107.3 (2008): 362-370.
4. Carls, Mark G., et al. "Fish embryos are damaged by dissolved PAHs, not oil particles." *Aquatic toxicology* 88.2 (2008): 121-127.
5. Choi, D.W. (1992). Excitotoxic cell death. *J. Neurobiol.* 23, 1261-1276
6. Cole, L., and L. Ross. "Apoptosis in the Developing Zebrafish Embryo." *Developmental Biology* 240.1 (2001): 123-42. Print.
7. de Soysa, T. Yvanka, et al. "Macondo crude oil from the Deepwater Horizon oil spill disrupts specific developmental processes during zebrafish embryogenesis." *BMC biology* 10.1 (2012): 40.
8. Freudenburg, William R., and Robert Gramling. *Blowout in the Gulf: The BP Oil Spill Disaster and the Future of Energy in America*. Cambridge, MA: MIT, 2011. Print.
9. Herrup, K., and Busser, J.C. (1995). The induction of multiple cell cycle events preceeds target-related neuronal death in Xenopus embryos. *Ann. N.Y. Acad. Sci.* 887, 105-119.
10. Hicken, Corinne E., et al. "Sublethal exposure to crude oil during embryonic development alters cardiac morphology and reduces aerobic capacity in adult fish." *Proceedings of the National Academy of Sciences* 108.17 (2011): 7086-7090.
11. Holth, Thor-Frederik, et al. "Differential gene expression and biomarkers in zebrafish (< i> Danio rerio</i>) following exposure to produced water components." *Aquatic Toxicology* 90.4 (2008): 277-291.
12. Hu, Norman, David Sedmera, H. Joseph Yost, and Edward B. Clark. "Structure and Function of the Developing Zebrafish Heart." *The Anatomical Record* 260.2 (2000): 148-57. Print.
13. Incardona, John P., et al. "Aryl hydrocarbon receptor–independent toxicity of weathered crude oil during fish development." *Environmental health perspectives* 113.12 (2005): 1755.
14. Jacobson, Michael D., Miguel Weil, and Martin C. Raff. "Programmed Cell Death in Animal Development." *Cell* 88.3 (1997): 347-54. Web.
15. Kelsh, Robert N., et al. "Zebrafish pigmentation mutations and the processes of neural crest development." *Development* 123.1 (1996): 369-389.
16. Kemadjou, Jules, and Martina Bauchrowitz. "Effects of Crude Oil on Zebrafish Embryos." *Http://www.eawag.ch/index_EN*. Eawag Aquatic Research, June 2008. Web. 27 Nov. 2012. <http://www.eawag.ch/medien/publ/eanews/news_64/en64e.pdf>.
17. Kerr, J.F., Wyllie, A.H., and Currie, A.R. (1972). Apoptosis: a basic biological phenomenon with wide-ranging implications in tissue kinetics. *Br. J. Cancer* 26, 239-257.

18. Kimmel, Charles B., William W. Ballard, Seth R. Kimmel, Bonnie Ullmann, and Thomas F. Schilling. "Stages of Embryonic Development of the Zebrafish." *American Journal of Anatomy* 203.3 (1995): 253-310. Print.
19. Liu, Jiandong, and Didier Stainier. "Zebrafish in the Study of Early Cardiac Development." *Circulation Research* (2012): 870-74. Print.
20. Menke, Aswin L., et al. "Normal anatomy and histology of the adult zebrafish." *Toxicologic pathology* 39.5 (2011): 759-775.
21. Meruvia-Pastor, Oscar E., et al. "Estimating cell count and distribution in labeled histological samples using incremental cell search." *Journal of Biomedical Imaging* 2011 (2011): 12.
22. Olson, E. N. "Sizing up the Heart: Development Redux in Disease." *Genes & Development* 17.16 (2003): 1937-956. Print.
23. Parichy, David M., et al. "Normal table of postembryonic zebrafish development: staging by externally visible anatomy of the living fish." *Developmental Dynamics* 238.12 (2009): 2975-3015.
24. Pauka, Luciana M., et al. "Embryotoxicity and biotransformation responses in zebrafish exposed to water-soluble fraction of crude oil." *Bulletin of environmental contamination and toxicology* 86.4 (2011): 389-393.
25. Raible, David W., and Judith S. Eisen. "Regulative interactions in zebrafish neural crest." *Development* 122.2 (1996): 501-507.
26. Sabaliauskas, Nicole A., et al. "High-throughput zebrafish histology." *Methods* 39.3 (2006): 246-254.
27. Schilling, Thomas F., Charline Walker, and Charles B. Kimmel. "The chinless mutation and neural crest cell interactions in zebrafish jaw development." *Development* 122.5 (1996): 1417-1426.
28. Stainier, D., and Mark Fishman. "Patterning the Zebrafish Heart Tube: Acquisition of Anteroposterior Polarity*1." *Developmental Biology* 153.1 (1992): 91-101. Print.
29. Stainier, Didier Y.R., and Mark C. Fishman. "The Zebrafish as a Model System to Study Cardiovascular Development." *Trends in Cardiovascular Medicine* 4.5 (1994): 207-12. Print.
30. Stainier, Didier. "Cardiovascular Development in the Zebrafish." *Development* (1993): 31-40. Print.
31. Thomas, G., K. Cheng, and J. Z. Wang. "Automated segmentation and classification of zebrafish histology images for high-throughput phenotyping." *Life Science Systems and Applications Workshop, 2007. LISA 2007.*
32. Truman, J.W., and Schwartz, L.M. (1984). Steroid regulation of neuronal death in the moth nervous system. *J. Neurosci.* 8, 4513-4530.
33. Trump, B.F., and Berezesky, I.K. (1995). Calcium-mediated cell injury and cell death. *FASEB J.* 9, 219-228.
34. Vaux, D.L., and Haecker, G., and Strasser, A., (1994). An evolutionary perspective on apoptosis. *Cell* 76, 777-779.
35. Webster, Joshua D., et al. "Quantifying histological features of cancer biospecimens for biobanking quality assurance using automated morphometric pattern recognition image analysis algorithms." *Journal of biomolecular techniques: JBT* 22.3 (2011): 108.
36. Williams, G.T., and Smith, C.A. (1993). Molecular regulation of apoptosis: Genetic

controls on cell death. *Cell* 74, 777-779.
37. Wood, K.A., and Youle, R.J. (1995). The role of free radicals and p53 in neuron apoptosis in vivo. *J. Neurosci.* 15, 5851-5857

Appendix A

East Carolina University

Animal Care and Use Commitee
212 Ed Warren Life Sciences Building
East Carolina University
Greenville, NC 27834

252-744-2436 office
252-744-2355 fax

September 18, 2012

Ed Stellwag, Ph.D.
Department of Biology
Howell Science Building
East Carolina University

Dear Dr. Stellwag:

The Amendment to your Animal Use Protocol entitled, "RAPID: Influence of Environmental Crude Oil Exposure on Genetic Mechanisms of Fish Development", (AUP #D248) was reviewed by this institution's Animal Care and Use Committee on 9/18/12. The following action was taken by the Committee:

"Approved as amended"

A copy of the Amendment is enclosed for your laboratory files. Please be reminded that all animal procedures must be conducted as described in the approved Animal Use Protocol. Modifications of these procedures cannot be performed without prior approval of the ACUC. The Animal Welfare Act and Public Health Service Guidelines require the ACUC to suspend activities not in accordance with approved procedures and report such activities to the responsible University Official (Vice Chancellor for Health Sciences or Vice Chancellor for Academic Affairs) and appropriate federal Agencies.

Sincerely yours,

Susan McRae, Ph.D.
Chair, Animal Care and Use Committee

SM/jd

enclosure

Appendix B

Supplemental Materials:

Video 1: 100x untreated zebrafish heart rate at 30 hpf

Video 1.1: 100x O+D zebrafish heart rate at 30 hpf

Video: 2: 100x untreated zebrafish heart rate at 36 hpf

Video 2.1: 100x O+D zebrafish heart rate at 36 hpf

Video 3: 100x untreated zebrafish heart rate at 48 hpf

Video 3.1: 100x O+D zebrafish heart rate at 48 hpf

Video 4: 100x untreated zebrafish heart rate at 72 hpf

Video 4.1: 100x O+D zebrafish heart rate at 72 hpf

Video 5: 100x untreated zebrafish heart rate at 96 hpf

Video 5.1: 100x O+D zebrafish heart rate at 96 hpf